SCHOOL OF ENGINEERING AND THE BUILT ENVIRONMENT

DEPARTMENT OF CIVIL ENGINEERING

THE USE OF THE SECTORIAL COORDINATE APPROACH TO DEMONSTRATE UNIQUE SHEAR CENTRE PROPERTIES OF NON-STANDARD MONOSYMMETRIC STEEL SECTIONS

A thesis submitted in partial fulfilment of the requirements for the degree of

Master of Engineering in Structural Engineering

at the

University of Cape Town

Presented by:	Mervin Mbakekua Muukua
Student Number:	MKXMER001
Supervisor:	Mr Kenny Mudenda
Submission date:	November 2019

Declaration of Authorship

I *Mervin Mbakekua Muukua, student number MKXMER001* hereby declare to the best of my knowledge that:

"I know the meaning of plagiarism and declare that all the work in this document, except for that, which is properly acknowledged is my own. This thesis/dissertation has been submitted to the Turnitin module (or equivalent similarity and originality checking software) and I confirm that my supervisor has seen my report and any concerns revealed by such have been resolved with my supervisor."

…. Signed by candidate …. Date: November 2019

Signature:

RETENTION AND USE OF THESIS

I, **Mervin Mbakekua Muukua** a candidate for the degree of **Master of Engineering specialising in Structural Engineering** accept the requirements of the University of Cape Town with regards to the retention and use of theses/mini-theses deposited in the Library and Information Services.

…Signed by candidate…. Date: November 2019

Signature:

METADATA

TITLE: The use of the sectorial coordinate approach to demonstrate unique shear centre properties of non-standard monosymmetric steel sections

AUTHOR:	Mr Mervin Mbakekua Muukua
SUPERVISOR:	Mr Kenny Mudenda
INSTITUTION:	University of Cape Town
DEPARTMENT:	Civil Engineering
MASTER IN:	Structural Engineering
KEYWORDS:	Sectorial method, Shear centre, non-standard monosymmetric sections
MAIN BODY of KNOWLEDGE:	Sectorial method use, Shear centre determination
METHODOLOGY:	Qualitative Approach, Calculation Research
TYPE OF RESEARCH:	Qualitative
SUBJECT:	Master's Thesis
STATUS:	Final Thesis
SITE:	University of Cape Town
DOCUMENT DATE:	November 2019
SPONSOR:	None

DEDICATION

I am wholeheartedly dedicating this thesis to my beloved family, friends and colleagues who have been my source of inspiration and have continually provided their moral and spiritual support throughout the completion of this thesis.

ACKNOWLEDGEMENTS

I would sincerely like to thank my mentors, Mr David Katale and Dr Victor Kamara for their unrelenting guidance and contributions. I am also grateful to my parents for their constant emotional support and having confidence in me throughout the entire academic journey. Another word of thanks goes to my supervisor, Mr Kenny Mudenda for his exemplary supervision and for enabling me to develop a better understanding of the topic.

Finally, I would like to thank the Almighty for the time and wisdom he has shed upon us all.

ABSTRACT

The study looks at how the sectorial coordinate approach can be used to solve the problem of unique shear centre property of non-standard monosymmetric sections. In solving the unique shear centres, the behaviour of the shear centre with reference to the centroid is carefully studied as the geometry of the section is changed.

The study shows investigations of the sections which are 152x152x30 UC H-section, the same H-section with 2/3 as well as 1/3 of the bottom flange width and a 203x178x30 T-section. Vertical plates of 8mm thickness are added to the ends of the upper flanges of the sections instigating increments of 12.5mm from 0 to 100mm height.

From the computations done, the following is observed:

- The difference between the sectorial coordinate approach results and those from Prokon is at most 3.1%. Also, as the end plate heights are increased, the difference in the results increases.
- Shear centres change in position with reference to the centroids as a result of the change in geometry of the sections.
- For the H-section the shear centre is initially with the centroid at zero plate height. It then moves upward (higher than the centroid) to a certain peak point, then decreases steadily, intersecting the centroid again and eventually ending up being lower than the centroid with upstanding plate height increases.
- A similar pattern follows the H-sections with reduced bottom flange widths, with the only difference being that the shear centre is initially higher than the centroid. It slightly increases to a peak then gradually decreases, intersecting the centroid at a certain point and ending up lower than the centroid.
- As for the T-section, the shear centre is initially at the highest point (furthest from the centroid) and decreases gradually, intersecting the centroid and ending up lower than the centroid.
- The H-section with upstanding plates offers itself as a section that has an envelope (gap) between the shear centre and centroid when the shear centre is above the centroid which is much lesser than the other sections.

With the usage of excel spreadsheets, the sectorial coordinate approach is an efficient and accurate method to find shear centres and related section properties.

TABLE OF CONTENTS

LIST OF FIGURES

LIST OF TABLES

LIST OF ACRONYMS

m, mass

h, height of section

b, breadth of section

t_f, thickness of flange

t_w, thickness of web

r_1, fillet radius

h_w, height of web

A, gross cross-sectional area

Z_e, elastic section modulus

Z_{pl}, plastic section modulus

r, radius gyration

E, youngs modulus

KL, effective length

β_x, coefficient of monosymmetry

C_w, warping torsional constant

G, shear modulus

J, St Venant torsional constant

ω_2, end moments effects factor

α, height of upstand plate

t_u, thickness of upstand plate

$\bar{y}$, first moment of area about the y-axis

$\bar{x}$, first moment of area about the x-axis

$\bar{y}_{sc}$, distance from bottom of section to shear centre

X, x-axis

Y, y-axis

C, centroid, centre of gravity

SC, shear centre

I_x, I_y, second moment of area about the x and y-axis

$I_{x\omega}$, $I_{y\omega}$, sectorial moment of area about the x and y-axis

ω, warping function

CHAPTER 1: RESEARCH OVERVIEW

1.1 Introduction

Steel is one of the materials commonly used in the construction industry. Due to the high cost and strength of steel, sections are dimensioned in such a manner as to optimise the resistance of forces induced. In other words, the sections utilized tend to deploy the cross-sectional area of the steel in such a manner that one gets the highest resistance of internal stresses for a certain amount of steel used (Jennings, 2004). As a result of this, we end up with sections of different shapes and sizes suitable for different loading scenarios and internally generated forces. The shapes used have structural properties which are related to the structural strengths and stiffnesses of the members (Mahachi, 2013). One of these section properties is the shear centre, which is the position through which if a load is transversely applied on a beam, twisting of the beam due to the applied load is avoided (Jennings, 2004).

This thesis examines one of the methods that can be used to determine the shear centre of any section. An analysis of a channel section is conducted as an example. Then an in-depth study of non-standard monosymmetric sections is undertaken.

1.2 Background

There are different sections available for use as structural members (SASCH, 2013). According to Mahachi (2013), these sections are required to resist externally applied loads by resisting internally induced stresses and strains. The resistance of these sections depends on a lot of parameters, with a few presented below:

- Magnitude, type and positions of loads
- Fixity of members (restrains on members)
- Material properties of sections
- **Cross-sectional properties of sections (derived from the geometry of the section)**

This thesis focuses more on the determination of the shear centre which is a cross-sectional property of the section. Also, the focus is on non-standard monosymmetric sections which are sections that are symmetric about one axis only, mostly about the y-axis. These sections do not have a common position for the shear centre and the centroid in general.

In view of the above, the aforementioned sections require more understanding of the section properties as they, in turn, affect the resistance capacities.

1.3 Problem Statement

The shear centre is a parameter that is of great importance with regards to the design of steel structures, as this position informs the designer on where to place a load on a beam member to prevent twisting of the member. A non-twisting member will result in a more stable member design and in turn, leads to stable structures which are aspired.

Determining the shear centre is not a straightforward process and there are different methods that can be used to determine this parameter. Two commonly known methods are the shear flow method and the sectorial coordinate approach. The shear flow method is less tedious; however, it is limited when arbitrary sections are considered. On the other hand, the sectorial coordinate approach is not limited and can address arbitrary sections.

In this thesis the sectorial coordinate approach is employed to find the shear centres of non-standard monosymmetric sections and to study the shear centre position with reference to the centroid as the structural geometry is altered. The relative position of the shear centre and centroid influences characteristics of the beam behaviour such as the critical buckling moment.

1.4 Research Objectives

1.4.1 Main Research Objective

The objective of this thesis is to demonstrate the usage of the sectorial coordinate approach in determining the shear centre of non-standard monosymmetric sections, as well as to observe the trend of the movement of the shear centre with reference to the centroid position, including a comparative analysis of the results obtained from Prokon software.

1.4.2 Specific Objectives

- To demonstrate the usage of the sectorial coordinate approach in determining the shear centre of non-standard monosymmetric sections.
- To analyse variances between results established through the sectorial coordinate approach and those obtained from Prokon software.
- To analyse the impact on the shear centre and centroid positions, of varying upstand plate heights on the top flanges of the sections.

1.5 Research Questions

The thesis seeks to address the following questions:

1.5.1 Main Research Question

How could the sectorial coordinate approach be employed in determining the shear centre of non-standard monosymmetric sections, as well as the impact of varying upstand plates on the beam top flange, on the shear centre and centroid position, including variances on the results obtained through the sectoral coordinate approach and those obtained from Prokon software?

1.5.2 Specific Questions

- How can the usage of the sectorial coordinate approach be employed in determining the shear centre of non-standard monosymmetric sections?
- What are the variances between results established through the sectorial coordinate approach and those obtained through Prokon software?
- How does changing upstanding plates on top flanges impact on shear centre and the centroid positions of the section?

1.6 Research Methodology

In this research, a desktop qualitative study research methodology was used. In this methodology, literature was reviewed to gain an understanding of the sectorial coordinate approach. Upon understanding of the sectorial coordinate approach, a channel section was used to explain the sectorial coordinate approach and how solutions were to be obtained. After which, the shear centres of chosen non-standard monosymmetric sections were determined. To validate the results of the sectorial coordinate approach, Prokon software was utilized to generate results of similar sections for comparison. The Prokon software was utilized as it is one of commonly used structural software in Southern Africa. It is what may Practicing Engineers have access to.

An analysis of the behaviour of the shear centres with altered geometry was then conducted. H-sections with vertical plates of varying heights welded on the ends of the upper flanges were studied. Similar H-sections with reduced bottom flanges as well as T-sections were also studied and the trend of how the shear centre position varied with reference to the centroid was analysed. The H-sections were used as

these are one of the frequently used sections as beam elements, the other being I-sections.

1.7 Research Rationale/Justification

The welding of upstanding plates on standard sections, hence forming non-standard sections, may be a necessity that some designers will require to implement on their members. This might be required to serve a few purposes practically such as:

- creating service ducts for cabling and pipes on the beams
- creating channels to transport fluids on the beams
- strengthening existing members

Hence, the outcome of this research may assist practitioners in the industry to understand how adding upstanding plates to a section affects the sections properties such as the shear centre. Knowing how the shear centre position varies with relation to the centroid at a certain plate height, informs the designer as to how the member may be expected to behave as a structural member and how best to load it.

For academia, this research shows the application of the sectorial area method and serve as an encouragement for the method to be frequently employed to conduct checks on results from the different software currently in use in the industry with the help of excel spreadsheets.

1.8 Research Limitations and Scope

The research was limited to a study of non-standard monosymmetric sections. The sections were an H-section, H-sections with reduced bottom flange widths and a T-section that had upstand flat plates welded on the ends of the upper flanges. The plates varied in height increments of 12.5mm from 0 to 100mm. A study of the variance in the shear centre position as the plate heights were adjusted was determined using the sectorial coordinate approach.

CHAPTER 2: LITERATURE REVIEW

2.1 Introduction

Steel sections are configured in different shapes such that the strength and stiffness of the material are optimised depending on the usage. The shape in which a cross-section of a member is formed is important. This is illustrated by means of a page shaped as shown in figure 2.1.

(a) 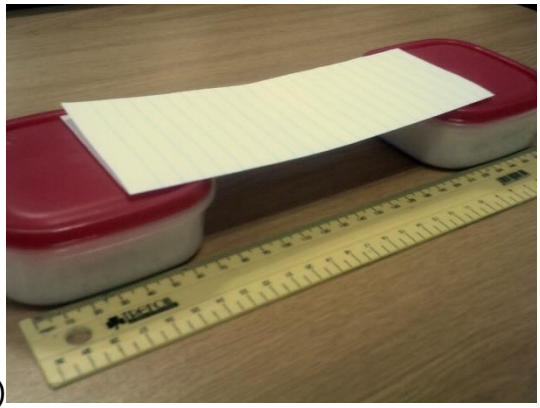 (b) 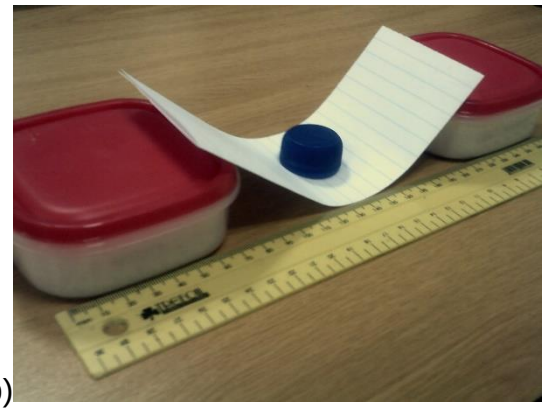

(c) 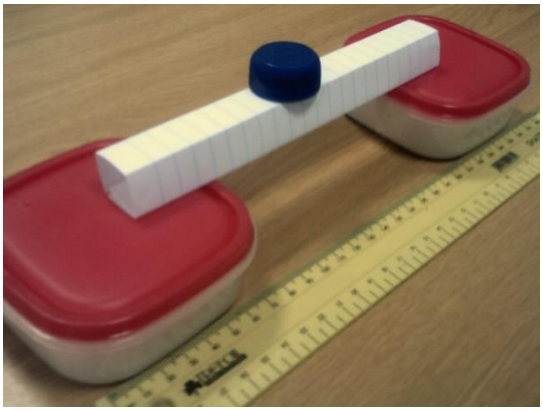

Figure 2.1: Page section beam, *Adapted from Jennings (2004)*

In figure 2.1, a page in insert (a), is folded in half and laid out flat on two supports (containers). Unloaded the page beam remains straight, able to carry its own weight. However, when loaded with a water bottle cap (b), the page sags and gives way under the load. Now, when the same page is taken and shaped in a square shape as can be seen in (c), the load-carrying capacity of the page is altered and the page beam is then able to carry the water bottle cap that it could not as a flat beam. From this simple illustration it is observed that, for a material of the same cross-sectional area, if the geometry of the cross-section is altered, the rigidity of the member changes. As a result, the member can potentially carry more loads.

Thus, structural sections have different geometries and each geometry brings forth unique aspects with regards to resistance of forces. Some of the sections are good at resisting axial loads (tension and compression), while others are good at resisting shear forces and bending moments. In certain scenarios, sections are expected to resist axial, shear forces and bending moments at the same time. The different type of sections and what they offer as structural members are discussed in the following section.

Regardless of the geometry, all sections require that sectional properties are calculated. This is important as these properties inform the designer as to how the structural members will behave when loaded and what their resistance capacities may be under certain conditions.

For example, if two sections are considered, a 305x165x40 kg/m I-section (highlighted in yellow/mustard) and a 356x171x45 kg/m I-section (highlighted in light grey) as shown in table 2.1 respectively. The sections have different geometries (h, b, t_w, t_f, r_1, h_w & A) and hence different section properties (I, Z_e, Z_{pl}, r, J & C_w).

Table 2.1: Section properties of I-Sections, *(SASCH, 2013)*

Designation	m	h	b	t_w	t_f	r_1	h_w	A
h x b x m	kg/m	mm	mm	mm	mm	mm	mm	10^3mm^2
305 x 165 x 40	40.3	303.8	165.1	6.1	10.2	8.9	266	5.16
46	46.1	307.1	165.7	6.7	11.8	8.9	266	5.88
54	54.0	310.9	166.8	7.7	13.7	8.9	266	6.82
356 x 171 x 45	45.0	352.0	171.0	6.9	9.7	10.2	312	5.70
51	51.0	355.6	171.5	7.3	11.5	10.2	312	6.46
57	57.0	358.6	172.1	8.0	13.0	10.2	312	7.22
67	67.1	364.0	173.2	9.1	15.7	10.2	312	8.55

	About x-x				About y-y				J	C_w
Designation	I	Z_e	Z_{pl}	r	I	Z_e	Z_{pl}	r		
h x b x m	10^6mm^4	10^3mm^3	10^3mm^3	mm	10^6mm^4	10^3mm^3	10^3mm^3	mm	10^3mm^4	10^9mm^6
305 x 165 x 40	85.5	563	626	129	7.66	92.8	142	38.5	149	165
46	99.3	647	722	130	8.96	108.0	166	39.0	223	195
54	117.0	752	843	131	10.60	127.0	195	39.4	345	234
356 x 171 x 45	121.0	686	773	146	8.10	94.7	146	37.7	160	237
51	142.0	796	895	148	9.68	113.0	174	38.7	238	287
57	161.0	896	1010	149	11.10	129.0	198	39.1	334	330
67	195.0	1070	1210	151	13.60	157.0	243	39.9	560	413

From table 2.2, we observe that a 305x165x40 kg/m I-section when laid out as a 5m long unrestrained beam can carry a moment of 110 kNm whereas the 356x171x45 kg/m I-section can carry a load of 127 kNm. Hence sections properties inform the designers of possible section behaviour.

Table 2.2: Moment resistance of I-Sections (max. moments not at end of unrestrained length), *(SASCH, 2013)*

Designation	M_{rx} (kN.m) Effective length KL of compression flange (m)									M_{ry}
h x b x m	0	2	4	5	6	7	8	9	10	kN.m
305 x 165 x 40	197.0	197.0	147.0	110.0	83.6	67.3	56.3	48.4		44.7
46	227.0	227.0	175.0	137.0	105.0	85.5	72.0	62.3		52.3
54	266.0	266.0	212.0	175.0	136.0	112.0	94.6	82.2		61.4
356 x 171 x 45	243.0	243.0	176.0	127.0	95.4	76.0	63.0	53.8	46.9	46.0
51	282.0	282.0	212.0	159.0	121.0	97.2	81.1	69.6	60.9	54.8
57	318.0	318.0	246.0	192.0	147.0	119.0	99.8	86.0	75.6	62.4
67	381.0	381.0	307.0	256.0	199.0	163.0	138.0	119.0	106.0	76.5

Amongst the many section properties, the shear centre is one of the properties required in the study of member strength and stability particularly for monosymmetric sections.

2.2 Steel Sections

There are many different steel sections used in the industry. In the Southern African context, the sections readily available off the shelf can be found in the South African Steel Construction Handbook (SASCH). Also known as the Red Book. Shown in figure 2.2 are the typical sections commonly used in the Southern African industry.

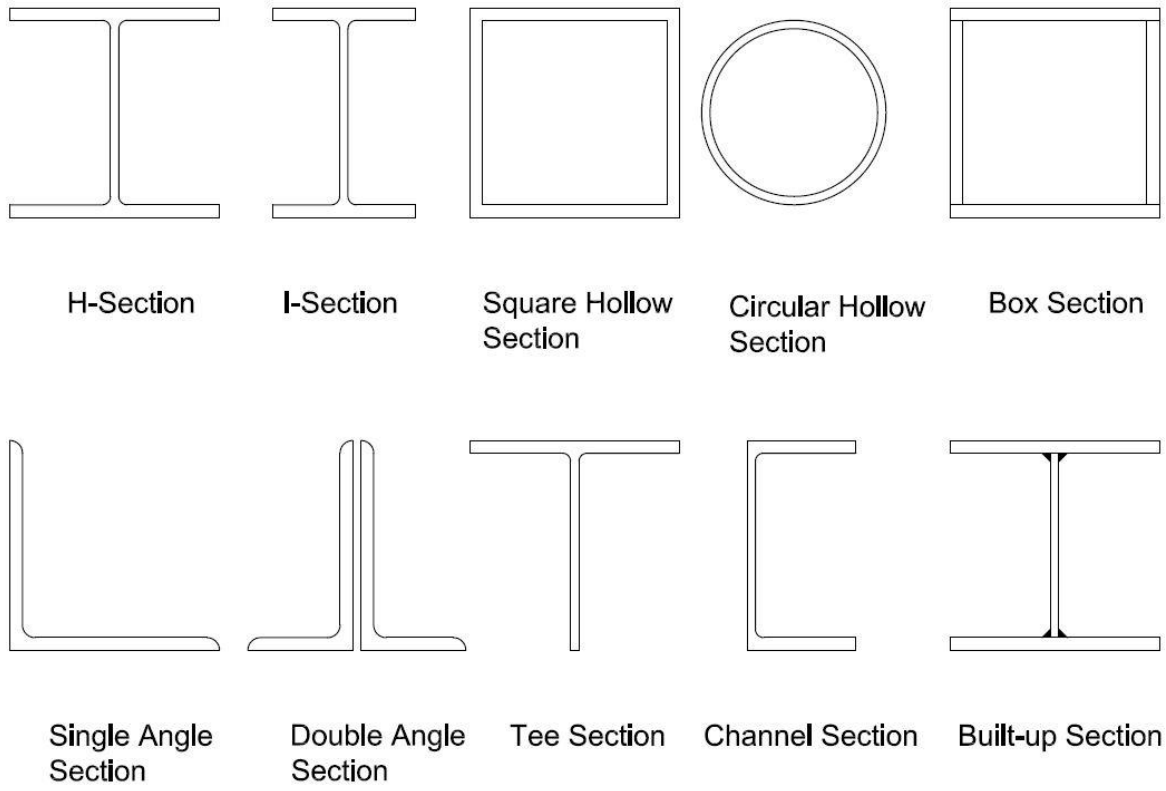

Figure 2.2: Types of section, *Adapted from Mahachi (2013)*

As per Mahachi (2013), the following sections tend to be used as members for axial forces in frames and in truss systems where moments are not of great concerns:

- Tee sections
- Angle sections (single and double)
- Hollow sections (circular, rectangular and square)
- H-sections (where axial forces predominate in frames)

Where moments are of significant value and should be considered in the design, the following members tend to be used:

- I-sections
- H-sections (dominantly moments about both axis)
- Built-up sections
- Channel sections

From the readily available sections, we get doubly symmetric, mono-symmetric and non-symmetric sections. The doubly symmetrical sections have symmetry about two axes, both the x-axis as well as the y-axis. Hence, if the section is folded in two about a certain axis, it will close itself in a mirror image. Sections that are doubly symmetric are sections such as the H-sections, I-sections, square and rectangular hollow sections.

Mono-symmetric sections are symmetrical about one axis only. These are sections such as channels and Tee sections.

The non-symmetric sections are sections that are not symmetrical about any of the axes. These are sections such as the Z and non-equal leg angle sections.

2.3 The behaviour of sections as beams

According to Mahachi (2013), a beam is a member that transmits loads normal to its longitudinal axis through to the supports. Beam elements are mostly composed of plates and they transfer the loads to the supports by generating two principle internal actions (forces), namely: shear and flexure (bending). Figure 2.3 shows a schematic of a simply supported beam and the internal stresses generated at a point within the section.

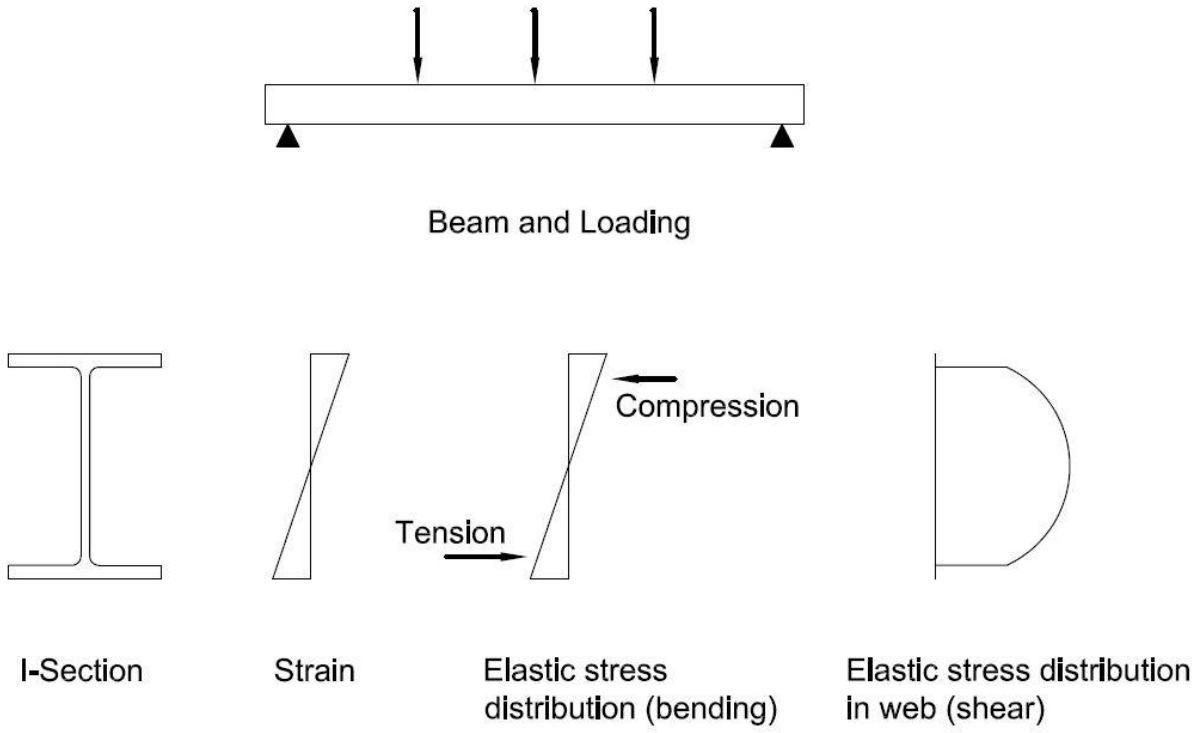

Figure 2.3: Loaded beam and internal stresses, *Adapted from Mahachi (2013)*

Figure 2.3 shows a beam which is experiencing a sagging moment. This yield tension stresses in the lower flange and compression stresses in the upper flange.

I-section, H-section and channel sections are the most commonly used sections as beams according to Mahachi (2013). This is because the distribution of the material in these sections provides the most efficient transfer of loads by means of bending and shear.

These sections tend to have high second moments of areas which are an important sectional property with regards to bending. This is because the largest amount of material is placed at the flanges (upper and lower ends of the section). Also, webs tend to have enough material to provide resistance for the shear stresses.

It is important to understand that when you have a beam which is loaded transversely, bending moments and shear forces will be present. This is because the two types of stresses co-exist.

In terms of loaded beams, we get laterally supported and laterally unsupported beams. When a laterally supported beam is loaded, the beam does not twist about the longitudinal axis as it is restrained from so doing. This is due to continuous lateral support that is provided along the flange in compression. The restrains in practice can be in the form of a cast concrete slab/deck, floorboards and roof claddings on top of the beam (Mahachi, 2013).

However, when loads are applied on a laterally unsupported beam, the beam can resist twisting and lateral displacement to a certain critical elastic bending moment.

This is an upper limit of the resistance strength of the beam to buckling according to Zhang, et al. (2017). Loading the beam with moments beyond that critical elastic moment, the beam can twist and displace laterally. The displacement and twist may affect other members attached to the member; hence the serviceability limit state of the members may be affected. In design the critical elastic moment for doubly symmetric beams is given by the formula (2.1a) as is provided in the steel design code:

$$M_{cr}= \frac{\omega_2\ \pi}{\mathrm{KL}}\sqrt{EI_yGJ+(\frac{\pi E}{KL})^2 I_y C_w}$$

… (2.1a)

Similarly, formula (2.1b) is the formula used to determine the critical elastic moment for monosymmetric sections as provided in the steel design code as well as the SASCH (2013).

$$M_{cr}= \frac{\omega_2\ \pi^2\ \mathrm{E}I_y\beta_x}{2(\mathrm{KL})^2}\{1+\sqrt{1+\frac{4}{{\beta_x}^2}[\frac{C_w}{I_y}+\frac{GJ(KL)^2}{\pi^2 EI_y}]}\}$$

… (2.1b)

Where:

E, youngs modulus

I_y, second moment of area about the y-axis

KL, effective length

β_x, coefficient of monosymmetry

C_w, warping torsional constant

G, shear modulus

J, St Venant torsional constant

ω_2, bending moments shape effects factor

The coefficient of monosymmetry (also known as the Wagner effect) is given by formula 2.1c (SASCH, 2013):

$$\beta_x = \{\frac{1}{I_x}[\int_A y(x^2+y^2)\,dA]\} - 2y_0$$

…(2.1c)

Where:

I_x, second moment of area about the x-axis

$x \text{ and } y$, cartesian coordinates of the infinitesimal area of dA

y_0, distance from shear centre to centre of gravity

The coefficient of monosymmetry is associated with the position of the shear centre in relation to the centre of gravity of the section and it affects the buckling resistance capacity of monosymmetric sections (Zhang, et al., 2017).

As mentioned earlier, laterally unsupported beams can buckle laterally and twist due to the critical loading of the internal moment. The way the load is applied to the member also plays a role in how the beam performs. Figure 2.4 shows the difference between a destabilising load and a stabilizing load.

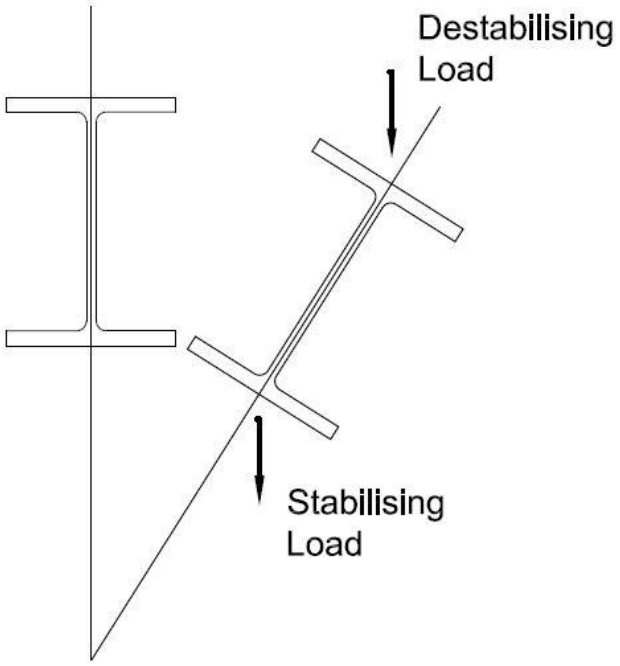

Figure 2.4: Destabilising and stabilising loads, *Adapted from Mahachi (2013)*

Assuming the loads shown in figure 2.4 are applied to a beam that is carrying sagging moments, hence the top flange is experiencing compression forces and the bottom flange, tension forces. If loads are applied on to the flange which is in compression due to the moment, this makes the twist worse (twist about the longitudinal axis) and hence the loads are termed as destabilizing. However, when the loads are applied to the flange which is experiencing tension forces due to the moments, the loads tend to correct the twist-action, hence termed as stabilising the beam.

2.4 Load application with regards to the Shear centre of a section

In addition to the above-mentioned phenomena that can cause the beam to twist under loading, there is another case that is also to be considered during design. This is the scenario of the load application with regards to the shear centre. The figures 2.5 and 2.6 show scenarios of beam twisting behaviour with respect to the point of application of a load from the shear centre.

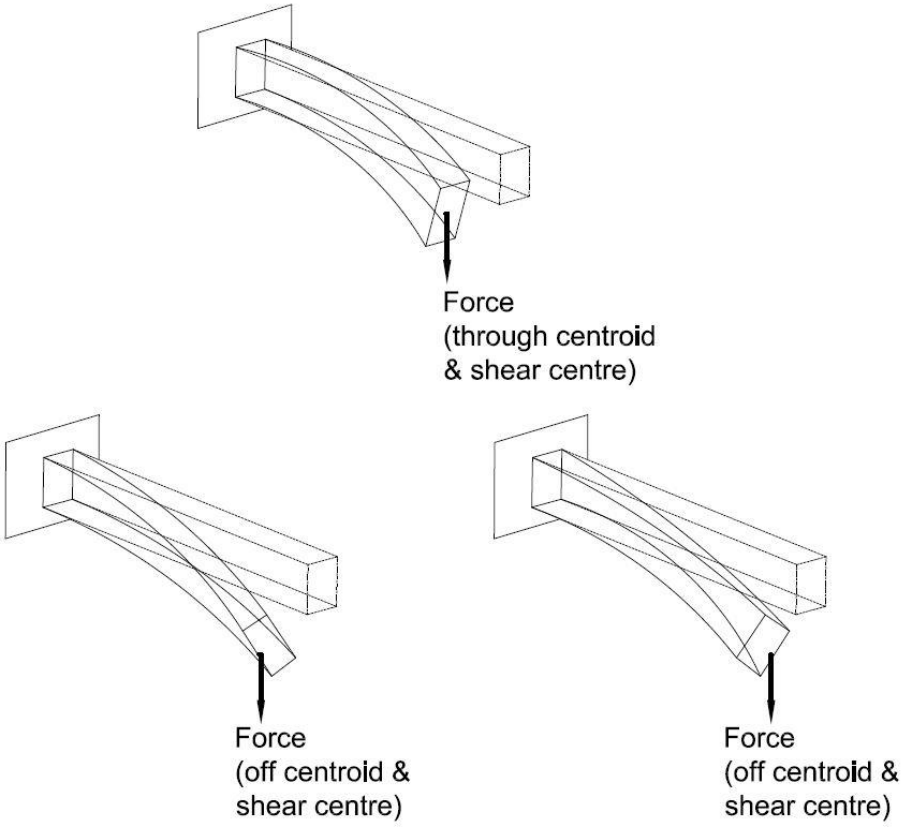

Figure 2.5: Load on the shear centre effect of a square section

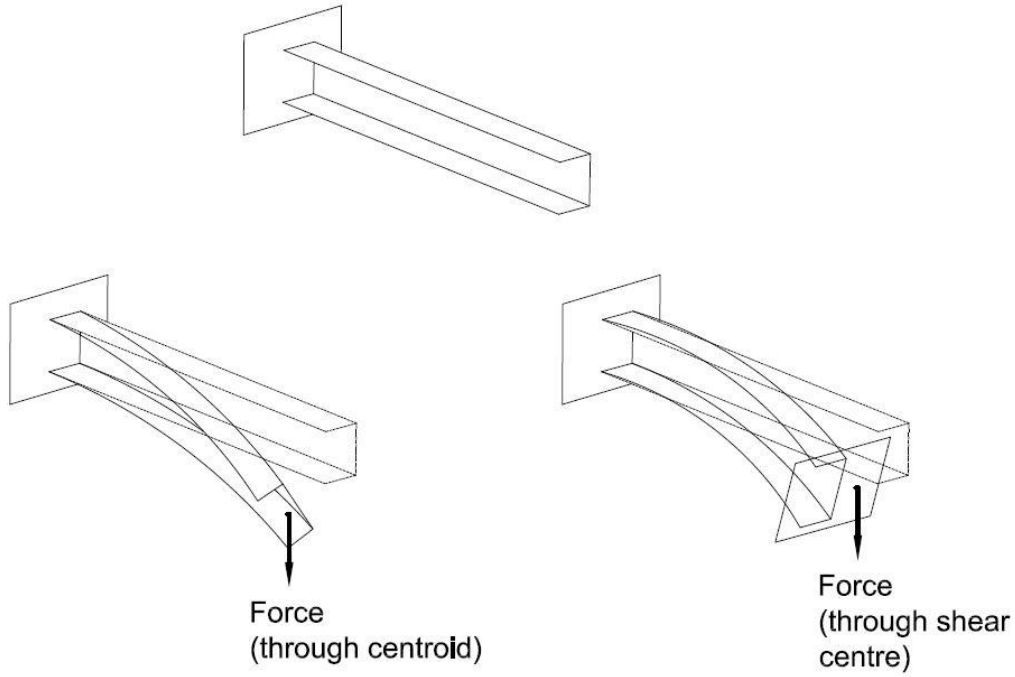

Figure 2.6: Load on the shear centre effect of a channel section

The square section has the centre of gravity and the shear centre coinciding at the same point. From figure 2.5 one can observe that application of the load at any position other than the shear centre, the beam tends to twist about the longitudinal length. In this case, the centroid and the shear centre happen to be in the same positions i.e. doubly symmetric.

For the channel section, the centroid and the shear centre are not in the same position. The first loaded case in figure 2.6 shows a load applied at the centroid position. This yields a twist of the section about the longitudinal axis together with sagging of the beam. However, when the load is applied at the shear centre position, the section does not twist about the longitudinal axis but only sags vertically.

Observing the behaviour of the load application with respect to the shear centre, it is eminent that the determination of the shear centre is crucial. It becomes important with regards to the stability of the structure and overall resistance capacity of the section to understand shear centre and know how to determine this section property.

When considering the resistance of monosymmetric sections the determination of their resistance is more complex compared to that of double symmetric sections. This is evident from equations 2.1a and 2.1b and is because of the Wagner effect. When a monosymmetric section twists during buckling the longitudinal bending stresses induce additional torque about the twisting axis and that the torque causes a change in the torsional stiffness of the member. The additional torque is a product of the major axis moment with a monosymmetric property termed as Wagner's coefficient (Morkhade & Gupta, 2013).

The norm is to have the upper flange of the monosymmetric section to be larger than the bottom flange as this offers better stability for simply support beams. The better

stability is offered by having the most material in the compression flange (upper flange) which tends to buckle furthest. Hence placing most of the material in that zone increases the beam stiffness, thus reducing the lateral-torsional buckling as compared to having the material the other way around (Trahair, 2011).

When a monosymmetric member is loaded the moment causes the internal forces to act about the shear centre creating torque (Wagner effect). The compression forces apply a torque in the one direction and the tension forces apply a torque in the other. Evidently, the force which has a greater lever arm (furthest from the shear centre) dominate the monosymmetric effect.

Morkhade & Gupta (2013) as well as, Yilmaz & Kirac (2016), state that the shear centre location is very important when it comes to monosymmetric sections lateral-torsional buckling resistance. Both papers indicate that monosymmetric sections are more economical when the larger flange is the one that carries the compression stresses and the smaller flange, the tension stresses, this once again agreeing with Trahair (2011). It was also shown that the resistance to buckling of monosymmetric beams are much higher when loads are applied below shear centre and lesser when applied above the shear centre for a beam carrying sagging moments (Yilmaz & Kirac, 2016).

In other words, the sections are more stable and twist less when the applied loads are below the shear centre.

2.5 Shear centre of a section

As discussed previously it is important to determine the position of the shear centre for consideration in the designing process with regards to stability.

The shear centre is the point in the cross-section of a member through which forces must be applied to avoid any twisting (Jennings, 2004). Some literature mention that the shear centre is the intersection of the longitudinal axis of a member with the line of action of a transverse load or transverse loads. It is the point through which the resultant shear forces act.

Chan & Syed (2009), have stated that:

> *The centroid is defined as the location where an axial load does not cause a change in curvature and a bending moment does not produce axial strain. Similarly, shear forces acting at the shear centre do not cause twist. In other words, the load acting at the centroid decouples the structural response between axial extension and bending, whereas, shear centre decouples bending and twisting, mechanisms of a beam.*

Geometric properties such as the centroid and shear centre of members depend on the geometry of the section for isotropic material (Chan & Syed, 2009).

Different sections due to their differences in geometry, yield shear centres in different positions. I and H-section will have their shear centres coinciding with their centroidal axes. Channels, on the other hand have their shear centre at an offset from the centroidal axis along the x-axis. All these differences are a result of their unique geometries.

Figure 2.7 shows a few common sections that have shear centres coinciding with the centroids of the sections. These are I/H-sections, rectangular hollow sections, circular hollow sections and Z-sections.

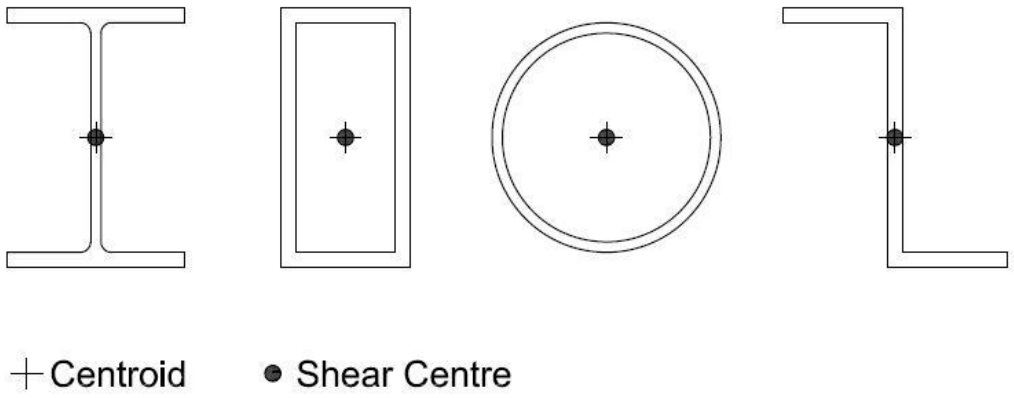

Figure 2.7: Shear centres of sections that coincide with the centroid

There is also another set of sections that provide a known position of the shear centre due to their geometry. These are the sections that have two elements meeting at a position. The intersection point of these sections ends up being their shear centres. It may however also be mentioned that the shear centre of these sections never coincides with the sections centre of gravity or centroid. Figure 2.10 shows examples of these types of sections, the angle and Tee sections.

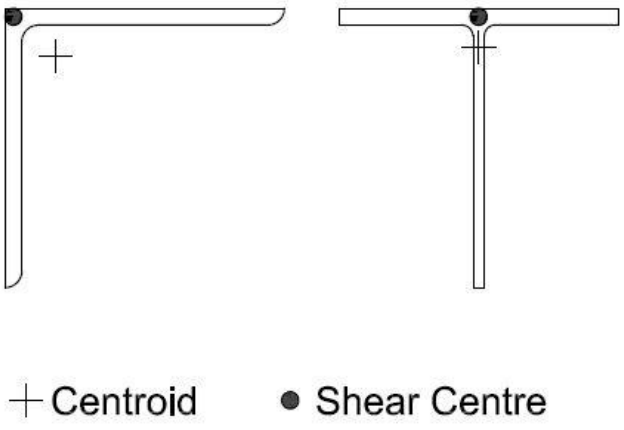

Figure 2.8: Shear centres of sections that coincide with element intersection

Not all the sections have shear centres that are as obvious as previously described in Figure 2.7 and 2.8. There are some sections such as the channel section with shear centres that do not coincide with the centroid of the section. Nor does it coincide with any of the elements of the section. Figure 2.9 shows a channel section with its centroid as well as the shear centre position indicated.

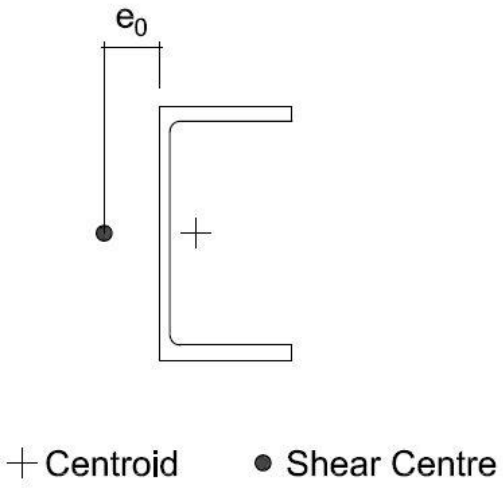

Figure 2.9: Shear centre and the centroid of a channel section

Sections such as the channel, require that the shear centres, as well as the centroids, are determined by means of calculations rather than by observation as with sections portrayed in Figures 2.7 and 2.8. The positions of this parameter are not always obvious due to the section's geometry.

The determination of the shear centre becomes a matter that must be addressed. As previously discussed, the shear centre determination is of importance for load application and the stability of the structure. Knowing how to apply a load to optimize the resistance capacity of the section is immensely beneficial as this will result in more economical designs.

CHAPTER 3: APPROACHES FOR THE DETERMINATION OF THE SHEAR CENTRE

3.1 Shear centre determination

To determine the shear centre of a section, there are different methods that can be employed. The two commonly used methods are:

- The determination of shear centre by means of shear flow
- The determination of shear centre by means of the sectorial coordinate approach

The shear flow method will be introduced; however, this approach will not be addressed in detail. The sectorial coordinate approach will also be introduced and dealt with in more detail as this is the method that will be employed in determining the shear centres in this study.

3.2 Shear flow method

To be able to find the shear centre of a section by employing the shear flow method one must first understand the shear stress, its distribution, the shear flow and forces generated as a result.

When a force is applied, internal shear forces are generated to counteract the applied force. The position where an external force may be applied such that the internally generated forces cancel out the external force is known as the shear centre.

The shear stress can be understood from the derivation of the shear stress equation. Figure 3.1 is used for the derivation of the shear stress equation.

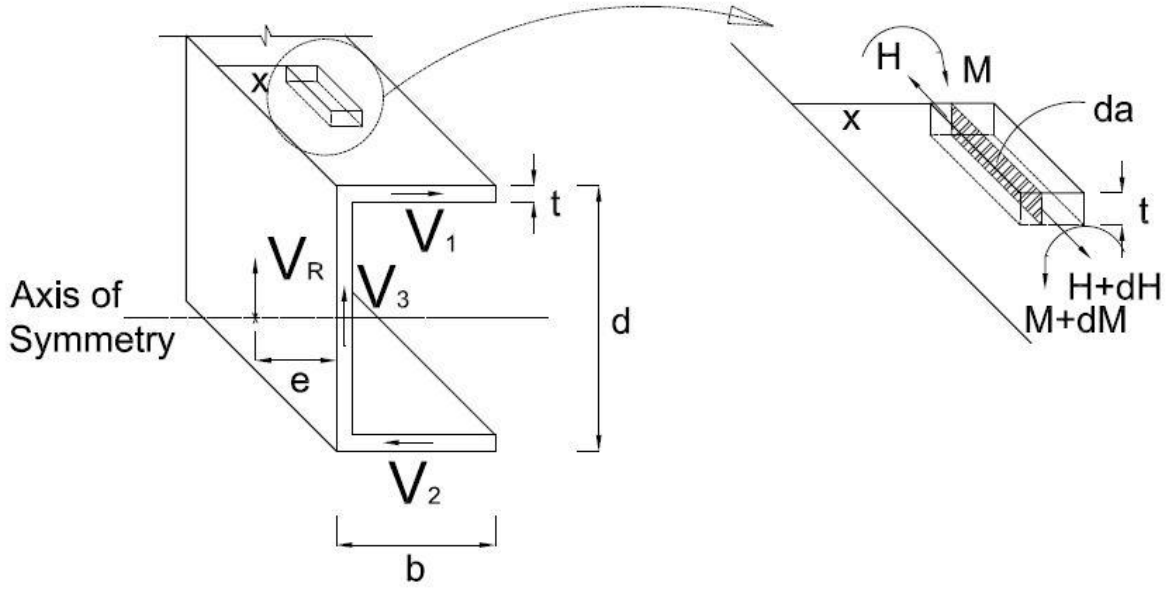

Figure 3.1: Shear stress equation derivation

To find the shear stress in the flange

$$H = \int \left(\frac{M}{I}\right) y \, da \qquad \ldots(3.1)$$

$$H+dH = \int \left(\frac{M+dM}{I}\right) y \, da \qquad \ldots(3.2)$$

dH, unbalanced longitudinal force = equation (3.2) – equation (3.1)

thus, $dH = \int \left(\frac{dM}{I}\right) y \, da$ …(3.3)

For equilibrium, this unbalanced force should be equal to the shear

$$\tau (t \, dz) = \frac{dM}{I} \int_x^b y \, da$$

$$\tau = \frac{dM}{dz} \frac{1}{It} \int_x^b y \, da \quad \text{... note that} \quad V = \frac{dM}{dz} \quad \text{which is the shear force}$$

Thus,

$$\tau = \frac{\mathbf{VQ}}{It} \qquad \ldots(3.4)$$

where, $Q = \int y \, da$

The equation (3.4) provides the shear stress in the section at any position (governed by **y**) due to the shear load, V (kN).

Using equation (3.4), a shear stress distribution diagram can be determined and drawn for each element of the section. Knowing the following:

$\text{Force} = \text{Stress x Area}$ we can conclude that in each element the force is the summation of the products of the stress and area,

$$Vi = \int \tau \, da = \int_{xi}^{xj} \frac{Vay}{It} \, dx \qquad \ldots(3.5)$$

Literature states that shear flows from the tension side of the moment stress distribution to the compression side. Figure 3.2 shows a schematic of the flow of shear stresses.

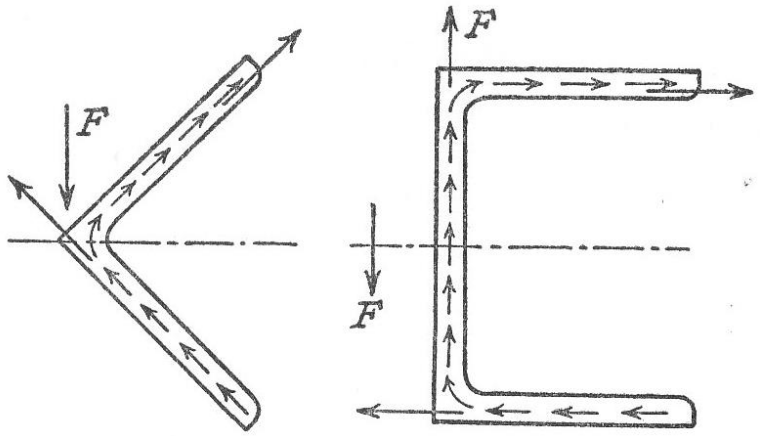

Figure 3.2: Shear stress flow (angle and channel sections in sag moment)

The shear flow shown in Figure 3.2 is for a member experiencing a sagging moment. Hence, the shear flows from the bottom elements that will be in tension to the upper elements that will be in compression as per Jennings (2004). From the stresses, equation (3.5) will be employed to determine the forces in each element as shown in Figure 3.3. Force F, in Figure 3.3 represents an applied shear force. With moments taken about the longitudinal axis at the centre of the vertical force F_3 (V_3), the eccentricity, e, at which the forces will be balancing out will be the offset of the shear centre.

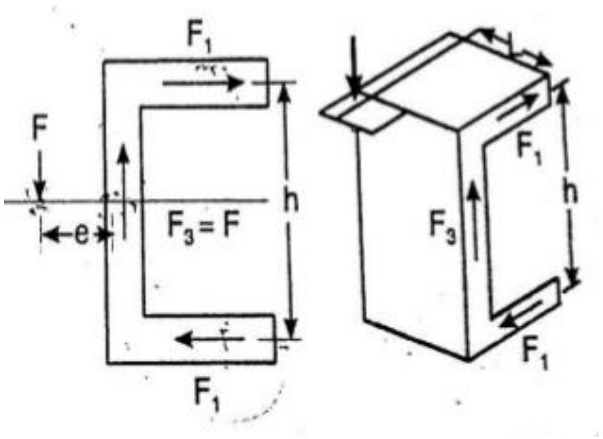

Figure 3.3: Shear forces in channel elements

With the above mentioned, the following formula is applicable:

$$Vr\,(e) = V_1 \frac{h}{2} + V_2 \frac{h}{2} \qquad \ldots(3.6)$$

$$Fr\,(e) = F_1 \frac{h}{2} + F_2 \frac{h}{2}$$

Using the above formulae, the eccentricity about the x-axis and y-axis can be determined which in turn is the shear centre position.

3.3 Sectorial coordinate approach

The sectorial coordinate approach can be used as an alternative in determining the shear centre of a section. This method is not restricted by geometry and is used to solve the properties of any arbitrary thin-walled section as shown in figure 3.4.

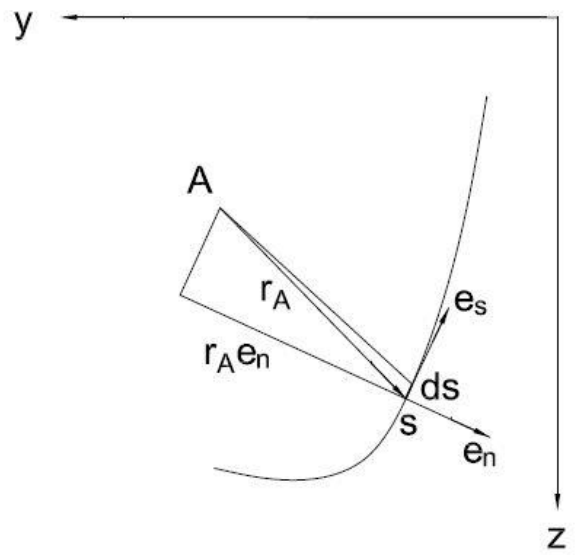

Figure 3.4: Arbitrary thin walled section, *Adopted from Pilkey & Kitis (1996)*

The sectorial coordinates that are derived from the thin-walled section are employed to determine unique sectorial properties of the section. These properties are the shear centre coordinates (position), as well as the warping constant of the section. This study will however not determine warping constants of sections. The warping constant of a section is calculated from the shear centre position of the section and is thus obtained after having determined the shear centre. These are important properties that must be attained in addition to the geometrical and flexural properties of any section such as, i.e. Area (A), Moments of Area about the axes (I_x, I_y, I_{xy}) and radius of gyration, r.

Referring to figure 3.4, the sectorial area of the thin-walled section about an arbitrary point is determined by multiplying the tangential distance and the segment considered from an arbitrary point. This is done in increments along the segment and then summed up.

Mathematically the double sectorial area is as stated by equation 3.7 (Pilkey & Kitis, 1996):

$$d\omega_A = \pm r_A(s)e_n(s)ds \qquad \text{(about } A\text{)} \qquad \ldots(3.7)$$

When we now want to consider the double sectorial area of the element from point S_o to S, we sum up all the little sectorial areas along the path of interest. This can be mathematically shown as follows:

$$\omega_A(s) = \int_{So}^{S} d\omega_A = \int_{So}^{S} r_A(s)e_n(s)ds \qquad \ldots(3.8)$$

Equation (3.8) yields the warping function for an element. Each element in a section may have a unique warping function depending on the geometry and the location/position of the arbitrary point. Also depending on the direction of the tangent vector, e_s, about the pivot point, the function may be positive for an anti-clockwise direction and negative for a clockwise direction. This is very important to note.

When poles *A* and *B* are at different positions but origins S_o and S_1 are the same, we can transform the warping function of *B* to *A* as follows:

$$\omega_A(s) = \omega_B(s) + (z_A - z_B)(y(s) - yo) - (y_A - y_B)(z(s) - zo) \qquad \ldots(3.9)$$

This expression can is expressed graphically as shown in figure 3.5.

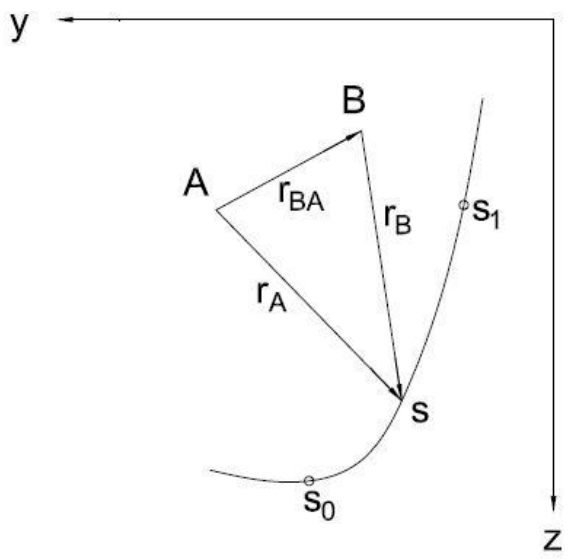

Figure 3.5: Arbitrary thin-walled section, *Adopted from Pilkey & Kitis (1996)*

Note that the shape of the sectorial area diagram for A will not be the same as for B when you draw it out graphically for the same section.

According to Pilkey & Kitis (1996), the integral of a warping function yields the first sectorial moment. This is also known as the sectorial static moment (Shama, 1974). The mathematical expression for it is:

$$Q\omega = \int_{A0}^{A} \omega(s)\, da \qquad \ldots(3.10)$$

This moment provides the direction of the principal radius i.e. the location of the principal pole according to Shama (1974).

A summation of the products of the sectorial areas with the segment distances about a certain axis yields the sectorial products of area, expressed mathematically by Pilkey [5] as:

$$I_{y\omega} = \int_{A0}^{A} y(s)\omega(s)\, da \qquad \ldots(3.11a)$$

$$I_{z\omega} = \int_{A0}^{A} z(s)\omega(s)\, da \qquad \ldots(3.11b)$$

Note that a transformation similar to that of the warping functions can also be done on the sectorial product of area. This provides the following:

$$I_{y\omega A} = I_{y\omega B} + (z_A - z_B)I_z - (y_A - y_B)I_{yz} \qquad \ldots(3.12a)$$

$$I_{z\omega A} = I_{z\omega B} + (z_A - z_B)I_{yz} - (y_A - y_B)I_y \qquad \ldots(3.12b)$$

The derivation of equations (3.9-12) are as per literature of Pilkey & Kitis (1996). This thesis only focuses on the usage of these equations.

According to Pilkey & Kitis (1996), the pole which causes both sectorial products of areas to be zero is called the principal pole. Meaning, for A to be a principle pole, $I_{y\omega A} = I_{z\omega A} = 0$.

Hence the coordinates for the pole may be solved by the following equations:

$$y_A = y_B + [(I_{z\omega B} I_z - I_{y\omega B} I_{yz}) / (I_y I_z - I_{yz}^2)] \quad \ldots(3.13a)$$

$$z_A = z_B + [(I_{z\omega B} I_{yz} - I_{z\omega B} I_y) / (I_y I_z - I_{yz}^2)] \quad \ldots(3.13b)$$

If the centroid is used as the pole for determining *A*, then $I_{xy} = 0$, thus

$$y_A = y_B + (I_{z\omega B}) / (I_y) \quad \ldots(3.14a)$$

$$z_A = z_B - (I_{y\omega B}) / (I_z) \quad \ldots(3.14b)$$

Thus equations (3.14a) and (3.14b) provide us with the values of the shear centre location.

Now it is important to note that the above-mentioned formulae from Pilkey & Kitis (1996) are derived using the following coordinate system:

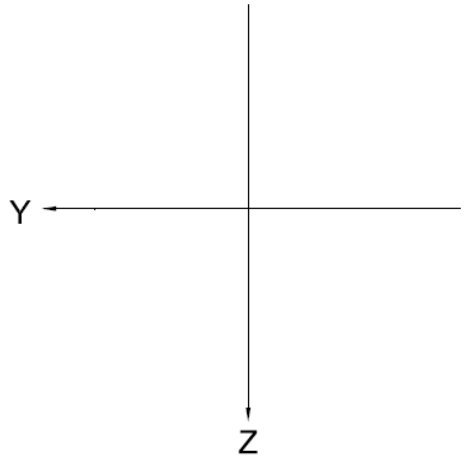

Figure 3.6: Pilkey coordinate system used

For the non-standard monosymmetric section the derivations of the functions and calculations in this thesis, the coordinate system which will be used is as shown in figure 3.7.

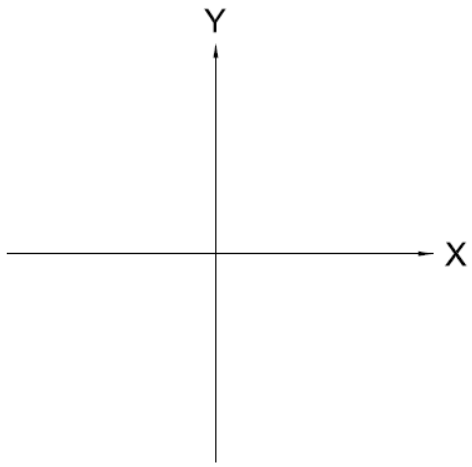

Figure 3.7: Thesis coordinate system used

The coordinate system used in this study is as that employed by Shama (1974). Hence the equations 3.9 to 3.14 changes to equations 3.15 to 3.20 as follows,

Warping functions:

$$\omega_A(s) = \int_{So}^{S} d\omega_A = \int_{So}^{S} r_A(s)e_n(s)ds \quad \ldots(3.8)$$

$$\omega_A(s) = \omega_B(s) + (y_A-y_B)(x(s)-x_o) - (x_A-x_B)(y(s)-y_o) \quad \ldots(3.15)$$

First sectorial moment:

$$Q\omega = \int_{A0}^{A} \omega(s)\, da \quad \ldots(3.16)$$

Sectorial product of area:

$$I_{x\omega} = \int_{A0}^{A} x(s)\omega(s)\, da \quad \ldots(3.17a)$$

$$I_{y\omega} = \int_{A0}^{A} y(s)\omega(s)\, da \quad \ldots(3.17b)$$

$$I_{x\omega A} = I_{x\omega B} + (y_A-y_B)I_y - (x_A-x_B)I_{xy} \quad \ldots(3.18a)$$

$$I_{y\omega A} = I_{y\omega B} + (y_A-y_B)I_{xy} - (x_A-x_B)I_x \quad \ldots(3.18b)$$

Coordinates of a principle pole, A, $I_{x\omega A} = I_{y\omega A} = 0$. thus:

$$x_A = x_B - [(I_{y\omega B}\, I_y - I_{x\omega B}\, I_{xy}) / (I_x\, I_y - I_{xy}^2)] \quad \ldots(3.19a)$$

$$y_A = y_B + [(I_{y\omega B}\, I_{xy} - I_{x\omega B}\, I_x) / (I_x\, I_y - I_{xy}^2)] \quad \ldots(3.19b)$$

If the centroid is used as the pole for determining *A*, then $I_{xy} = 0$, thus:

$$x_A = x_B - (I_{y\omega B}) / (I_x) \quad \ldots(3.20a)$$

$$y_A = y_B - (I_{x\omega B}) / (I_y) \quad \ldots(3.20b)$$

The formulae (3.8) and (3.15 to 3.20b) are the formulae employed in this thesis to determine the shear centres.

3.4 Shear Centre Determination in Prokon

The Prokon Software used in this thesis for verification of the shear centres uses numerical solutions to determine the section properties. As per provided content in the help function of ProSec in Prokon, the calculations in the program are based on a Finite Difference method which is a numerical technique that solves differential equations by means of approximating derivatives with finite differences.

The program recognises polygons and distinct circles to formulate the equations, hence sections of different multiple shapes can be formulated. In solving for the shear centres, the content in the section, Section Analysis, states that:

> *The shear stress distributions in the Y and X-directions are determined for a unit load applied in the Y-direction. The shear centre is then calculated by considering the moment of the shear stresses about the centre of mass.*

Thus, from the above-mentioned statement, one can observe that the Prokon Software uses the shear flow method to determine these properties. This method is as discussed in section 3.2 of this Chapter.

CHAPTER 4: SECTORIAL COORDINATE APPROACH PROCEDURE USED FOR CALCULATION

4.1 Simple Channel Example

To explain the procedures used, a simple channel section with known results was employed. The sections dimensions were named, b for the heights as well as the breadth and t for thickness, see figure 4.1. The section had the following properties as per [7]:

$I_y = 1/3\ b^3\ t$

$I_x = 7/12\ b^3\ t$

The centroid of the section was as shown at C in figure 4.1.

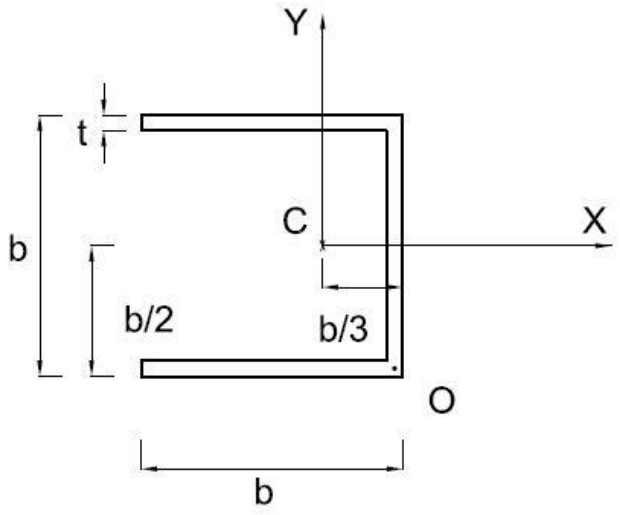

Figure 4.1: Channels dimensions

To determine the warping functions a pole "O" at the bottom right-hand corner of the section was chosen. Note that this pole could have been at any position, however, choosing a position resulting in fewer calculations was ideal. Using point "O" as the pole, the tangential ($\mathbf{s}_{\#}$) and normal ($\mathbf{n}_{\#}$) components of displacement for each element were obtained, see figure 4.2. Moving from the pole along the elements being considered following a path to the end of the elements, the components of displacement were obtained using the right-hand rule.

The right-hand rule states: *Following the path of the elements with your right-hand palm facing upward, the pointing finger assigns the tangential component while the thumb gives the normal component of the displacement*.

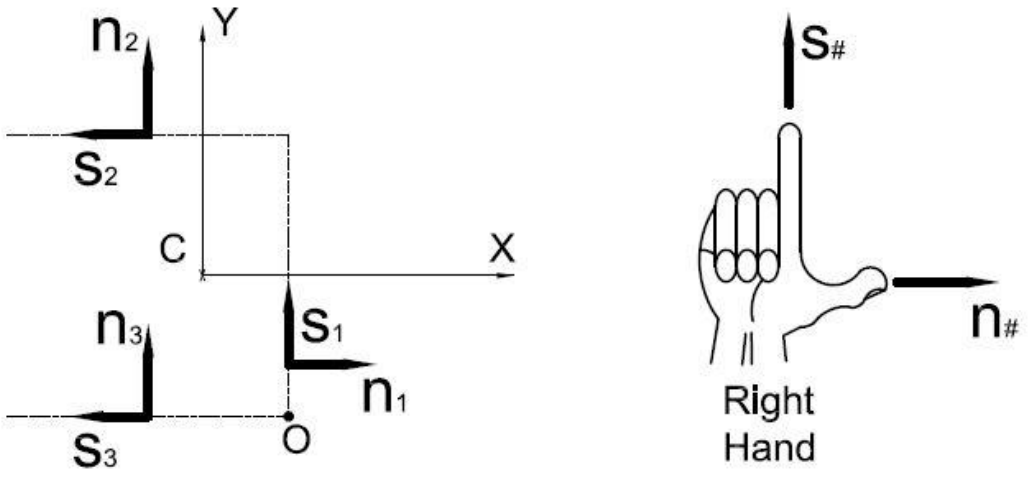

Figure 4.2: Channels Tangential and normal components of displacement

The warping functions for the three elements (1-3) were determined as follows:

$\omega_o(s_1) = \int_{So}^{S} d\omega_o = 0$

$\omega_o(s_2) = \int_{So}^{S} d\omega_o = b\ s_2$ (anticlockwise = +)

$\omega_o(s_3) = \int_{So}^{S} d\omega_o = 0$

Note that $\omega_o(s_2)$ was positive because it rotated counter clockwise about "O" respectively. On the other hand, the other two functions were zero because the tangential components ran through the pole and hence did not have a perpendicular distance through which they were acting. As for $\omega_o(s_2)$, the perpendicular distance through which S_2 was acting was the height of the section, b.

Once the warping functions were determined, the sectorial product areas were then determined.

The y and x coordinates that were used in each calculation of the sectorial product areas were distances from the Centroid "C" to the element that was being considered. Also, dA was taken as the appropriate tds. Note that the perpendicular distance function for s_2 along the y-axis from the centroid was a constant function equal to half the breadth. Thus y = b/2 for s_2 from s_0 to s.

$$I_{y\omega o} = \int y_{\omega o}\, dA = \int_0^b \left(\frac{b}{2}\right)(bs_2)\, tds = \left(\frac{b^2 t}{2}\right)\left[\frac{s^2}{2}\right]_b = \frac{b^4 t}{4}$$

On the other hand, the perpendicular distance function for s_2 along the x-axis from the centroid was a varying function equal to $(b/3 - s_2)$. This means that the function for s_2 along the axis started at a position b/3 and we would be subtracting the distance covered by s_2. The subtraction is a result of the s_2 vector which increased in the negative direction along the x-axis.

Thus, $x = (b/3 – s_2)$ leading to the sectorial product area about the x-axis being:

$$I_{x\omega o} = \int x_{\omega o}\, dA = \int_0^b \left(\frac{b}{3} - s_2\right)(bs_2)\, tds$$

$$= -\int_0^b bts^2 ds + \int_0^b \frac{b^2 ts}{3} ds$$

$$= (bt)\left[\frac{s^3}{3}\right]^b + \left(\frac{b^2 t}{3}\right)\left[\frac{s^2}{2}\right]^b = \frac{-b^4 t}{3} + \frac{b^4 t}{6} = \frac{-b^4 t}{6}$$

Knowing that:

$$x_A = x_o - [(I_{y\omega o} I_y - I_{x\omega o} I_{xy}) / (I_x I_y - I_{xy}^2)]$$

$$y_A = y_o + [(I_{y\omega o} I_{xy} - I_{x\omega o} I_x) / (I_x I_y - I_{xy}^2)]$$

Additionally, since the centroid was used as the pole for determining *A* therefore Ixy = 0, hence:

$$x_A = x_o - (I_{y\omega o}) / (I_x)$$

$$x_A = \frac{b}{3} - \left[\frac{\left(\frac{-b^4 t}{4}\right)}{\frac{7b^3 t}{12}}\right] = \frac{b}{3} + \frac{3b}{7} = \frac{16b}{21}$$

$$y_A = y_o - (I_{x\omega o}) / (I_y)$$

$$y_A = \frac{-b}{2} - \left[\frac{\left(\frac{-b^4 t}{6}\right)}{\frac{b^3 t}{3}}\right] = -\frac{b}{2} + \frac{b}{2} = 0$$

The results obtained were equivalent to those given in the literature reviewed, therefore it is safe to say that the approach used was accurate and can be proven. This is a simple example of a channel section illustrated on how the sectorial area method could be used to determine shear centres of sections. This approach was used for the non-standard monosymmetric section.

CHAPTER 5: MONOSYMMETRIC SECTION OF AN I OR H-SECTION WITH UPSTAND PLATES SHEAR CENTRE DEMONSTRATION

5.1 Formulae derivation for I or H-Sections with upstand plates

To create a non-standard monosymmetric section, a standard doubly symmetric H-section was used. Upstand plates were welded on the ends of the upper flanges to create the section of interest. The section studied was as shown in figure 5.1.

The desire was to compare the variation of the shear centre with that of the centroid as we changed the upstand heights. Thus, the plate height parameter 'α' in figure 5.1 was treated as the parameter that would vary.

The weld geometry at the positions where the flanges met the web was not considered. It was assumed that the elements met at right angles. This was to simplify the calculations considering that the areas of the chamfers in comparison to the entire cross-section would be negligible, hence it was ignored. The plate elements were numbered 1 to 4 with the bottom flange being 1, the web 2, top flange 3 and the two upstanding plates 4.

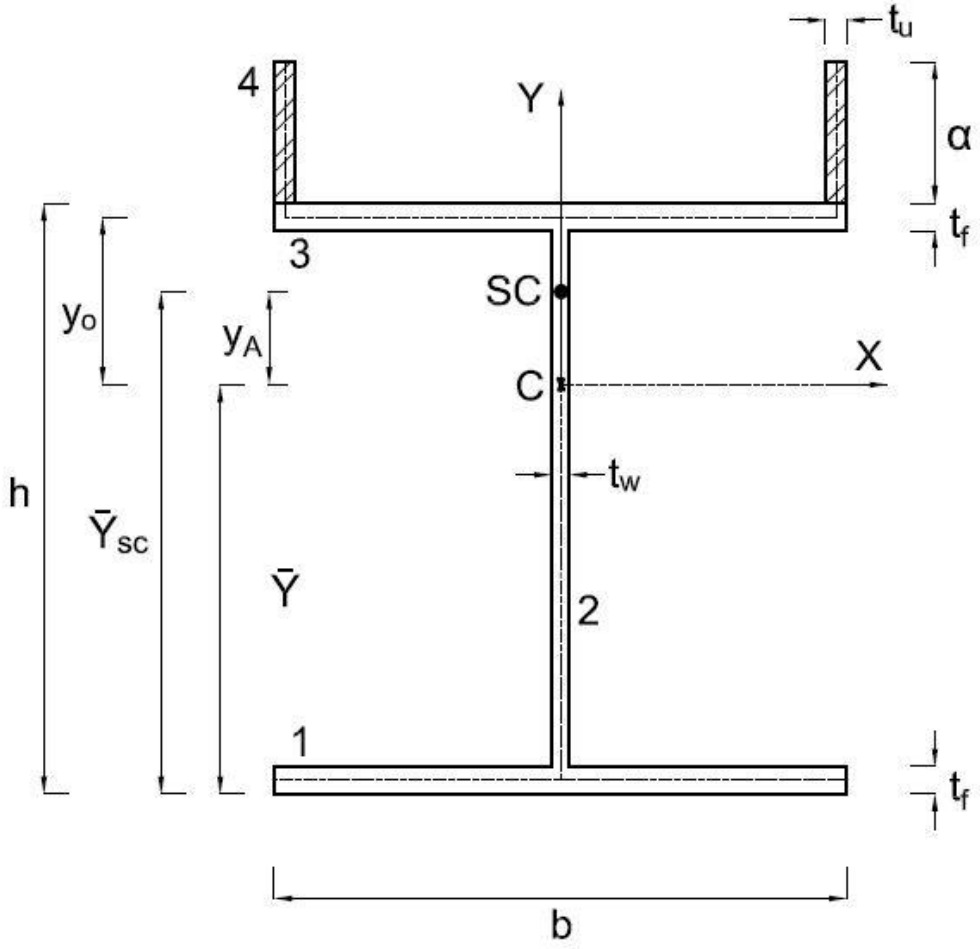

Figure 5.1: Mono-symmetric I or H section dimensions

The sections properties were as follows:

h = height of section

b = breadth of section

t_f = thickness of the flange

t_w = thickness of the web

α = height of upstand plate

t_u = thickness of upstand plate

$\bar{y}$ = the first moment of area about the y-axis

$\bar{x}$ = first moment of area about the x-axis

$\bar{y}_{sc}$ = distance from the bottom of the section to shear centre

X = x-axis

Y = y-axis

C = centroid, the centre of gravity

SC = shear centre

The formulae were derived in the following order: centroids, second moments of area, warping functions, sectorial product areas, shear centre and shear centre distances from the bottom of the section. All the formulae were derived in four parts being, (1) the bottom flanges, (2) web, (3) top flanges and (4) the upstanding plates.

Centroid:

In deriving the formulae for the centroid, the standard formula for determining first moments of area was utilized.

$\bar{x} = 0$

Due to the symmetry of the section.

$$\bar{y} = \sum_{0}^{n} \frac{A_i\, y_i}{A_i}$$

$$\bar{y} = \frac{\left\{\left[(b\ t_f)\left(\frac{t_f}{2}\right)\right] + \left[\left((h\text{-}2t_f)t_w\right)\left(\left(\frac{h\text{-}2t_f}{2}\right)+t_f\right)\right] + \left[(b\ t_f)\left(h\text{-}\frac{t_f}{2}\right)\right] + 2\left[(\alpha\ t_u)\left(h+\frac{\alpha}{2}\right)\right]\right\}}{\{[(b\ t_f)]+[(h\text{-}2t_f)t_w]+[(b\ t_f)]+[2(\alpha\ t_u)]\}}$$

The second moment of area:

The second moment of area formula was used, and the shift of the areas was also considered for each of the elements. The shift is denoted as C in the formula below and A is the area of the element in question.

$$I = \frac{b\,d^3}{12} + AC^2$$

$$I_{x1} = \left(\frac{b\,t_f^3}{12}\right) + \left[(b\,t_f)\left(\bar{y} - \frac{t_f}{2}\right)^2\right]$$

$$I_{x2} = \left(\frac{t_w(h-2t_f)^3}{12}\right) + \left[(t_w(h-2t_f))\left(\bar{y} - \left(\frac{h-2t_f}{2}\right) + t_f\right)^2\right]$$

$$I_{x3} = \left(\frac{b\,t_f^3}{12}\right) + \left[(b\,t_f)\left((h - \left(\frac{t_f}{2}\right)) - \bar{y}\right)^2\right]$$

$$I_{x4} = 2\left\{\left(\frac{t_u\,\alpha^3}{12}\right) + \left[(\alpha\,t_u)\left((h-\bar{y}) + (\alpha/2)\right)^2\right]\right\}$$

$$I_x = I_{x1} + I_{x2} + I_{x3} + I_{x4}$$

$$I_{y1} = \left(\frac{t_f\ b^3}{12}\right)$$

$$I_{y2} = \left(\frac{(h-2t_f)t_w^3}{12}\right)$$

$$I_{y3} = \left(\frac{t_f\ b^3}{12}\right)$$

$$I_{y4} = 2\left\{\left(\frac{\alpha\,t_u^3}{12}\right) + \left[(\alpha\,t_u\ )\left(\frac{b}{2} - \frac{t_u}{2}\right)^2\right]\right\}$$

$$I_y = I_{y1} + I_{y2} + I_{y3} + I_{y4}$$

Warping functions:

To determine the warping functions, the tangential and normal components of displacement for the different elements were drawn about a pole “O”. this pole was at the centre of the top flanges. Figure 5.2 shows the pole “O” and the different components of displacements drawn using the right-hand rule.

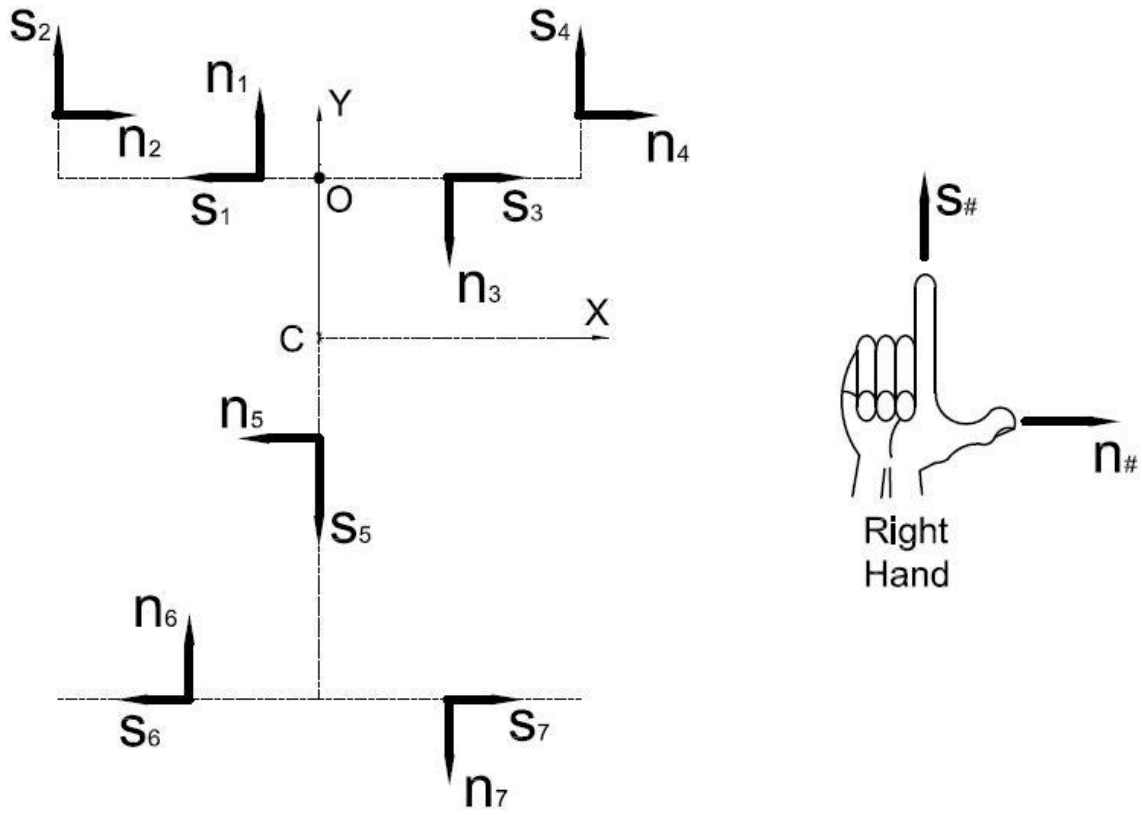

Figure 5.2: Mono-symmetric section Tangential and normal components of displacement

Having chosen “O” as the pole, meant that the warping functions s_1, s_3 and s_5 were zero as the tangential components ran through the pole. Another important point was that the tangential components are acting along the centre lines of the different elements. Hence, the perpendicular distance for s_2 was half the flange width minus half the upstand plate thickness. This was a similar approach to s_4. For s_6 and s_7 the perpendicular distance between the top and bottom flanges centre lines were given by the height of the section minus the thickness of the flanges. Meaning, half the thickness of the top flange plus half the thickness of the bottom flange was taken away from the height of the section, the flanges end-to-end.

Vectors are taken about the pole “O”.

$$\omega_o(s_1) = \int_{So}^{S} d\omega_o = 0$$

$$\omega_o(s_2) = \int_{So}^{S} d\omega_o = -\left(\frac{b}{2} - \frac{t_u}{2}\right) s_2 = \frac{t_u}{2} s_2 - \frac{b}{2} s_2$$

(clockwise = -)

$$\omega_o(s_3) = \int_{So}^{S} d\omega_o = 0$$

$$\omega_o(s_4) = \int_{So}^{S} d\omega_o = \left(\frac{b}{2} - \frac{t_u}{2}\right) s_4 = \frac{b}{2} s_4 - \frac{t_u}{2} s_4$$

(anticlockwise = +)

$$\omega_o(s_5) = \int_{So}^{S} d\omega_o = 0$$

$$\omega_o(s_6) = \int_{So}^{S} d\omega_o = -(h-t_f)s_6 = t_f\ s_6 - h\ s_6$$

(clockwise = -)

$$\omega_o(s_7) = \int_{So}^{S} d\omega_o = (h-t_f)s_7 = h\ s_7 - t_f\ s_7$$

(anticlockwise = +)

Sectorial product areas:

The x & y values were taken from centroid "C" to the elements being studied. The perpendicular distances functions along the y-axis and x-axis were not constant functions. They were varying functions and the first parameters in the warping functions. Also, the direction (start to the end of a vector) in which the vector s was pointed played a role.

$$I_{y\omega o} = \int_{So}^{S} y\omega_o\, dA$$

Let,

$$A = h - \bar{y}$$

$$I_{y\omega o2} = \int_{So}^{S} y\omega_{o2}\, dA$$

$$= \int_0^{\alpha} ((h-\bar{y})+s_2)\left(\left(\frac{t_u}{2}\ s_2\right) - \left(\frac{b}{2}\ s_2\right)\right) t_u\, ds$$

$$= \int_0^{\alpha} (A+s_2)\left(\left(\frac{t_u}{2}\ s_2\right) - \left(\frac{b}{2}\ s_2\right)\right) t_u\, ds$$

$$= \int_0^{\alpha} \left(\frac{At_u}{2} s_2\right) t_u\, ds - \int_0^{\alpha} \left(\frac{Ab}{2} s_2\right) t_u\, ds + \int_0^{\alpha} \left(\frac{t_u}{2} s_2^2\right) t_u\, ds - \int_0^{\alpha} \left(\frac{b}{2} s_2^2\right) t_u\, ds$$

$$= \frac{A\ t_u^2}{2}\left[\frac{s^2}{2}\right]^{\alpha} - \frac{A\ b\ t_u}{2}\left[\frac{s^2}{2}\right]^{\alpha} + \frac{t_u^2}{2}\left[\frac{s^3}{3}\right]^{\alpha} - \frac{b t_u}{2}\left[\frac{s^3}{3}\right]^{\alpha}$$

$$I_{y\omega o2} = \frac{A\ t_u^2}{4}\alpha^2 - \frac{A\ b\ t_u}{4}\alpha^2 + \frac{t_u^2}{6}\alpha^3 - \frac{b\ t_u}{6}\alpha^3$$

$$I_{y\omega o4} = \int_{So}^{S} y\omega_{o4}\, dA$$

$$= \int_0^{\alpha} (A + s_4)\left(\left(\frac{b}{2}\, s_4\right) - \left(\frac{t_u}{2} s_4\right)\right) t_u\, ds$$

$$= \int_0^{\alpha} \left(\frac{Ab}{2} s_4\right) t_u\, ds - \int_0^{\alpha} \left(\frac{At_u}{2} s_4\right) t_u\, ds + \int_0^{\alpha} \left(\frac{b}{2} s_4^{\,2}\right) t_u\, ds - \int_0^{\alpha} \left(\frac{t_u}{2} s_4^{\,2}\right) t_u\, ds$$

$$= \frac{A\, b\, t_u}{2}\left[\frac{s^2}{2}\right]^{\alpha} - \frac{A\, t_u^2}{2}\left[\frac{s^2}{2}\right]^{\alpha} + \frac{bt_u}{2}\left[\frac{s^3}{3}\right]^{\alpha} - \frac{t_u^2}{2}\left[\frac{s^3}{3}\right]^{\alpha}$$

$$I_{y\omega o4} = \frac{A\, b\, t_u}{4}\alpha^2 - \frac{A\, t_u^2}{4}\alpha^2 + \frac{b\, t_u}{6}\alpha^3 - \frac{t_u^2}{6}\alpha^3$$

Let,

$$B = \bar{y} - \frac{t_f}{2}$$

$$I_{y\omega o6} = \int_{So}^{S} y\omega_{o6}\, dA$$

$$= \int_0^{b/2} (-B)\left((t_f\, s_6) - (h\, s_6)\right) t_f\, ds$$

$$= \int_0^{b/2} (B\, h\, s_6) t_f\, ds - \int_0^{b/2} (B\, t_f\, s_6) t_f\, ds$$

$$= B\, h\, t_f \left[\frac{s^2}{2}\right]^{b'^2} - B\, t_f^2 \left[\frac{s^2}{2}\right]^{b'^2}$$

$$I_{y\omega o6} = \frac{B\, h\, t_f}{8} b^2 - \frac{B\, t_f^2}{8} b^2$$

$$I_{y\omega o7} = \int_{So}^{S} y\omega_{o7}\, dA$$

$$= \int_0^{b/2} (-B)\left((h\, s_7) - (t_f\, s_7)\right) t_f\, ds$$

$$= \int_0^{b/2} (B\, t_f\, s_7) t_f\, ds - \int_0^{b/2} (B\, h\, s_7) t_f\, ds$$

$$= B\, t_f^2 \left[\frac{s^2}{2}\right]^{b'^2} - B\, h\, t_f \left[\frac{s^2}{2}\right]^{b'^2}$$

$$I_{y\omega o7} = \frac{B\, t_f^2}{8} b^2 - \frac{B\, h\, t_f}{8} b^2$$

$$I_{y\omega o} = I_{y\omega o2} + I_{y\omega o4} + I_{y\omega o6} + I_{y\omega o7}$$

$$I_{x\omega o} = \int_{So}^{S} x\omega_o \, dA$$

Let,

$$C = \frac{b}{2} - \frac{t_u}{2}$$

$$I_{x\omega o2} = \int_{So}^{S} x\omega_{o2} \, dA$$

$$= \int_0^{\alpha} -\left(\frac{b}{2} - \frac{t_u}{2}\right)\left(\left(\frac{t_u}{2}\, s_2\right) - \left(\frac{b}{2}\, s_2\right)\right) t_u \, ds$$

$$= \int_0^{\alpha} -C\left(\left(\frac{t_u}{2}\, s_2\right) - \left(\frac{b}{2}\, s_2\right)\right) t_u \, ds$$

$$= \int_0^{\alpha} \left(\frac{C\, b}{2} s_2\right) t_u \, ds - \int_0^{\alpha} \left(\frac{C\, t_u}{2} s_2\right) t_u \, ds$$

$$= \frac{C\, b\, t_u}{2}\left[\frac{s^2}{2}\right]_{\alpha} - \frac{C\, t_u^2}{2}\left[\frac{s^2}{2}\right]_{\alpha}$$

$$I_{x\omega o2} = \frac{C\, b\, t_u}{4}\alpha^2 - \frac{C\, t_u^2}{4}\alpha^2$$

$$I_{x\omega o4} = \int_{So}^{S} x\omega_{o4} \, dA$$

$$= \int_0^{\alpha} C\left(\left(\frac{b}{2}\, s_4\right) - \left(\frac{t_u}{2} s_4\right)\right) t_u \, ds$$

$$= \int_0^{\alpha} \left(\frac{Cb}{2} s_4\right) t_u \, ds - \int_0^{\alpha} \left(\frac{Ct_u}{2} s_4\right) t_u \, ds$$

$$= \frac{C\, b\, t_u}{2}\left[\frac{s^2}{2}\right]_{\alpha} - \frac{C\, t_u^2}{2}\left[\frac{s^2}{2}\right]_{\alpha}$$

$$I_{x\omega o4} = \frac{C\, b\, t_u}{4}\alpha^2 - \frac{C\, t_u^2}{4}\alpha^2$$

$$I_{x\omega o6} = \int_{So}^{S} x\omega_{o6} \, dA$$

$$= \int_0^{b/2} (-s_6)\left((t_f\, s_6) - (h\, s_6)\right) t_f \, ds$$

$$= \int_0^{b/2} (h\, s_6^2) t_f \, ds - \int_0^{b/2} (t_f\, s_6^2) t_f \, ds$$

$$= h\, t_f \left[\frac{s^3}{3}\right]_{b'2} - t_f^2 \left[\frac{s^3}{3}\right]_{b'2}$$

$$I_{x\omega o6} = \frac{h\, t_f}{24} b^3 - \frac{t_f^2}{24} b^3$$

$$I_{x\omega o7} = \int_{So}^{S} x\omega_{o7}\, dA$$

$$= \int_0^{b/2} s_7((h\, s_7) - (t_f\, s_7))\, t_f\, ds$$

$$= \int_0^{b/2} (h\, s_7^2) t_f\, ds - \int_0^{b/2} (t_f\, s_7^2) tf\, ds$$

$$= h\, t_f \left[\frac{s^3}{3}\right]_{b'^2} - t_f^2 \left[\frac{s^3}{3}\right]_{b'^2}$$

$$I_{x\omega o7} = \frac{h\, t_f}{24} b^3 - \frac{t_f^2}{24} b^3$$

$$I_{x\omega o} = I_{x\omega o2} + I_{x\omega o4} + I_{x\omega o6} + I_{x\omega o7}$$

Since the distances for x and y in determining $I_{x\omega o}$ and $I_{y\omega o}$ were measured from the centroid to the elements of consideration, it was concluded that $I_{xy} = 0$.

Hence to determine the shear centre, the following equations were used.

$$x_A = x_o - [(I_{y\omega o} I_y - I_{x\omega o} I_{xy}) / (I_x I_y - I_{xy}^2)]$$

$$y_A = y_o + [(I_{y\omega o} I_{xy} - I_{x\omega o} I_x) / (I_x I_y - I_{xy}^2)]$$

Because Ixy = 0, thus:

$$x_A = x_o - (I_{y\omega o}) / (I_x)$$

$$y_A = y_o - (I_{x\omega o}) / (I_y)$$

Note: x_0 and y_0 were the coordinates from the centroid “C” to the origin “O”. These were determined to be as shown below.

$x_0 = 0$, due to symmetry.

$y_0 = h - \bar{y} - (t_f/2)$

$\bar{y}_{sc} = y_A + \bar{y}$

These formulae were then inputted in an excel spreadsheet to determine the results.

5.2 Calculations, outputs and observations for H-Section with upstand plates

The section used in this study was a 152x152x30 UC H-section. Flat plates were welded on the upper flanges of the section at the ends. These plates were considered to vary in height and the effect on the shear centre determined.

The section properties that were used were as follow:

h = 157.5mm

b = 152.9mm

t_w = 6.6mm

t_f = 9.4mm

A = 3840mm^2

m = 30kg/m

Note that the chamfers of the section were ignored and an assumption that the flanges and webs met at right angles was made.

α = 0 to 100mm @ 12.5mm increments

The thickness of the upstanding plates was assumed to be 8mm thick plates. Hence, t_u = 8mm. This thickness which was used for all sections was the average thickness of the flanges and web of the 152x152x30 UC H-Section.

5.2.1 Formulae inputted into Excel for H-Section with upstand plates calculations

The following formulae were formulated in an excel spreadsheet to provide solutions to all the variables.

Centroid:

$\bar{x} = 0$

$$\bar{y} = \frac{\left\{\left[(b\ t_f)\left(\frac{t_f}{2}\right)\right] + \left[\left((h-2t_f)t_w\right)\left(\left(\frac{h-2t_f}{2}\right)+t_f\right)\right] + \left[(b\ t_f)\left(h-\frac{t_f}{2}\right)\right] + 2\left[(\alpha\ t_u)\left(h+\frac{\alpha}{2}\right)\right]\right\}}{\{[(b\ t_f)]+[(h-2t_f)t_w]+[(b\ t_f)]+[2(\alpha\ t_u)]\}}$$

The second moment of area:

$$I_{x_1} = \left(\frac{b\ t_f^3}{12}\right) + [(b\ t_f)(\bar{y} - \frac{t_f}{2})^2]$$

$$I_{x_2} = \left(\frac{t_w(h-2t_f)^3}{12}\right) + [(t_w(h-2t_f))(\bar{y} - (\frac{h-2t_f}{2}) + t_f)^2]$$

$$I_{x_3} = \left(\frac{b\ t_f^3}{12}\right) + [(b\ t_f)((h - (\frac{t_f}{2})) - \bar{y})^2]$$

$$I_{x_4} = 2\{(\frac{t_u\ \alpha^3}{12}) + [(\alpha\ t_u)\left((h - \bar{y}) + (\alpha/2)\right)^2]\}$$

$$I_x = I_{x_1} + I_{x_2} + I_{x_3} + I_{x_4}$$

$$I_{y_1} = \left(\frac{t_f\ b^3}{12}\right)$$

$$I_{y_2} = \left(\frac{(h-2t_f)t_w^3}{12}\right)$$

$$I_{y_3} = \left(\frac{t_f\ b^3}{12}\right)$$

$$I_{y_4} = 2\{(\frac{\alpha\ t_u^3}{12}) + [(\alpha\ t_u)(\frac{b}{2} - \frac{t_u}{2})^2]\}$$

$$I_y = I_{y_1} + I_{y_2} + I_{y_3} + I_{y_4}$$

Sectorial product areas:

$$I_{y\omega o2} = \frac{A\ t_u^2}{4}\alpha^2 - \frac{A\ b\ t_u}{4}\alpha^2 + \frac{t_u^2}{6}\alpha^3 - \frac{b\ t_u}{6}\alpha^3$$

$$I_{y\omega o4} = \frac{A\ b\ t_u}{4}\alpha^2 - \frac{A\ t_u^2}{4}\alpha^2 + \frac{b\ t_u}{6}\alpha^3 - \frac{t_u^2}{6}\alpha^3$$

$$I_{y\omega o6} = \frac{B\ h\ t_f}{8}b^2 - \frac{B\ t_f^2}{8}b^2$$

$$I_{y\omega o7} = \frac{B\ t_f^2}{8}b^2 - \frac{B\ h\ t_f}{8}b^2$$

$$I_{y\omega o} = I_{y\omega o2} + I_{y\omega o4} + I_{y\omega o6} + I_{y\omega o7}$$

$$I_{x\omega o2} = \frac{C\ b\ t_u}{4}\alpha^2 - \frac{C\ t_u^2}{4}\alpha^2$$

$$I_{y\omega o4} = \frac{C\ b\ t_u}{4}\alpha^2 - \frac{C\ t_u^2}{4}\alpha^2$$

$$I_{x\omega o6} = \frac{h\ t_f}{24}b^3 - \frac{t_f^2}{24}b^3$$

$$I_{x\omega o7} = \frac{h\ t_f}{24}b^3 - \frac{t_f^2}{24}b^3$$

$$I_{x\omega o} = I_{x\omega o2} + I_{x\omega o4} + I_{x\omega o6} + I_{x\omega o7}$$

Let,

$$A = h - \bar{y}, \quad B = \bar{y} - \frac{t_f}{2}, \quad C = \frac{b}{2} - \frac{t_u}{2}$$

$x_0 = 0$, due to symmetry.

$y_0 = h - \bar{y} - (t_f/2)$

$\bar{y}_{sc} = y_A + \bar{y}$

$x_A = x_o - (I_{y\omega o}) / (I_x)$

$y_A = y_o - (I_{x\omega o}) / (I_y)$

5.2.2 Excel Spreadsheets and Prokon outputs for H-Section with upstand plates

Having inputted the formulae in excel, the results given in Table 5.1 were obtained and they show the second moment of areas for the varying upstand plate heights. It was observed that the calculated values for the second moment of areas were the same as those obtained from Prokon (ProSec), (Prokon, 2013). As the plate heights increased so did the second moment of areas.

Table 5.1: Second moment of areas for varying upstand plate heights

α (mm)	I_{xTotal} (mm^4)	I_{yTotal} (mm^4)
0	17,250,863	5,603,465
12.5	18,626,035	6,654,332
25	20,284,358	7,705,200
37.5	22,245,359	8,756,067
50	24,527,889	9,806,934
62.5	27,150,257	10,857,801
75	30,130,342	11,908,668
87.5	33,485,677	12,959,535
100	37,233,511	14,010,403

The sectorial product areas along the x-axis increased as the plate heights increased. However, the sectorial product areas along the y-axis remained zero. The zero value for the I_{yw0} made sense as we did not expect to have the shear centre offset along the x-axis due to the symmetry of the section about the y-axis. This can be seen in Table 5.2.

Table 5.2: Sectorial product areas for varying upstand plate heights

α (mm)	$I_{x\omega oTotal}$	$I_{y\omega oTotal}$
0	414,690,534	0
12.5	421,251,787	0
25	440,935,547	0
37.5	473,741,812	0
50	519,670,584	0
62.5	578,721,862	0
75	650,895,647	0
87.5	736,191,937	0
100	834,610,734	0

The output for the shear centre calculations showed that, as the plate heights increased the shear centre shifted further apart (upward) from the centroid. See reading y_a in table 5.3 for the distances between the centroid and shear centre. This phenomenon occurred up to a range between 25 and 37.5mm plate heights. Somewhere after the plate height of 25mm, the two centres started coming together and by heights of 62.5mm plates, the shear centre was below the centroid. Table 5.3 shows the results of how the shear centres and centroids changed as the upstanding plates increased in height.

Table 5.3: Sectorial coordinate approach shear centres for varying upstand plate heights.

α (mm)	$\bar{x}$ (mm)	$\bar{y}$ (mm)	x_o (mm)	y_o (mm)	x_a (mm)	y_a (mm)	$\bar{y}_{sc}$ (mm)
0	0	78.75	0	74.05	0	0.04	78.79
12.5	0	83.01	0	69.79	0	6.48	89.50
25	0	87.46	0	65.34	0	8.11	95.57
37.5	0	92.08	0	60.72	0	6.62	98.70
50	0	96.83	0	55.97	0	2.98	99.81
62.5	0	101.71	0	51.09	0	-2.21	99.50
75	0	106.71	0	46.09	0	-8.56	98.14
87.5	0	111.79	0	41.01	0	-15.80	95.99
100	0	116.97	0	35.83	0	-23.74	93.23

The results from the spreadsheets were also compared to results from the Prokon (ProSec) software and are shown in table 5.4.

Table 5.4: Sectorial coordinate approach vs Prokon shear centre results for varying

	Sectorial coordinate approach			Prokon (ProSec) software			
α (mm)	**$\bar{x}$ (mm)**	**$\bar{y}$ (mm)**	**$\bar{y}_{sc}$ (mm)**	**$\bar{x}$ (mm)**	**$\bar{y}$ (mm)**	**$\bar{y}_{sc}$ (mm)**	**Δ $\bar{y}_{sc}$ (mm)**
0	0	78.75	78.79	0	78.75	78.80	-0.01
12.5	0	83.01	89.50	0	83.01	88.80	0.70
25	0	87.46	95.57	0	87.46	94.30	1.27
37.5	0	92.08	98.70	0	92.08	97.00	1.70
50	0	96.83	99.81	0	96.83	97.90	1.91
62.5	0	101.71	99.50	0	101.71	97.30	2.20
75	0	106.71	98.14	0	106.71	95.70	2.44
87.5	0	111.79	95.99	0	111.79	93.50	2.49
100	0	116.97	93.23	0	116.97	90.50	2.73

From Table 5.4 it can be observed that the two approaches yielded results that had a minor difference in value. Also, the greater the plate heights were, the greater the difference.

The behaviour observed above can be compared to the study by Mudenda & Zingoni (2018). These two studies show similar outcomes; however, the former study used the shear flow approach (Mudenda & Zingoni, 2018).

5.3 Calculations, outputs and observations for H-Section of a trimmed bottom flange with upstand plates

The section that was used in the study was a 152x152x30 UC section and for trimmed section, the bottom flange was **trimmed to 2/3 and 1/3 of the normal width**. Flat plates were welded on the upper flanges of the section at the ends. These plates were considered to vary in height and the effect on the shear centre determined.

The section properties that were used were as follow:

h = 157.5mm

b = 152.9mm

t_w = 6.6mm

t_f = 9.4mm

A = Less than 3840mm^2 according to trimmed width

m = Less than 30kg/m according to trimmed width

Note that the chamfers of the section were ignored and an assumption that the flanges and webs met at right angles was made.

α = 0 to 100mm @ 12.5mm increments

The thickness of the upstanding plates was assumed to be 8mm thick plates. Hence, t_u = 8mm.

Figure 5.3 shows the trimmed section and the different parameters.

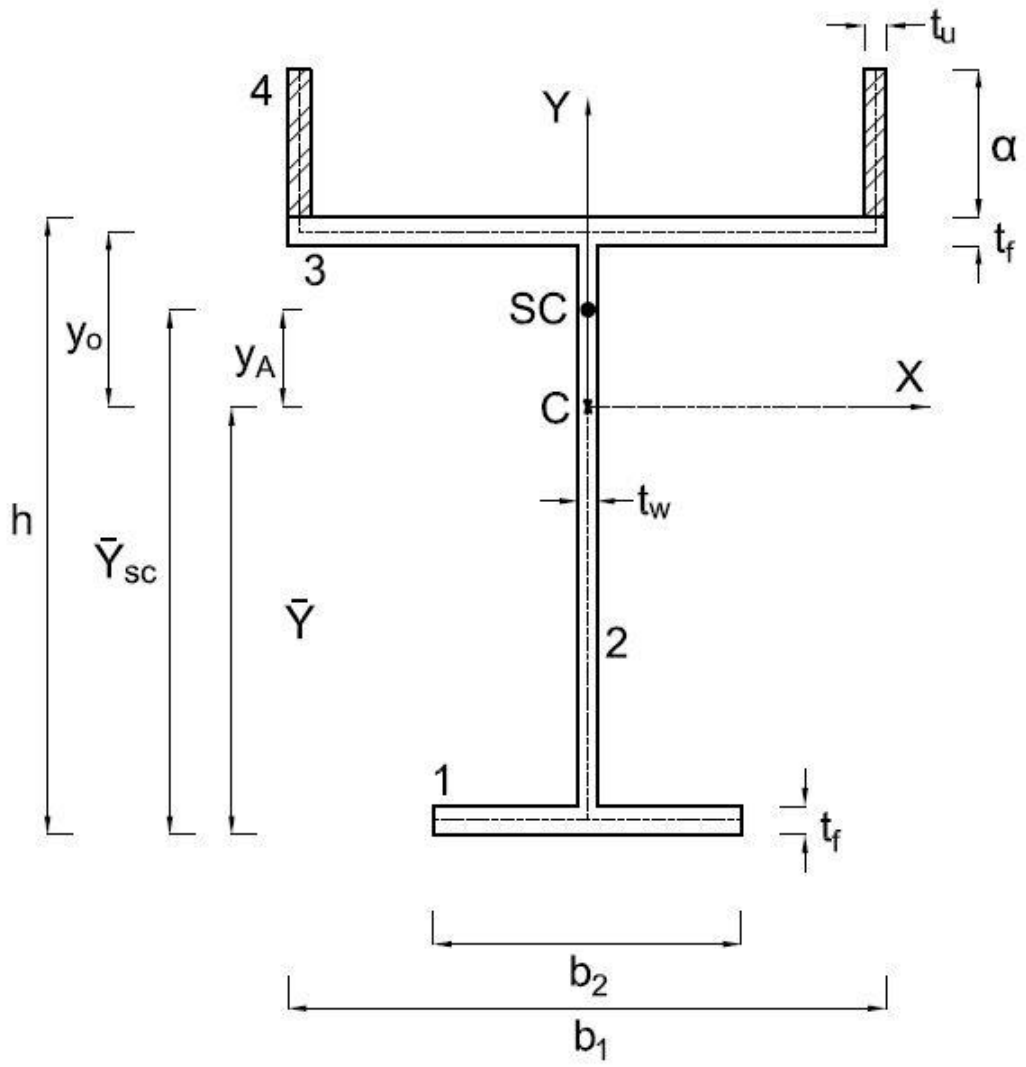

Figure 5.3: Mono-symmetric I or H section of trimmed bottom flange dimensions

A similar procedure to that of the H-section was followed in determining the warping functions for the new sections. The tangential and normal components of displacement for the different elements were drawn about a pole “O”. this pole was at the centre of the top flanges. Figure 5.4 shows the pole “O” and the different components of displacements drawn using the right-hand rule.

As was mentioned before, in determining the warping functions for the different elements, elements whose tangential components went through the pole yielded no warping functions (zero). This was because for the elements having the tangential components running through the pole of consideration had a lever arm equal to zero, hence yielding a product result of zero for those warping functions.

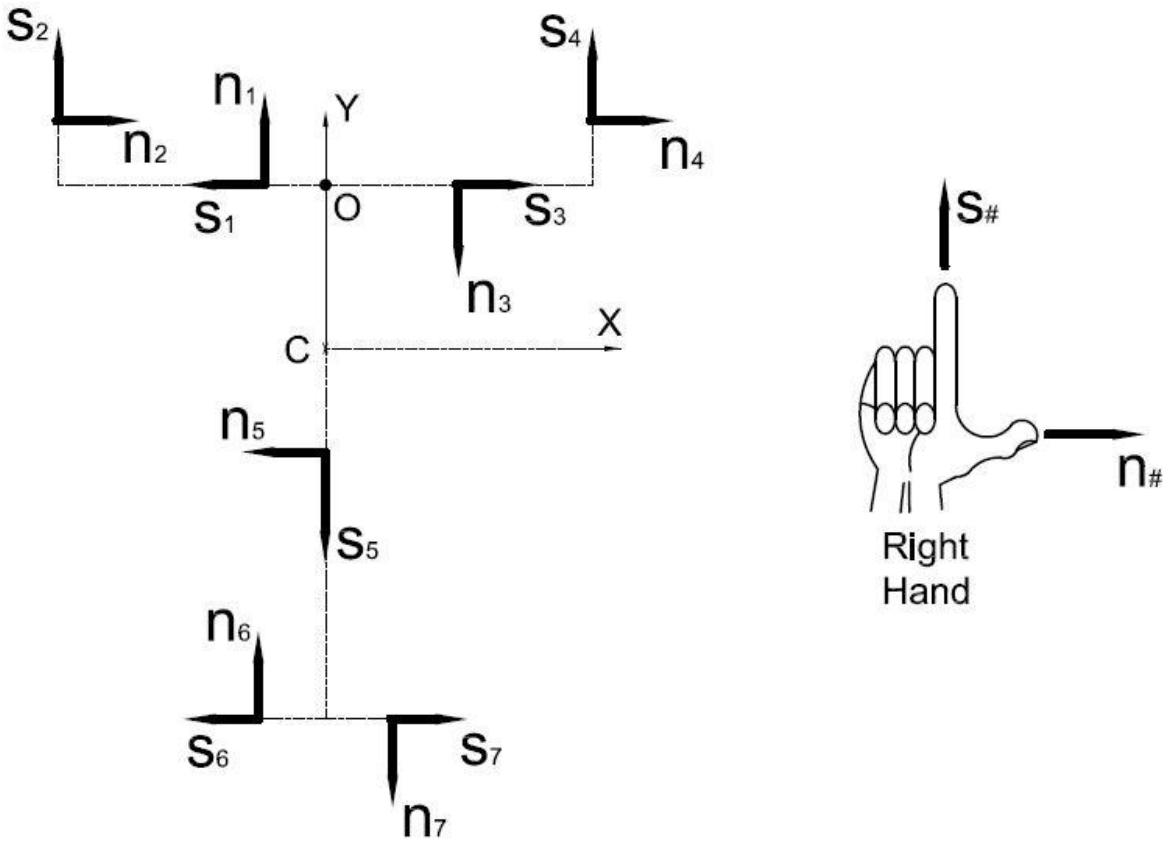

Figure 5.4: Mono-symmetric I or H section of trimmed bottom flange, Tangential and normal components of displacement

5.3.1 Formulae inputted into Excel for H-Section of trimmed bottom flange with upstand plates calculations

The following formulae were formulated in an excel spreadsheet to provide solutions to all the variables. Note that the formulae are similar to those in section 5.2 however there was an introduction of parameter b_1 for the top flange and b_2 for the bottom flange. Hence, yielding a slight difference in the obtained formulae.

Centroid:

$\bar{x} = 0$

$$\bar{y} = \frac{\left\{\left[(b_2\ tf)\left(\frac{t_f}{2}\right)\right] + \left[((h-2t_f)t_w)\left(\left(\frac{h-2t_f}{2}\right)+t_f\right)\right] + \left[(b_1\ t_f)\left(h-\frac{t_f}{2}\right)\right] + 2\left[(\alpha\ t_u)\left(h+\frac{\alpha}{2}\right)\right]\right\}}{\{[(b_2\ t_f)]+[(h-2t_f)t_w]+[(b_1\ t_f)]+[2(\alpha\ t_u)]\}}$$

The second moment of area:

$$I_{x1} = \left(\frac{b_2\ t_f^3}{12}\right) + [(b_2\ t_f)(\bar{y}-\frac{t_f}{2})^2]$$

$$I_{x2} = \left(\frac{t_w(h-2t_f)^3}{12}\right) + [(t_w(h-2t_f))(\bar{y} - (\frac{h-2t_f}{2}) + t_f)^2]$$

$$I_{x3} = \left(\frac{b_1\ t_f^3}{12}\right) + [(b_1\ t_f)((h - (\frac{t_f}{2})) - \bar{y})^2]$$

$$I_{x4} = 2\{(\frac{t_u\ \alpha^3}{12}) + [(\alpha\ t_u)\left((h - \bar{y}) + (\alpha/2)\right)^2]\}$$

$$I_x = I_{x1} + I_{x2} + I_{x3} + I_{x4}$$

$$I_{y1} = \left(\frac{t_f\ b_2^3}{12}\right)$$

$$I_{y2} = \left(\frac{(h-2t_f)t_w^3}{12}\right)$$

$$I_{y3} = \left(\frac{t_f\ b_1^3}{12}\right)$$

$$I_{y4} = 2\{(\frac{\alpha\ t_u^3}{12}) + [(\alpha\ t_u)(\frac{b}{2}-\frac{t_u}{2})^2\}$$

$$I_y = I_{y1} + I_{y2} + I_{y3} + I_{y4}$$

Sectorial product areas:

$$I_{y\omega o2} = \frac{A\ t_u^2}{4}\alpha^2 - \frac{A\ b_1\ t_u}{4}\alpha^2 + \frac{t_u^2}{6}\alpha^3 - \frac{b_1\ t_u}{6}\alpha^3$$

$$I_{y\omega o4} = \frac{A\ b_1\ t_u}{4}\alpha^2 - \frac{A\ t_u^2}{4}\alpha^2 + \frac{b_1\ t_u}{6}\alpha^3 - \frac{t_u^2}{6}\alpha^3$$

$$I_{y\omega o6} = \frac{B\ h\ t_f}{8}b_2^2 - \frac{B\ t_f^2}{8}b_2^2$$

$$I_{y\omega o7} = \frac{B\ t_f^2}{8}b_2^2 - \frac{B\ h\ t_f}{8}b_2^2$$

$I_{y\omega o} = I_{y\omega o2} + I_{y\omega o4} + I_{y\omega o6} + I_{y\omega o7}$

$$I_{x\omega o2} = \frac{C\, b_1\, t_u}{4}\alpha^2 - \frac{C\, t_u^2}{4}\alpha^2$$

$$I_{x\omega o4} = \frac{C\, b_1\, t_u}{4}\alpha^2 - \frac{C\, t_u^2}{4}\alpha^2$$

$$I_{x\omega o6} = \frac{h\, t_f}{24}b_2^3 - \frac{t_f^2}{24}b_2^3$$

$$I_{x\omega o7} = \frac{h\, t_f}{24}b_2^3 - \frac{tf^2}{24}b_2^3$$

$I_{x\omega o} = I_{x\omega o2} + I_{x\omega o4} + I_{x\omega o6} + I_{x\omega o7}$

Let,

$$A = h - \bar{y}, \quad B = \bar{y} - \frac{t_f}{2}, \quad C = \frac{b_1}{2} - \frac{t_u}{2}$$

$x_0 = 0$, due to symmetry.

$y_0 = h - \bar{y} - (t_f/2)$

$\bar{y}_{sc} = y_A + \bar{y}$

$x_A = x_o - (I_{y\omega o}) / (I_x)$

$y_A = y_o - (I_{x\omega o}) / (I_y)$

5.3.2 Excel Spreadsheets and Prokon outputs for H-Section of the trimmed bottom flange with upstand plates

Having inputted the formulae in excel, the following results were obtained. Table 5.5 shows the second moment of areas for the varying upstand plate heights. It was observed that the calculated values for the second moment of areas were the same as those obtained from Prokon (ProSec). Also, as the plate heights increased, so did the second moment of areas.

Table 5.5: Second moment of areas for varying upstand plate heights of trimmed sections

Case 1: 2/3 of the bottom flange

α (mm)	I_{xTotal} (mm^4)	I_{yTotal} (mm^4)
0	14,237,921	3,632,231
12.5	15,281,072	4,683,098
25	16,572,964	5,733,965
37.5	18,133,139	6,784,833
50	19,980,375	7,835,700
62.5	22,132,864	8,886,567
75	24,608,346	9,937,434
87.5	27,424,198	10,988,301
100	30,597,513	12,039,168

Case 2: 1/3 of the bottom flange

α (mm)	I_{xTotal} (mm^4)	I_{yTotal} (mm^4)
0	10,215,046	2,907,304
12.5	10,889,149	3,958,171
25	11,772,139	5,009,038
37.5	12,884,535	6,059,906
50	14,245,777	7,110,773
62.5	15,874,512	8,161,640
75	17,788,783	9,212,507
87.5	20,006,178	10,263,374
100	22,543,931	11,314,241

The sectorial product areas along the x-axis also increased as the plate heights increased and as was expected the sectorial product areas along the y-axis remained zero. This can be seen in Table 5.6.

Table 5.6: Sectorial product areas for varying upstand plate heights of the trimmed bottom flange sections

Case 1: 2/3 of the bottom flange

α (mm)	$I_{x\omega oTotal}$	$I_{y\omega oTotal}$
0	122,750,768	0
12.5	129,312,021	0
25	148,995,781	0
37.5	181,802,046	0
50	227,730,818	0
62.5	286,782,096	0
75	358,955,881	0
87.5	444,252,171	0
100	542,670,968	0

Case 2: 1/3 of the bottom flange

α (mm)	$I_{x\omega oTotal}$	$I_{y\omega oTotal}$
0	15,389,064	0
12.5	21,950,317	0
25	41,634,076	0
37.5	74,440,342	0
50	120,369,114	0
62.5	179,420,392	0
75	251,594,176	0
87.5	336,890,467	0
100	435,309,264	0

The output for the calculations shows that for both sections (2/3 & 1/3 trimmed sections) the shear centre was above the centroid for the sections without plates. This was because trimming the bottom flanges already introduced monosymmetry into the section. It was also noted that the section which had the bottom flange trimmed to 1/3 of the normal width had the shear centre furthest from the centroid then that of which was trimmed to 2/3 of the normal width.

The results as shown in table 5.7 for both sections and are discussed further.

Table 5.7: Sectorial coordinate approach shear centres for varying upstand plate heights

Case 1: 2/3 of the bottom flange

α (mm)	$\bar{x}$ (mm)	$\bar{y}$ (mm)	x_o (mm)	y_o (mm)	x_a (mm)	y_a (mm)	$\bar{y}_{sc}$ (mm)
0	0	89.47	0	63.33	0	29.53	119.01
12.5	0	93.70	0	59.10	0	31.48	125.19
25	0	98.15	0	54.65	0	28.66	126.82
37.5	0	102.79	0	50.01	0	23.22	126.00
50	0	107.58	0	45.22	0	16.16	123.74
62.5	0	112.50	0	40.30	0	8.02	120.53
75	0	117.55	0	35.25	0	-0.87	116.68
87.5	0	122.69	0	30.11	0	-10.32	112.37
100	0	127.93	0	24.87	0	-20.21	107.72

Case 2: 1/3 of the bottom flange

α (mm)	$\bar{x}$ (mm)	$\bar{y}$ (mm)	x_o (mm)	y_o (mm)	x_a (mm)	y_a (mm)	$\bar{y}_{sc}$ (mm)
0	0	103.80	0	49.00	0	43.71	147.51
12.5	0	107.75	0	45.05	0	39.50	147.25
25	0	111.99	0	40.81	0	32.50	144.49
37.5	0	116.46	0	36.34	0	24.05	140.52
50	0	121.13	0	31.67	0	14.74	135.87
62.5	0	125.96	0	26.84	0	4.85	130.82
75	0	130.94	0	21.86	0	-5.45	125.49
87.5	0	136.03	0	16.77	0	-16.06	119.98
100	0	141.23	0	11.57	0	-26.91	114.33

It was also noted that as the plate heights increased, the shear centre shifted further apart (upward) from the centroid over the first step and then the gap decreased steadily until the shear centre was below the centroid for the 2/3 trimmed section. Whereas, for the 1/3 trimmed section, the shear centre started furthest apart from the centroid and the gap between the two decreased as the plate heights increased. The decrease remained constant and eventually, the shear centre fell below the centroid. See reading y_a in table 5.7 for the distances between the centroid and shear centre.

Overall, looking at the centroids and shear centres it was observed that the shear centres were always above the centroids up to the ranges of heights 62.5 to 75mm.

The results from the spreadsheets were also compared to results from the Prokon software (ProSec section). From table 5.8 it can be observed that the two approaches yielded results that had a minor difference in value. Also, the greater the plate heights were, the greater the difference.

Table 5.8: Sectorial coordinate approach vs Prokon shear centre results for reduced bottom flanges

Case 1: 2/3 of the bottom flange

	Sectorial coordinate approach			**Prokon (ProSec) software**			
α (mm)	**$\bar{x}$ (mm)**	**$\bar{y}$ (mm)**	**$\bar{y}_{sc}$ (mm)**	**$\bar{x}$ (mm)**	**$\bar{y}$ (mm)**	**$\bar{y}_{sc}$ (mm)**	**Δ $\bar{y}_{sc}$ (mm)**
0	0	89.47	119.01	0	89.47	119.00	0.01
12.5	0	93.70	125.19	0	93.70	124.00	1.19
25	0	98.15	126.82	0	98.15	125.00	1.82
37.5	0	102.79	126.00	0	102.80	124.00	2.00
50	0	107.58	123.74	0	107.60	121.00	2.74
62.5	0	112.50	120.53	0	112.50	118.00	2.53
75	0	117.55	116.68	0	117.50	114.00	2.68
87.5	0	122.69	112.37	0	122.70	109.00	3.37
100	0	127.93	107.72	0	127.90	105.00	2.72

Case 2: 1/3 of the bottom flange

	Sectorial coordinate approach			**Prokon (ProSec) software**			
α (mm)	**$\bar{x}$ (mm)**	**$\bar{y}$ (mm)**	**$\bar{y}_{sc}$ (mm)**	**$\bar{x}$ (mm)**	**$\bar{y}$ (mm)**	**$\bar{y}_{sc}$ (mm)**	**Δ $\bar{y}_{sc}$ (mm)**
0	0	103.80	147.51	0	103.80	147.00	0.51
12.5	0	107.75	147.25	0	107.80	146.00	1.25
25	0	111.99	144.49	0	112.00	143.00	1.49
37.5	0	116.46	140.52	0	116.50	138.00	2.52
50	0	121.13	135.87	0	121.10	133.00	2.87
62.5	0	125.96	130.82	0	126.00	128.00	2.82
75	0	130.94	125.49	0	130.90	122.00	3.49
87.5	0	136.03	119.98	0	136.00	117.00	2.98
100	0	141.23	114.33	0	141.20	111.00	3.33

CHAPTER 6: MONOSYMMETRIC SECTION OF A T-SECTION WITH UPSTAND PLATES SHEAR CENTRE DEMONSTRATION

6.1 Formulae derivation for T-Section with upstand plates

Another non-standard monosymmetric section that was considered was formed by welding the upstanding plates onto a standard monosymmetric T-section. The upstanding plates were welded on the ends of the upper flanges as with the previous sections. The section studied was as shown in figure 6.1.

The aim was to compare the variation of the shear centre with that of the centroid as the upstand heights were changed. Thus, the upstanding plate height parameter varied to show the change.

The chamfering at the positions where the flanges met the web were not considered. It was assumed that the elements met at right angles. This was to simplify the calculations considering that the areas of the chamfers in comparison to the entire cross-section was negligible, hence it was ignored. The elements were numbered from 1 to 3, as can be seen in figure 6.1.

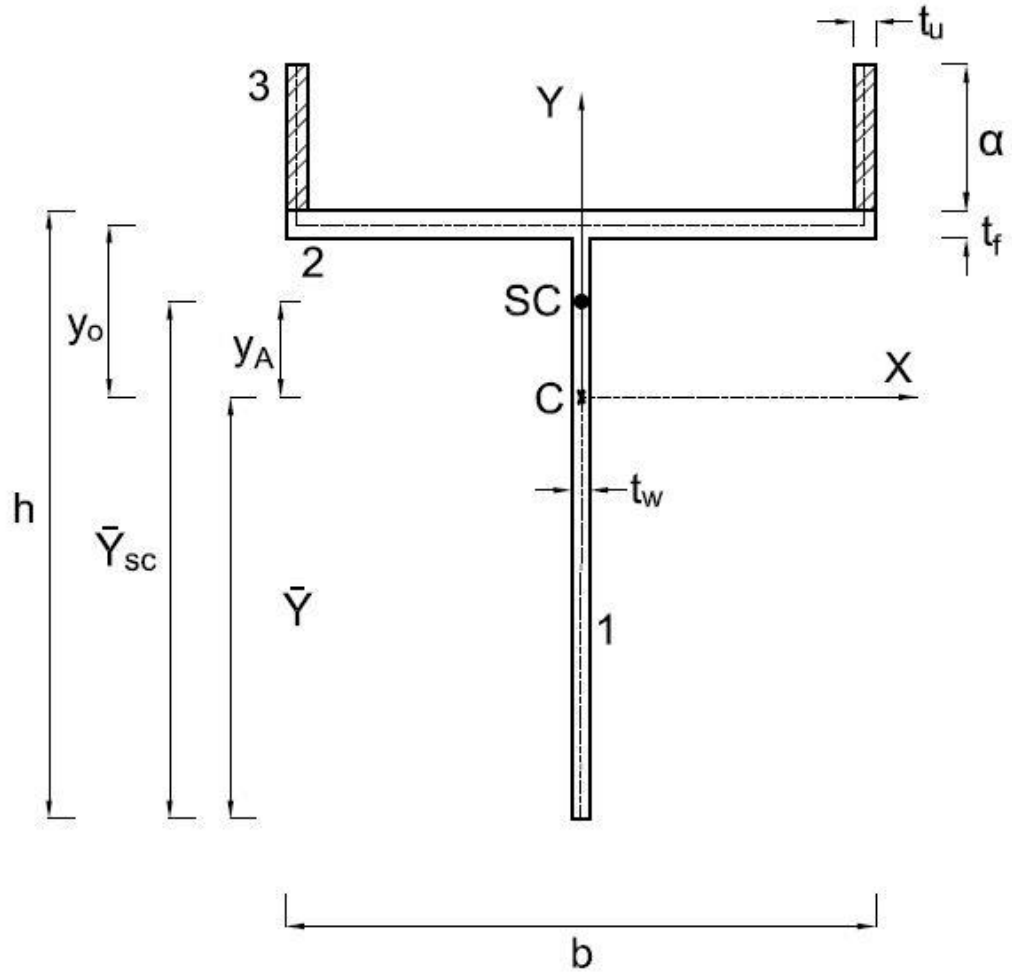

Figure 6.1: Mono-symmetric T-section dimensions

The sections properties were as follows:

h = height of section

b = breadth of section

t_f = thickness of the flange

t_w = thickness of the web

α = height of upstand plate

t_u = thickness of upstand plate

$\bar{y}$ = y bar, the first moment of area about the y-axis

x bar = first moment of area about the x-axis

$\bar{y}_{sc}$ = distance from the bottom of the section to shear centre

X = x-axis

Y = y-axis

C = centroid, the centre of gravity

SC = shear centre

The formulae were derived in the following order: centroids, second moments of area, warping functions, sectorial product areas, shear centre and shear centre distances from the bottom of the section. All the formulae were derived in three parts being, (1) the web, (2) top flanges and (3) the upstanding plates.

Centroid:

In deriving the formulae for the centroid, the standard formula for determining first moments of area was utilized.

$\bar{x} = 0$

Due to the symmetry of the section.

$$\bar{y} = \sum_{0}^{n} \frac{A_i\, y_i}{A_i}$$

$$\bar{y} = \frac{\left\{\left[((h-t_f)t_w)\left(\left(\frac{h-t_f}{2}\right)\right)\right] + \left[(b\ t_f)\left(h-\frac{t_f}{2}\right)\right] + 2\left[(\alpha\ t_u)\left(h+\frac{\alpha}{2}\right)\right]\right\}}{\{[(h-t_f)t_w]+[(b\ t_f)]+[2(\alpha\ t_u)]\}}$$

The second moment of area:

The second moment of area formula was used, and the shift of the areas was also considered for each of the elements.

$$I = \frac{b\,d^3}{12} + AC^2$$

$$I_{x1} = \left(\frac{t_w(h-t_f)^3}{12}\right) + \left[(t_w(h - t_f))\left(\bar{y} - \left(\frac{h-2t_f}{2}\right)\right)^2\right]$$

$$I_{x2} = \left(\frac{b\,t_f^3}{12}\right) + \left[(b\,t_f)\left((h - \left(\frac{t_f}{2}\right)) - \bar{y}\right)^2\right]$$

$$I_{x3} = 2\left\{\left(\frac{t_u\,\alpha^3}{12}\right) + \left[(\alpha\,t_u)\left((h - \bar{y}) + (\alpha/2)\right)^2\right]\right\}$$

$$I_x = I_{x1} + I_{x2} + I_{x3}$$

$$I_{y1} = \left(\frac{(h-t_f)t_w^3}{12}\right)$$

$$I_{y2} = \left(\frac{t_f\,b^3}{12}\right)$$

$$I_{y3} = 2\left\{\left(\frac{\alpha\,t_u^3}{12}\right) + \left[(\alpha\,t_u)\left(\frac{b}{2} - \frac{t_u}{2}\right)^2\right]\right\}$$

$$I_y = I_{y1} + I_{y2} + I_{y3}$$

Warping functions:

To determine the warping functions, the tangential and normal components of displacement for the different elements were drawn about a pole “O”. this pole was at the centre of the top flanges. Figure 6.2 shows the pole “O” and the different components of displacements drawn using the right-hand rule.

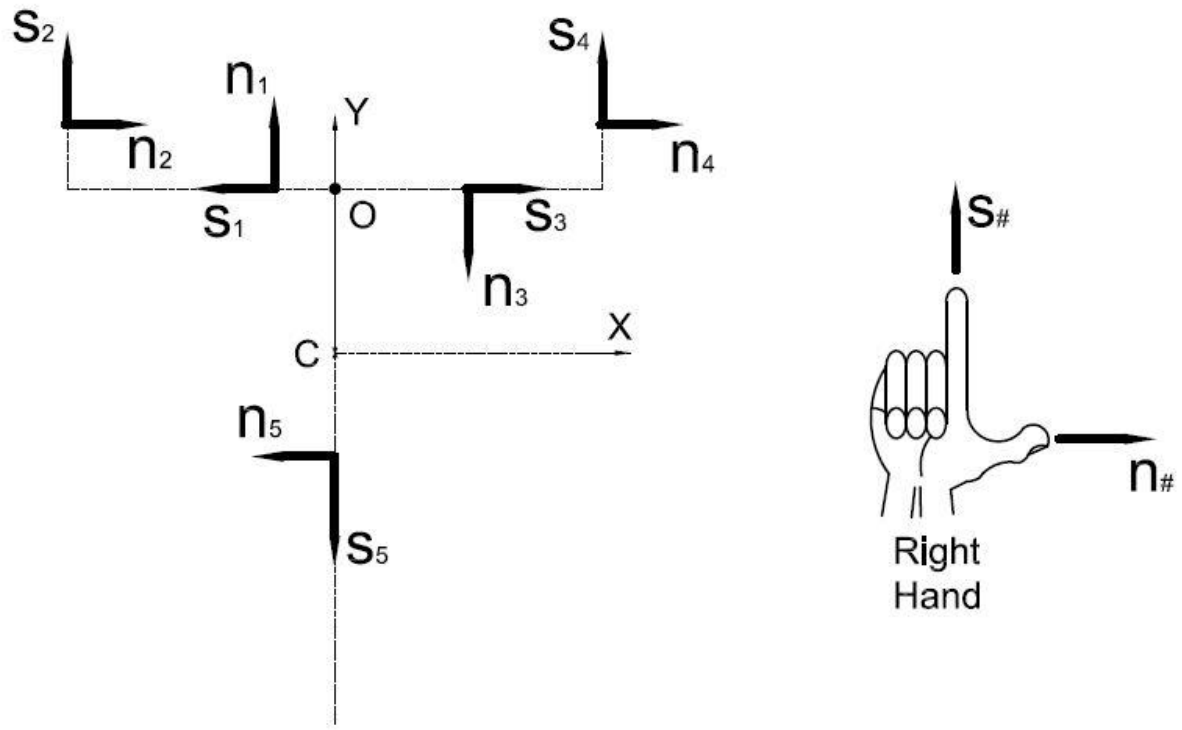

Figure 6.2: Mono-symmetric T-section Tangential and normal components of displacement

Having chosen “O” as the pole, meant that the warping functions s_1, s_3 and s_5 were zero as the tangential components ran through the pole. Another important point to note was that the tangential components were taken along the centre lines of the different elements. That is why the perpendicular distance for s_2 was half the flange width subtracted by half the upstand plate thickness. This was a similar approach to s_4.

Vectors are taken about the pole “O”.

$$\omega_o(s_1) = \int_{So}^{S} d\omega_o = 0$$

$$\omega_o(s_2) = \int_{So}^{S} d\omega_o = -\left(\frac{b}{2} - \frac{t_u}{2}\right) s_2 = \frac{t_u}{2} s_2 - \frac{b}{2} s_2$$

(clockwise = -)

$$\omega_o(s_3) = \int_{So}^{S} d\omega_o = 0$$

$$\omega_o(s_4) = \int_{So}^{S} d\omega_o = \left(\frac{b}{2} - \frac{t_u}{2}\right) s_4 = \frac{b}{2} s_4 - \frac{t_u}{2} s_4$$

(anticlockwise = +)

$$\omega_o(s_5) = \int_{So}^{S} d\omega_o = 0$$

Sectorial product areas:

The x & y values were taken from centroid “C” to the elements being studied. The perpendicular distances functions along the y-axis and x-axis were not constant functions as they were varying functions and were the first parameters in the warping functions. The direction (start to the end of a vector) in which the vector s was pointed played a role.

$$I_{y\omega o} = \int_{So}^{S} y\omega_o \, dA$$

Let,

$A = h - \bar{y}$

$$I_{y\omega o2} = \int_{So}^{S} y\omega_{o2} \, dA$$

$$= \int_0^{\alpha} ((h-\bar{y})+s_2)\left(\left(\frac{t_u}{2} s_2\right) - \left(\frac{b}{2} s_2\right)\right) t_u \, ds$$

$$= \int_0^{\alpha} (A+s_2)\left(\left(\frac{t_u}{2} s_2\right) - \left(\frac{b}{2} s_2\right)\right) t_u \, ds$$

$$= \int_0^{\alpha} \left(\frac{At_u}{2} s_2\right) t_u \, ds - \int_0^{\alpha} \left(\frac{Ab}{2} s_2\right) t_u \, ds + \int_0^{\alpha} \left(\frac{t_u}{2} s_2^2\right) t_u \, ds - \int_0^{\alpha} \left(\frac{b}{2} s_2^2\right) t_u \, ds$$

$$= \frac{A\, t_u^2}{2}\left[\frac{s^2}{2}\right]^{\alpha} - \frac{A\, b\, t_u}{2}\left[\frac{s^2}{2}\right]^{\alpha} + \frac{t_u^2}{2}\left[\frac{s^3}{3}\right]^{\alpha} - \frac{b t_u}{2}\left[\frac{s^3}{3}\right]^{\alpha}$$

$$I_{y\omega o2} = \frac{A\, t_u^2}{4}\alpha^2 - \frac{A\, b\, t_u}{4}\alpha^2 + \frac{t_u^2}{6}\alpha^3 - \frac{b\, t_u}{6}\alpha^3$$

$$I_{y\omega o4} = \int_{So}^{S} y\omega_{o4} \, dA$$

$$= \int_0^{\alpha} (A+s_4)\left(\left(\frac{b}{2} s_4\right) - \left(\frac{t_u}{2} s_4\right)\right) t_u \, ds$$

$$= \int_0^{\alpha} \left(\frac{Ab}{2} s_4\right) t_u \, ds - \int_0^{\alpha} \left(\frac{At_u}{2} s_4\right) t_u \, ds + \int_0^{\alpha} \left(\frac{b}{2} s_4^2\right) t_u \, ds - \int_0^{\alpha} \left(\frac{t_u}{2} s_4^2\right) t_u \, ds$$

$$= \frac{A\, b\, t_u}{2}\left[\frac{s^2}{2}\right]^{\alpha} - \frac{A\, t_u^2}{2}\left[\frac{s^2}{2}\right]^{\alpha} + \frac{bt_u}{2}\left[\frac{s^3}{3}\right]^{\alpha} - \frac{t_u^2}{2}\left[\frac{s^3}{3}\right]^{\alpha}$$

$$I_{y\omega o4} = \frac{A\, b\, t_u}{4}\alpha^2 - \frac{A\, t_u^2}{4}\alpha^2 + \frac{b\, t_u}{6}\alpha^3 - \frac{t_u^2}{6}\alpha^3$$

$I_{y\omega o} = I_{y\omega o2} + I_{y\omega o4}$

$$I_{x\omega o} = \int_{So}^{S} x\omega_o \, dA$$

Let,

$$C = \frac{b}{2} - \frac{t_u}{2}$$

$$I_{x\omega o2} = \int_{So}^{S} x\omega_{o2} \, dA$$

$$= \int_0^{\alpha} -\left(\frac{b}{2} - \frac{t_u}{2}\right)\left(\left(\frac{t_u}{2}\, s_2\right) - \left(\frac{b}{2}\, s_2\right)\right) t_u \, ds$$

$$= \int_0^{\alpha} -C\left(\left(\frac{t_u}{2}\, s_2\right) - \left(\frac{b}{2}\, s_2\right)\right) t_u \, ds$$

$$= \int_0^{\alpha} \left(\frac{C\, b}{2} s_2\right) t_u \, ds - \int_0^{\alpha} \left(\frac{C\, t_u}{2} s_2\right) t_u \, ds$$

$$= \frac{C\, b\, t_u}{2}\left[\frac{s^2}{2}\right]_{\alpha} - \frac{C\, t_u^2}{2}\left[\frac{s^2}{2}\right]_{\alpha}$$

$$I_{x\omega o2} = \frac{C\, b\, t_u}{4}\alpha^2 - \frac{C\, t_u^2}{4}\alpha^2$$

$$I_{x\omega o4} = \int_{So}^{S} x\omega_{o4} \, dA$$

$$= \int_0^{\alpha} C\left(\left(\frac{b}{2}\, s_4\right) - \left(\frac{t_u}{2} s_4\right)\right) t_u \, ds$$

$$= \int_0^{\alpha} \left(\frac{Cb}{2} s_4\right) t_u \, ds - \int_0^{\alpha} \left(\frac{Ct_u}{2} s_4\right) t_u \, ds$$

$$= \frac{C\, b\, t_u}{2}\left[\frac{s^2}{2}\right]_{\alpha} - \frac{C\, t_u^2}{2}\left[\frac{s^2}{2}\right]_{\alpha}$$

$$I_{y\omega o4} = \frac{C\, b\, t_u}{4}\alpha^2 - \frac{C\, t_u^2}{4}\alpha^2$$

$I_{x\omega o} = I_{x\omega o2} + I_{x\omega o4}$

Since the distances for x and y in determining $I_{x\omega o}$ and $I_{y\omega o}$ were measured from the centroid to the elements of consideration, it was concluded that $I_{xy} = 0$. Therefore, to determine the shear centre the following equations were used:

$x_A = x_o - [(I_{y\omega o} I_y - I_{x\omega o} I_{xy}) / (I_x I_y - I_{xy}^2)]$

$y_A = y_o + [(I_{y\omega o} I_{xy} - I_{x\omega o} I_x) / (I_x I_y - I_{xy}^2)]$

Because $I_{xy} = 0$, thus:

$x_A = x_o - (I_{y\omega o}) / (I_x)$

$y_A = y_o - (I_{x\omega o}) / (I_y)$

Note: x_0 and y_0 were the coordinates from the centroid “C” to the origin “O”. These were determined to be as shown below.

$x_0 = 0$, due to symmetry.

$y_0 = h - \bar{y} - (tf/2)$
$\bar{y}_{sc} = y_A + \bar{y}$

These formulae were then inputted in an excel spreadsheet to determine the results.

6.2 Calculations, outputs and observations of T-Section with upstand plates

The section used in the study was a 203x178x30 T-Section, cut from a406x178x60 I-Section. This section was chosen as it was the standard T-Section with a mass per meter length similar to that of the H-Section used in this study. This was done to ensure we had sections of different shapes that had the same amount of material (steel).

Flat plates were welded on the upper flanges of the section at the ends. These plates were considered to vary in height and the effect on the shear centre was determined.

The section properties that were used were as follow:

h = 203.2mm

b = 177.8mm

t_w = 7.8mm

t_f = 12.8mm

A = 3810mm^2

m = 30kg/m

Note that the chamfers of the section were ignored and an assumption that the flanges and webs met at right angles was made.

α = 0 to 100mm @ 12.5mm increments

The thickness of the upstanding plates was assumed to be 8mm thick plates. Hence, t_u = 8mm.

6.2.1 Formulae inputted into Excel Spreadsheets for the T-Sections with upstand plates calculation

The following formulae were formulated in an excel spreadsheet to provide solutions to all the variables.

Centroid:

$\bar{x}$ = 0

$$\bar{y} = \frac{\left\{\left[((h-t_f)t_w)\left(\left(\frac{h-t_f}{2}\right)\right)\right] + \left[(b\ t_f)\left(h-\frac{t_f}{2}\right)\right] + 2\left[(\alpha\ t_u)\left(h+\frac{\alpha}{2}\right)\right]\right\}}{\{[(h-t_f)t_w]+[(b\ t_f)]+[2(\alpha\ t_u)]\}}$$

The second moment of area:

$$I_{x_1} = \left(\frac{t_w(h-t_f)^3}{12}\right) + [(t_w(h-t_f))(\bar{y} - (\frac{h-2t_f}{2}))^2]$$

$$I_{x_2} = \left(\frac{b\ t_f^3}{12}\right) + [(b\ t_f)((h - (\frac{t_f}{2})) - \bar{y})^2]$$

$$I_{x_3} = 2\{(\frac{t_u\ \alpha^3}{12}) + [(\alpha\ t_u)\left((h - \bar{y}) + (\alpha/2)\right)^2]\}$$

$$I_x = I_{x_1} + I_{x_2} + I_{x_3}$$

$$I_{y_1} = \left(\frac{(h-t_f)t_w^3}{12}\right)$$

$$I_{y_2} = \left(\frac{t_f\ b^3}{12}\right)$$

$$I_{y_3} = 2\{(\frac{\alpha\ t_u^3}{12}) + [(\alpha\ t_u\ )(\frac{b}{2} - \frac{t_u}{2})^2\}$$

$$I_y = I_{y_1} + I_{y_2} + I_{y_3}$$

Sectorial product areas:

$$I_{y\omega o2} = \frac{A\ t_u^2}{4}\alpha^2 - \frac{A\ b\ t_u}{4}\alpha^2 + \frac{t_u^2}{6}\alpha^3 - \frac{b\ t_u}{6}\alpha^3$$

$$I_{y\omega o4} = \frac{A\ b\ t_u}{4}\alpha^2 - \frac{A\ t_u^2}{4}\alpha^2 + \frac{b\ t_u}{6}\alpha^3 - \frac{t_u^2}{6}\alpha^3$$

$$I_{y\omega o} = I_{y\omega o2} + I_{y\omega o4}$$

$$I_{x\omega o2} = \frac{C\ b\ t_u}{4}\alpha^2 - \frac{C\ t_u^2}{4}\alpha^2$$

$$I_{x\omega o4} = \frac{C\ b\ t_u}{4}\alpha^2 - \frac{C\ t_u^2}{4}\alpha^2$$

$I_{x\omega o} = I_{x\omega o2} + I_{x\omega o4}$

Let,

$$A = h - \bar{y}, \quad B = \bar{y} - \frac{t_f}{2}, \quad C = \frac{b}{2} - \frac{t_u}{2}$$

$x_0 = 0$, due to symmetry.

$y_0 = h - \bar{y} - (t_f/2)$
$\bar{y}_{sc} = y_A + \bar{y}$

$x_A = x_o - (I_{y\omega o}) / (I_x)$

$y_A = y_o - (I_{x\omega o}) / (I_y)$

6.2.2 Excel Spreadsheets and Prokon outputs for T-Section with upstand plates

Having inputted the formulae in excel, the following results transpired. Table 6.1 shows the second moment of areas for the varying upstand plate heights. It was observed that the calculated values for the second moment of areas were the same as those obtained from Prokon (ProSec). As with the previous sections, as the plate heights increased, so did the second moment of areas.

Table 6.1: Second moment of areas for varying upstand plate heights on T-section

α (mm)	I_{xTotal} (mm^4)	I_{yTotal} (mm^4)
0	13,794,307	6,003,010
12.5	14,325,717	7,445,679
25	15,074,523	8,888,347
37.5	16,069,016	10,331,016
50	17,335,265	11,773,685
62.5	18,897,583	13,216,353
75	20,778,883	14,659,022
87.5	23,000,947	16,101,691
100	25,584,641	17,544,359

The sectorial product areas along the x-axis also increased as the plate heights increased. However, the sectorial product areas along the y-axis remained zero as was expected. This can be seen in table 6.2.

Table 6.2: Sectorial product areas for varying upstand plate heights on T-section

α (mm)	$I_{x\omega oTotal}$	$I_{y\omega oTotal}$
0	0	0
12.5	9,010,013	0
25	36,040,050	0
37.5	81,090,113	0
50	144,160,200	0
62.5	225,250,313	0
75	324,360,450	0
87.5	441,490,613	0
100	576,640,800	0

The output for the calculations showed that the shear centre at the initial stage was furthest from the centroid. It started off at the joint of the web and flange and as the plate heights increased, the shear centre gradually moved downward, closing the gap with the centroid which was moving upward. See reading y_a in table 6.3 for the distances between the centroid and shear centre. This phenomenon occurred up to a range between 62.5 and 75mm of plate heights where the shear centre eventually ended up being below the centroid.

Table 6.3: Sectorial coordinate approach shear centres for varying upstand plate heights on T-section

α (mm)	$\bar{x}$ (mm)	$\bar{y}$ (mm)	x_o (mm)	y_o (mm)	x_a (mm)	y_a (mm)	$\bar{y}_{sc}$ (mm)
0	0	156.68	0	40.12	0	40.12	196.80
12.5	0	159.34	0	37.46	0	36.25	195.59
25	0	162.35	0	34.45	0	30.39	192.75
37.5	0	165.66	0	31.14	0	23.29	188.95
50	0	169.23	0	27.57	0	15.33	184.56
62.5	0	173.02	0	23.78	0	6.74	179.76
75	0	177.00	0	19.80	0	-2.33	174.67
87.5	0	181.17	0	15.63	0	-11.79	169.38
100	0	185.49	0	11.31	0	-21.55	163.93

The results from the spreadsheets were also compared to results from the Prokon (ProSec) software. From table 6.4 it can be observed that the two approaches yielded results that had a minor difference in value. Also, the greater the plate heights were, the greater the difference. It is important to note that Prokon uses the shear flow approach to determine the shear centres.

Table 6.4: Sectorial coordinate approach vs Prokon shear centre results for varying upstand plate heights on T-section

	Sectorial coordinate approach			**Prokon (ProSec) software**			
α (mm)	**$\bar{x}$ (mm)**	**$\bar{y}$ (mm)**	**$\bar{y}_{sc}$ (mm)**	**$\bar{x}$ (mm)**	**$\bar{y}$ (mm)**	**$\bar{y}_{sc}$ (mm)**	**Δ $\bar{y}_{sc}$ (mm)**
0	0	156.68	196.80	0	156.70	197.00	-0.20
12.5	0	159.34	195.59	0	159.30	194.00	1.59
25	0	162.35	192.75	0	162.40	191.00	1.75
37.5	0	165.66	188.95	0	165.70	186.00	2.95
50	0	169.23	184.56	0	169.20	181.00	3.56
62.5	0	173.02	179.76	0	173.00	176.00	3.76
75	0	177.00	174.67	0	177.00	171.00	3.67
87.5	0	181.17	169.38	0	181.20	165.00	4.38
100	0	185.49	163.93	0	185.50	160.00	3.93

CHAPTER 7: DISCUSSION

7.1 Discussion

Plotting a graph of the shear centre ($\bar{y}_{sc}$) and centroid ($\bar{y}$), the behaviour of both centres as the plate heights were increased could be observed. Graph 7.1 showed that for H-Sections with no end plates resembled an H-section hence the two centres coincided. However, as the plates were introduced, the shear centre was higher than the centroid up to the range between 50 and 62.5mm of plate height from which then it fell below the centroid.

Another noticeable fact was that the centroid increased linearly while the shear centre followed an upward then downward curve which peaked at about 50mm height of upstand plate.

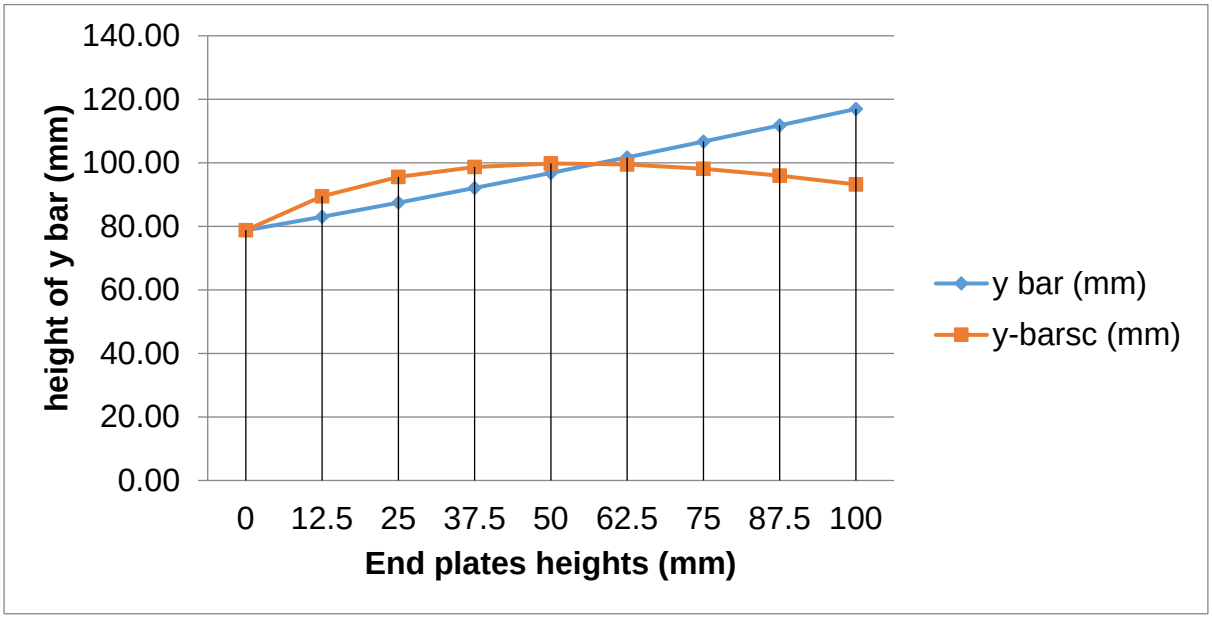

Figure 7.1: H-Section "y" bar position vs shear centre (y_sc) position

The reduction of the bottom flanges by 2/3 and 1/3 of the normal widths had an impact on the shear centre curve. While the centroid remained a linear line, the shear centre had a jump from the initial stage. For the section which was reduced to two-thirds of the bottom flange, the shear centre was 29.54mm higher than the centroid at the initial stage of no upstand plate. Whereas for the section which was reduced to one-third of the bottom flange had the shear centre positioned 43.71mm above the centroid. The H-Section which was reduced to two thirds (2/3) of the bottom width had a curve similar to the unreduced section but the shear centre curve was smoothening out from the beginning and the peak which was at 50mm of plate height now occurred at 25mm. Smoothening of the curve was more evident for the

H-Section which was reduced to one third (1/3) of the bottom flange. The peak was at the first stage were no plates were added and the decrease of the shear centre followed the decreasing pattern observed with the other two sections. Both reduced sections had the two centres coinciding in the range between 62.5 to 75mm of plate height. These behaviours can be seen in graphs 7.2 and 7.3 respectively.

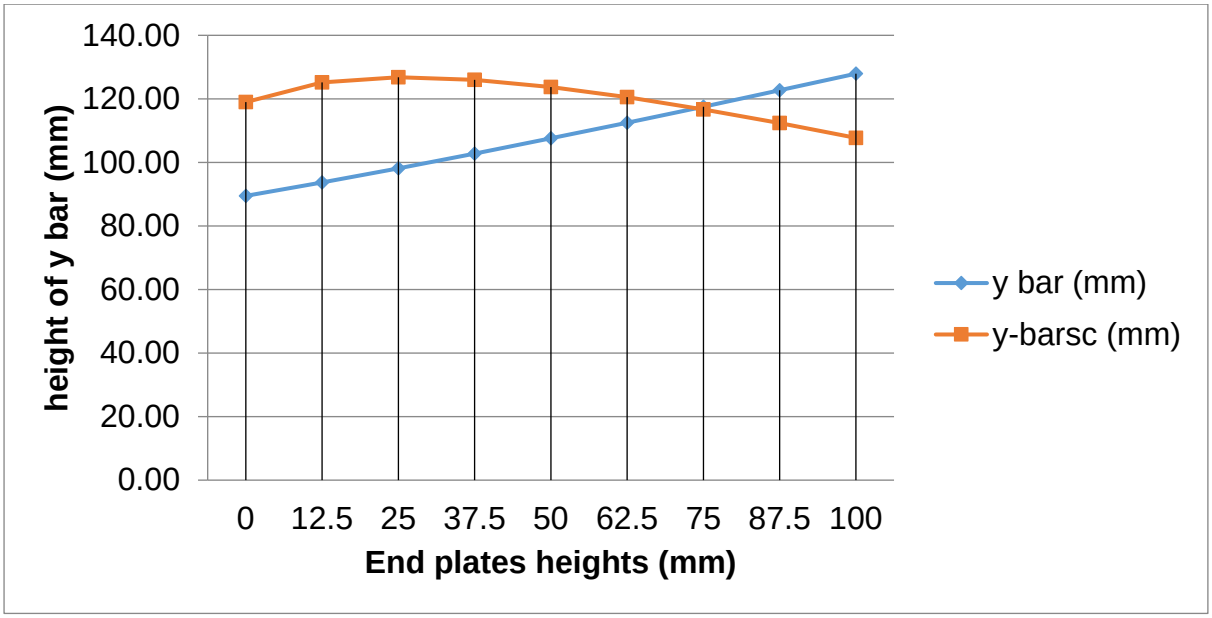

Figure 7.2: H-Section with 2/3 bottom flange "y" bar position vs shear centre (y_sc) position

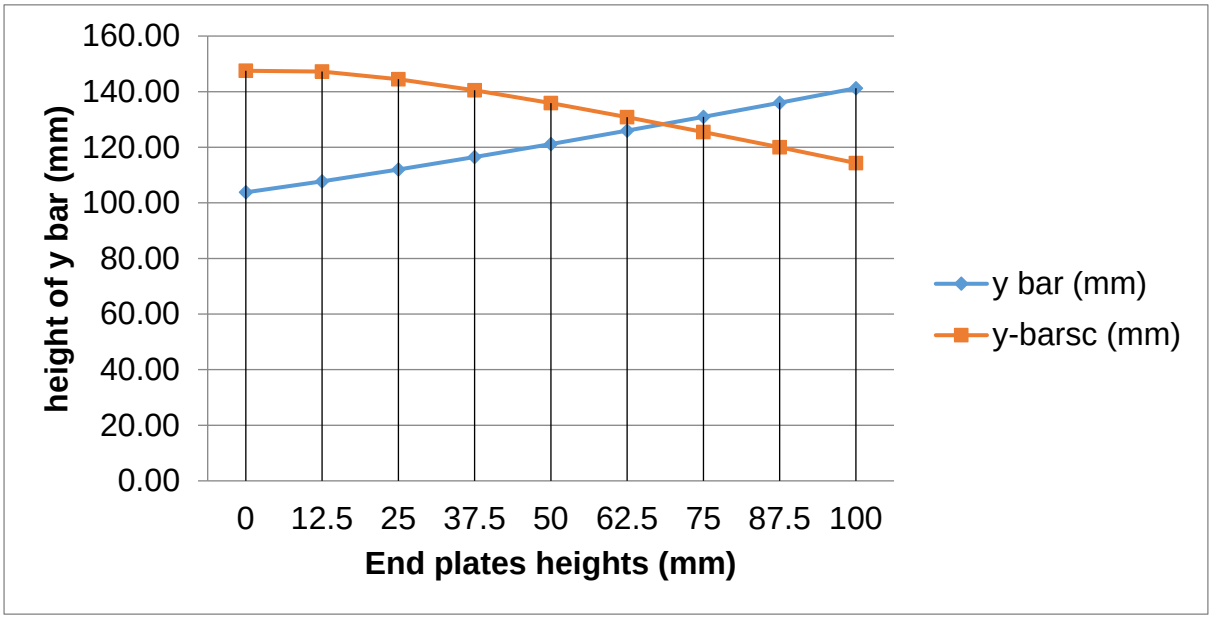

Figure 7.3: H-Section with 1/3 bottom flange "y" bar position vs shear centre (y_sc) position

The T-Section followed the trend set by the H-Section which had the bottom flange reduced to 1/3 of the normal width. The only difference was that the curve was smoother/linear than that of the aforementioned and the two curves intersected in the range of 62.5 to 75mm plate height similar to the H-Sections with reduced bottom flanges. Graph 7.4 shows the plot for the T-section.

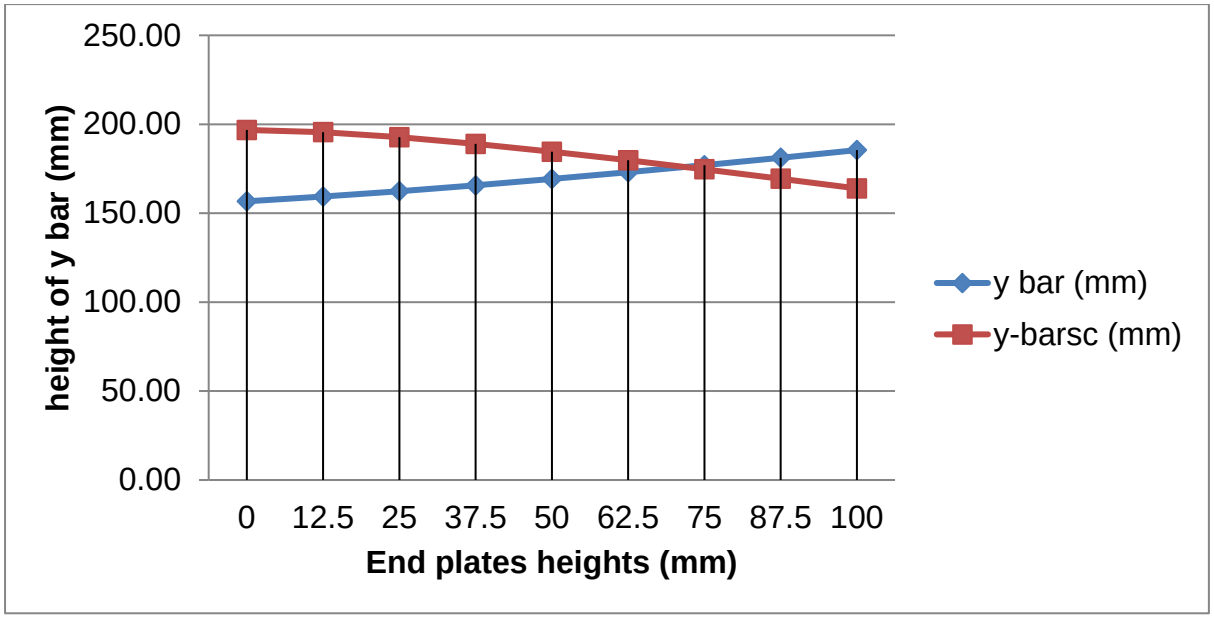

Figure 7.4: T-Section "y" bar position vs shear centre (y_sc) position

At zero plate heights, the T-Section had the shear centre at a position 40.12mm above the centroid and this was the furthest the two centres were, hence the peak.

Finally, the be variance in the results obtained by the Sectorial Area Method and that of Prokon plotted in Figures 7.5-7.8 as shown below.

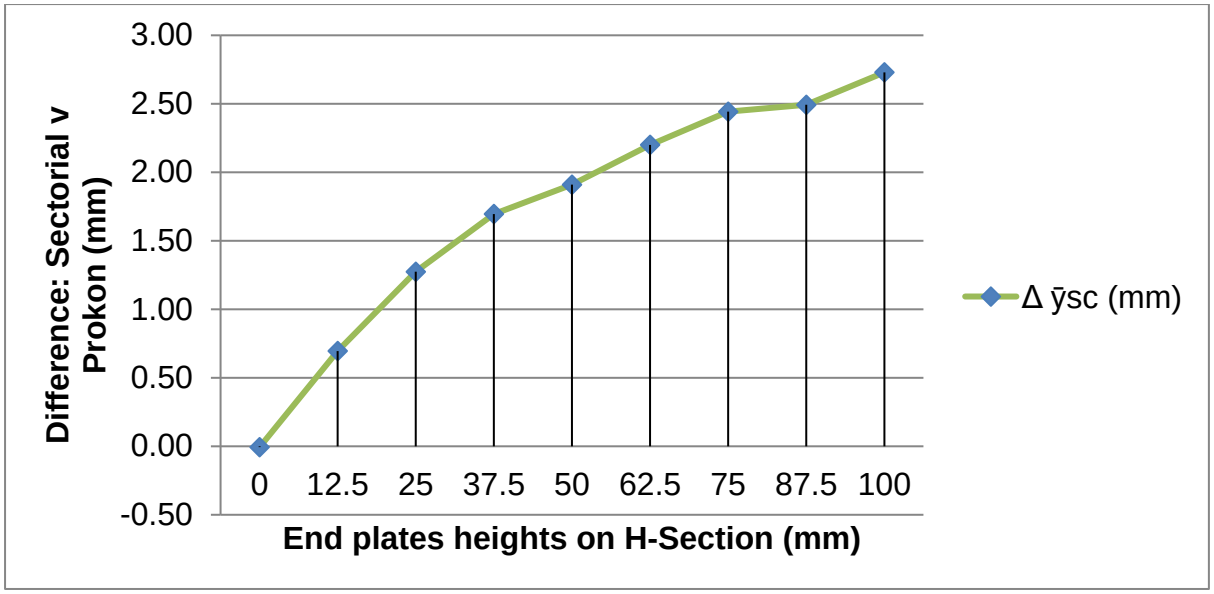

Figure 7.5: H-Section difference between Sectorial and Prokon results

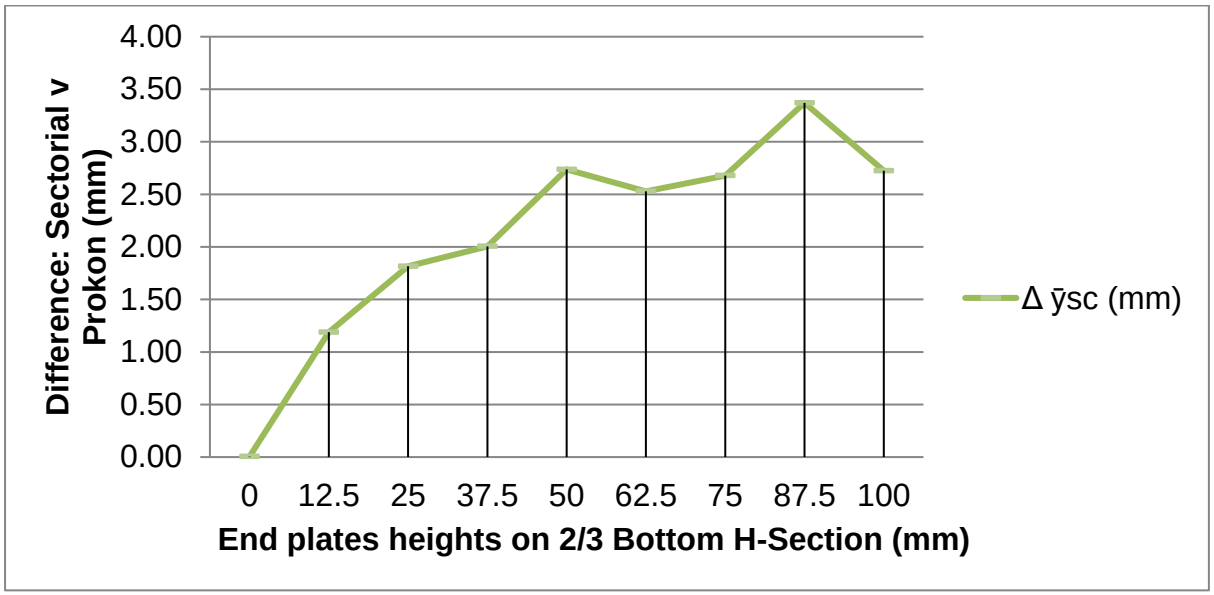

Figure 7.6: H-Section with 2/3 bottom flange difference between Sectorial and Prokon results

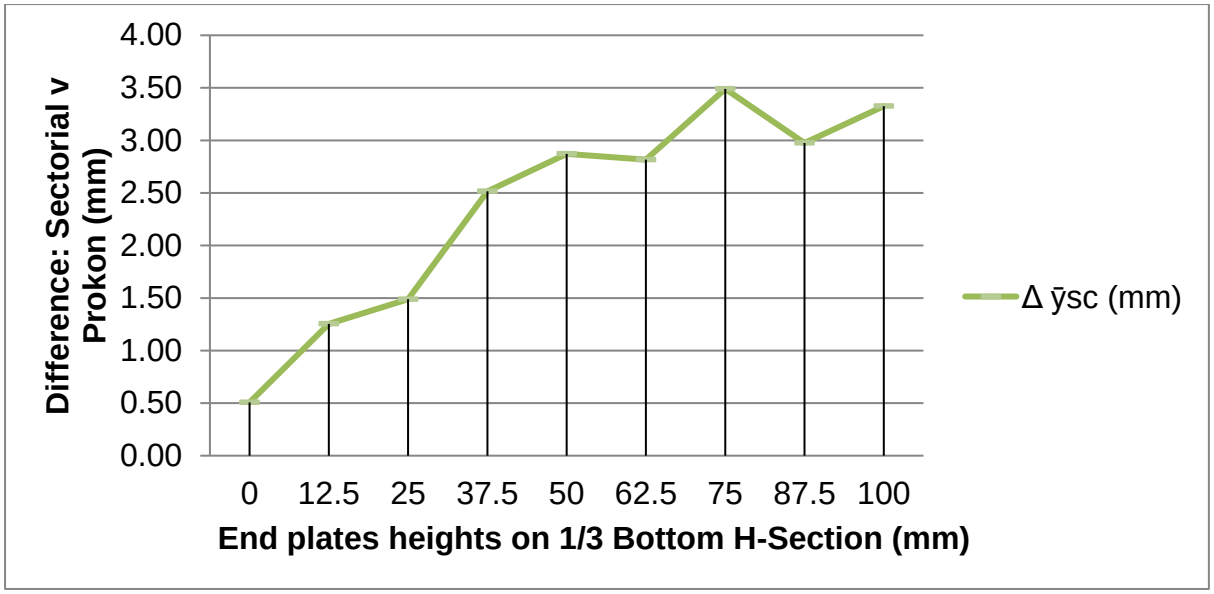

Figure 7.7: H-Section with 1/3 bottom flange difference between Sectorial and Prokon results

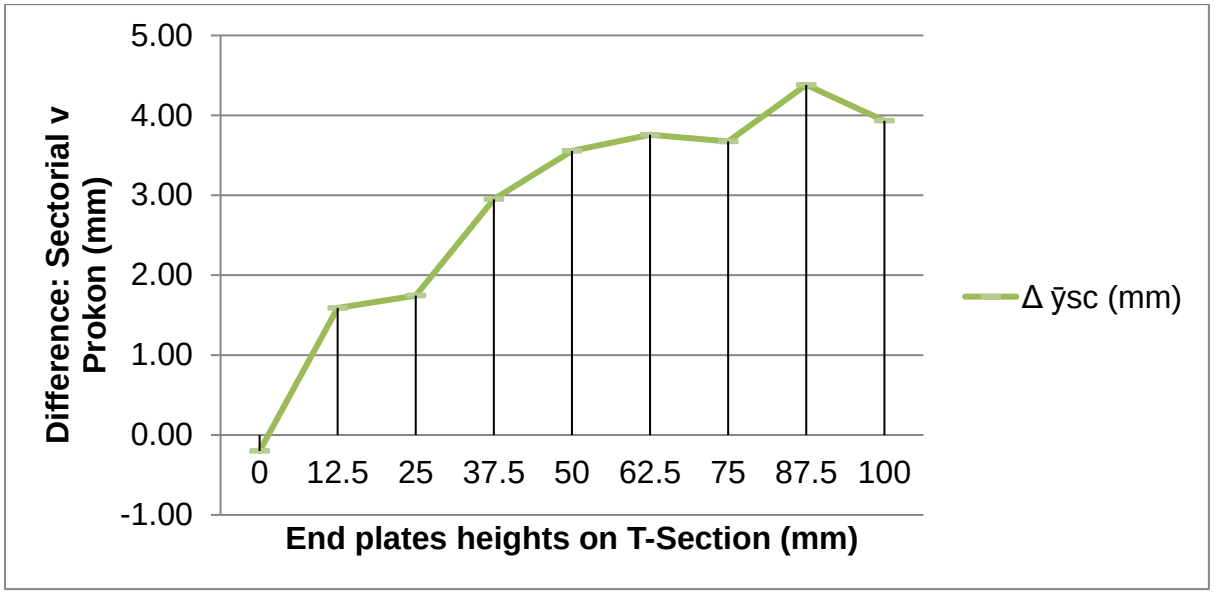

Figure 7.8: T-Section difference between Sectorial and Prokon results

From the figures above, it was noticed that the larger the end plates where, the larger the difference became for the results of the two methods. The increase followed a similar incremental pattern.

CHAPTER 8: CONCLUSION AND RECOMMENDATIONS

8.1 Conclusion

In conclusion, it is safe to say that the sectorial coordinate approach is not a challenging approach to apply. Backed up with the usage of excel spreadsheets, the method is well suited for complex problems such as the one that was just studied which is not catered by the standard formulae provided in codes of practice.

The results which are obtained using the sectorial area method are almost similar to those from the Prokon software. Differences between the results increased as the height of the end plates increased. The largest difference of about 3.1% between the two results was obtained. This was determined by finding the percentage of the shear centre difference over the Prokon results. This is not a huge difference and designers may vindicate the usage of either method.

With regards to the behaviour of the shear centres and centroids of the studied non-standard monosymmetric sections, the results provide us with interesting observations. The shear centres jump at the initial stages (no upstand plate) were larger as the bottom flanges were reduced, hence the gap between the two centres, the shear centre and centroid become more. Noticeably, the H-Section with a 1/3 bottom flange has a jump that is 3.59mm higher than that of the T-Section. Hence this then informs us that there is an optimum width that will yield the highest initial jump and this width may lie in the range between the 2/3 & 1/3 width respectively. Also, as the bottom flanges are reduced, the shear centre plot follows a path that is less curved.

All sections resulted in having the shear centre below the centroid due to the height of the plates increases. For the H-section, this occurs in the range of 50 to 62.5mm of plate height. Whereas for the other sections, this occurs in the range of 62.5 to 70mm of plate height.

The envelope between the shear centre and the centroid for the case when the shear centre is above the centroid, this envelope is least for the H-section. Thus, the shear centre is not that much higher above the centroid for plate heights up to under 60mm as compared to the other sections with reduced widths for the bottom flanges which have a much wider envelope as the shear centres are much higher than the centroids. This, in turn, may yield an effect on the constant of monosymmetry as it is related to the distance between the two centres. Hence, the higher envelope may have a correlation with the value of the constant on monosymmetry which was not part of this study.

Knowing the positions of shear centres informs the designers as to where to place any horizontal loads as well should there be any to prevent twisting of members due to the loads.

8.2 Recommendations

The usage of the Sectorial coordinate approach is highly recommended as it offers solutions that are comparable to those of the Prokon software. Furthermore, a study using Finite Element Modelling (FEM) programs must be conducted to validate the 3.1% difference obtained between the results from the Prokon Software and the sectorial coordinate approach. Also, to address the query of why an increase in end plate heights results in an increase in the difference of the results.

Employment of upstanding plates offers stability opportunities, and these should be investigated further to determine what the load-carrying capacities of the different sections would be. Also, considering the stability of the plates with the heights increased should be looked into as the higher the plates are, the slenderer they become hence the more prone they are to buckling.

The H-section with upstanding plates offers itself as a section that has an envelope (gap) between the shear centre and centroid when the shear centre is above the centroid which is much lesser than the other sections. A study is to be conducted to determine the effect on the lateral-torsional buckling resistance of a section with a smaller envelope and that of a larger envelope. In so doing, an optimum section and plate height that provides better resistance to lateral-torsional buckling may be obtained. This too will guide designers as to what envelope ranges, they should be working with for better economy.

CHAPTER 9: References

Chan, W. & Syed, K., 2009. Determination of centroid and shear centre locations of composite box beams. *ICCM International conferences on composite materials*, 01.

Jennings, A., 2004. *Structures: From theory to practice.* 1st ed. New York: Spon Press.

Mahachi, J., 2013. *Design of structural steelwork to SANS 10162.* 3rd ed. Randburg: Xsi-tek.

Morkhade, S. & Gupta, L., 2013. Effect of load height on buckling resistance of steel beams. *Procedia Engineering,* Issue 51, pp. 151-158.

Mudenda, K. & Zingoni, A., 2018. Lateral-torsional buckling behavior of hot-rolled steel beams with flange upstands. *Journal of constructional steel research,* Volume 144, pp. 53-64.

Pilkey, W. D. & Kitis, L., 1996. *Notes on the linear analysis of thin-walled beams,* Charlottesville: University of Virginia.

Prokon, 2013. *Version W3.1.05,* Randburg: Xsi-tek.

SASCH, S. A. I. o. S. C., 2013. *Southern african steel construction handbook.* 8th ed. s.l.:Southern African Institude of Steel Construction.

Shama, M., 1974. *Calculation of sectorial properties, shear centre and warping constant of open sections,* Alexandria: M.K. Aleandria Press.

Trahair, N., 2011. *Wagner's beam cycle,* Sydnew: School of Civil Engineering, The University of Sydney.

Yilmaz, T. & Kirac, N., 2016. On the evaluation of critical lateral-torsional buckling loads of monosymmetric beam-columns. *International journal of Civil and Environmental Engineering,* 10(7).

Zhang, W.-F., Liu, Y.-C., Chen, K.-S. & Deng, Y., 2017. Dimensionless analytical solution and new design formula for lateral-torsional buckling of I-beams under linear distributed moment via linear stability theory. *Hindawi,* 2017(ID 4838613).

APPENDIX A: EXCEL SPREADSHEET DATA

Below is the general geometry figure of the H-section and tables extracted from Excel that were used to determine the shear centres.

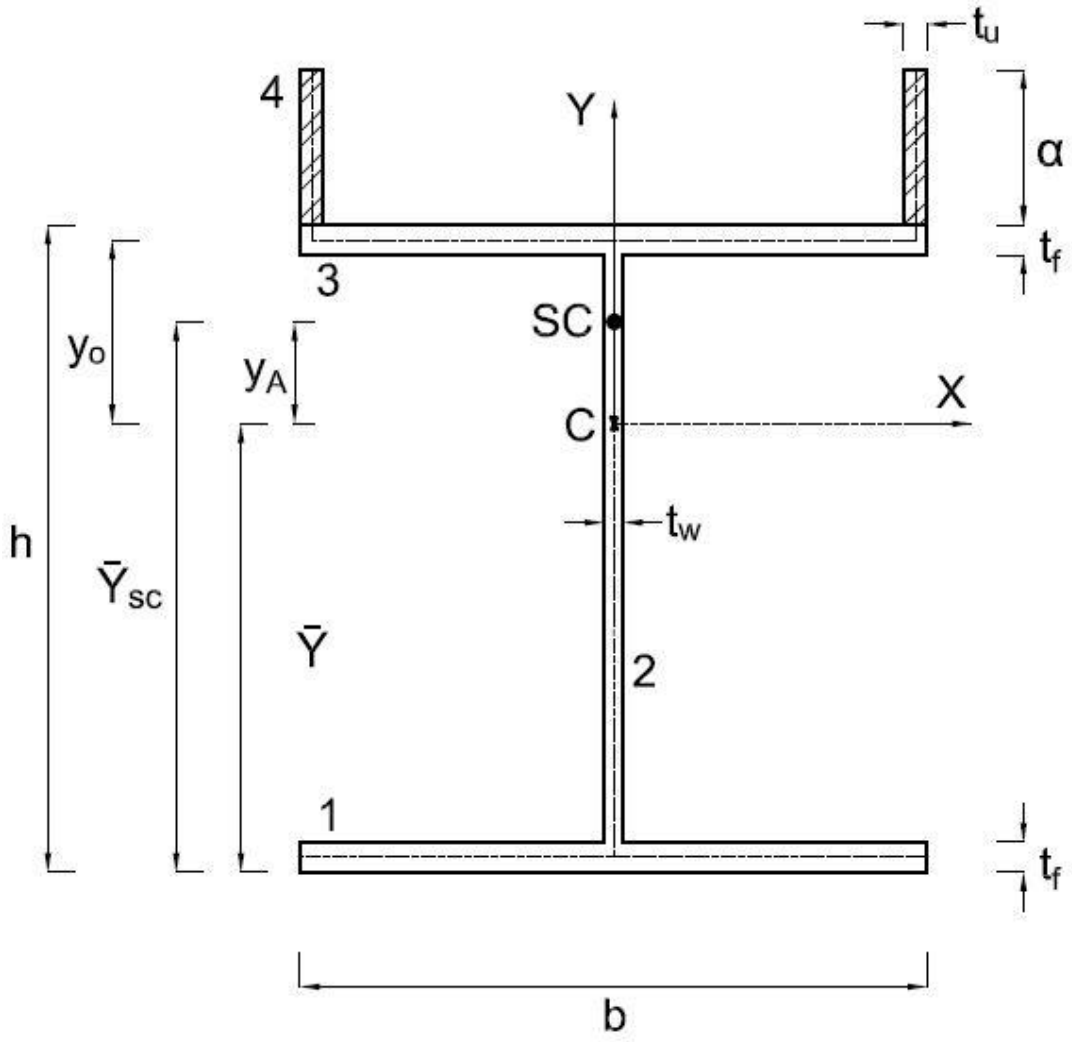

Section	152x152x30 UC								
h (mm)	157.5			I_x (mm4)	17,500,000				
b (mm)	152.9			I_y (mm4)	5,600,000				
t_w (mm)	6.6								
t_f (mm)	9.4								
α incriment (mm)	12.5								
α (mm)	0	12.5	25	37.5	50	62.5	75	87.5	100
t_u (mm)	8	8	8	8	8	8	8	8	8
Output from equations									
First Moments of Areas									
x bar (mm)	**0**	**0**	**0**	**0**	**0**	**0**	**0**	**0**	**0**
y bar (mm)	**78.75**	**83.01**	**87.46**	**92.08**	**96.83**	**101.71**	**106.71**	**111.79**	**116.97**
Second Moments of Areas									
I_{x1}	7,891,658	8,824,678	9,855,009	10,983,419	12,210,756	13,537,889	14,965,668	16,494,912	18,126,393
I_{x2}	1,467,547	1,484,165	1,537,016	1,630,108	1,766,886	1,950,323	2,182,995	2,467,142	2,804,718
I_{x3}	7,891,658	7,010,821	6,146,448	5,310,355	4,512,516	3,761,398	3,064,234	2,427,242	1,855,788
I_{x4}	0	1,306,371	2,745,885	4,321,478	6,037,731	7,900,647	9,917,444	12,096,381	14,446,611
I_{xTotal} (mm^4)	**17,250,863**	**18,626,035**	**20,284,358**	**22,245,359**	**24,527,889**	**27,150,257**	**30,130,342**	**33,485,677**	**37,233,511**
I_{y1}	2,800,071	2,800,071	2,800,071	2,800,071	2,800,071	2,800,071	2,800,071	2,800,071	2,800,071
I_{y2}	3,323	3,323	3,323	3,323	3,323	3,323	3,323	3,323	3,323
I_{y3}	2,800,071	2,800,071	2,800,071	2,800,071	2,800,071	2,800,071	2,800,071	2,800,071	2,800,071
I_{y4}	0	1,050,867	2,101,734	3,152,602	4,203,469	5,254,336	6,305,203	7,356,070	8,406,937
I_{yTotal} (mm^4)	**5,603,465**	**6,654,332**	**7,705,200**	**8,756,067**	**9,806,934**	**10,857,801**	**11,908,668**	**12,959,535**	**14,010,403**
A	79	74	70	65	61	56	51	46	41
B	74	78	83	87	92	97	102	107	112
C	72	72	72	72	72	72	72	72	72

Sectorial Product Areas									
α (mm)	0	12.5	25	37.5	50	62.5	75	87.5	100
$I_{x\omega o2}$	0	3,280,627	13,122,506	29,525,639	52,490,025	82,015,664	118,102,556	160,750,702	209,960,100
$I_{x\omega o4}$	0	3,280,627	13,122,506	29,525,639	52,490,025	82,015,664	118,102,556	160,750,702	209,960,100
$I_{x\omega o6}$	207,345,267	207,345,267	207,345,267	207,345,267	207,345,267	207,345,267	207,345,267	207,345,267	207,345,267
$I_{x\omega o7}$	207,345,267	207,345,267	207,345,267	207,345,267	207,345,267	207,345,267	207,345,267	207,345,267	207,345,267
$I_{x\omega oTotal}$	**414,690,534**	**421,251,787**	**440,935,547**	**473,741,812**	**519,670,584**	**578,721,862**	**650,895,647**	**736,191,937**	**834,610,734**
$I_{y\omega o2}$	0	-3,750,312	-15,704,502	-36,850,637	-68,103,223	-110,318,562	-164,306,415	-230,838,973	-310,657,825
$I_{y\omega o4}$	0	3,750,312	15,704,502	36,850,637	68,103,223	110,318,562	164,306,415	230,838,973	310,657,825
$I_{y\omega o6}$	301,254,095	318,587,762	336,694,033	355,467,312	374,820,406	394,680,687	414,987,169	435,688,269	456,740,057
$I_{y\omega o7}$	-301,254,095	-318,587,762	-336,694,033	-355,467,312	-374,820,406	-394,680,687	-414,987,169	-435,688,269	-456,740,057
$I_{y\omega oTotal}$	**0**	**0**	**0**	**0**	**0**	**0**	**0**	**0**	**0**
Origin Co-ordinates from Centroid									
x_o (mm)	0	0	0	0	0	0	0	0	0
y_o (mm)	74.05	69.79	65.34	60.72	55.97	51.09	46.09	41.01	35.83
Shear Centre Co-ordinates from Centroid									
x_a (mm)	0	0	0	0	0	0	0	0	0
y_a (mm)	0.04	6.48	8.11	6.62	2.98	-2.21	-8.56	-15.80	-23.74
Shear Centre from bottom of Section									
y-bar$_{sc}$ (mm)	78.79	89.50	95.57	98.70	99.81	99.50	98.14	95.99	93.23

Below is the general geometry figure of the H-section with 2/3 width of the bottom flange and tables extracted from Excel that were used to determine the shear centres.

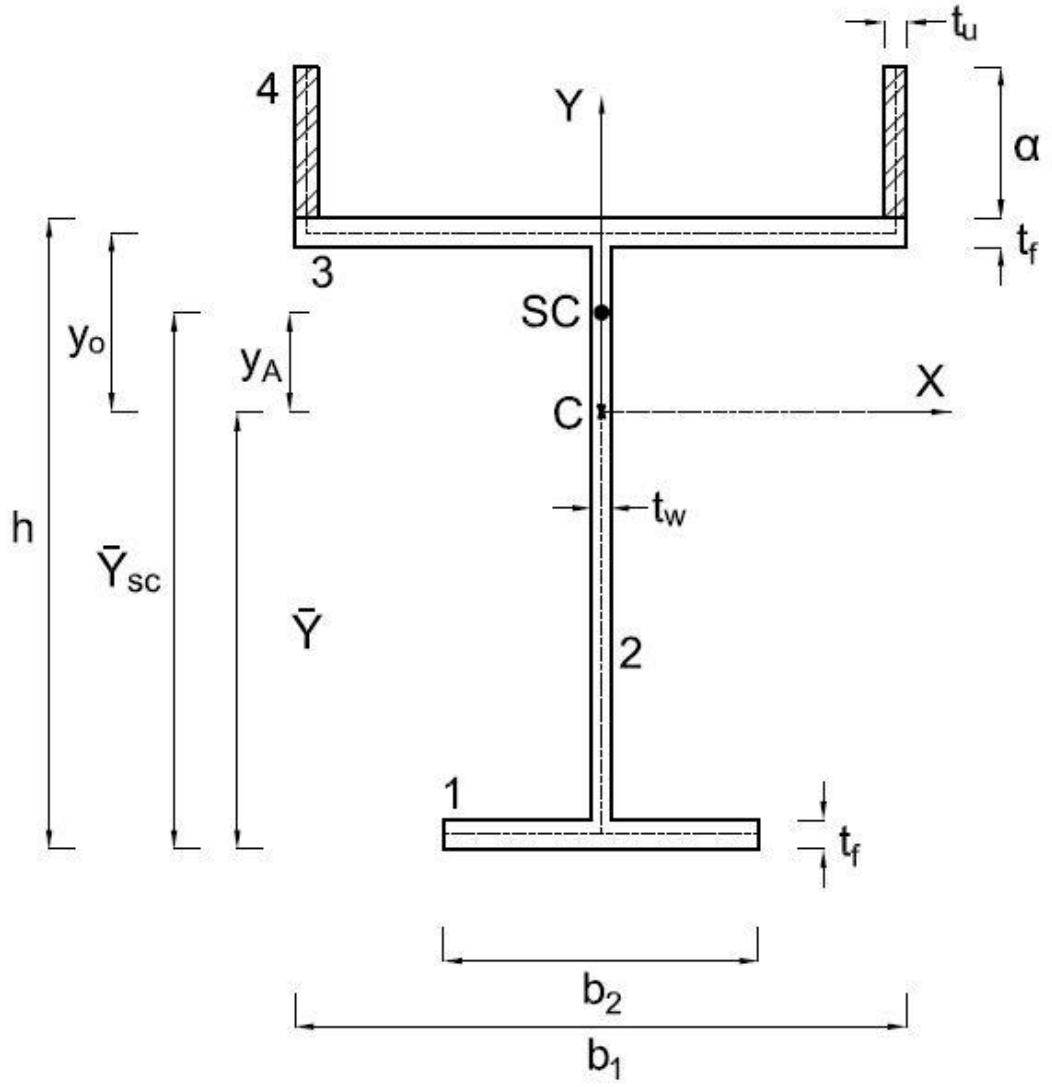

Section	152x152x30 UC								
h (mm)	157.5			I_x (mm4)	17,500,000				
b_1 (mm)	152.9			I_y (mm4)	5,600,000				
b_2 (mm)	101.9	2/3 of bottom flange ... 101,9mm							
t_w (mm)	6.6								
t_f (mm)	9.4								
α incriment (mm)	12.5								
α (mm)	0	12.5	25	37.5	50	62.5	75	87.5	100
t_u (mm)	8	8	8	8	8	8	8	8	8
Output from equations									
First Moments of Areas									
x bar (mm)	**0**	**0**	**0**	**0**	**0**	**0**	**0**	**0**	**0**
y bar (mm)	**89.47**	**93.70**	**98.15**	**102.79**	**107.58**	**112.50**	**117.55**	**122.69**	**127.93**
Second Moments of Areas									
I_{x1}	6,890,709	7,595,088	8,372,679	9,222,773	10,144,975	11,139,094	12,205,068	13,342,920	14,552,726
I_{x2}	1,572,809	1,672,278	1,812,219	1,996,478	2,228,322	2,510,538	2,845,509	3,235,285	3,681,634
I_{x3}	5,774,404	5,029,837	4,302,497	3,605,531	2,949,793	2,344,316	1,796,679	1,313,281	899,564
I_{x4}	0	983,869	2,085,569	3,308,357	4,657,285	6,138,917	7,761,090	9,532,711	11,463,590
I_{xTotal} (mm^4)	**14,237,921**	**15,281,072**	**16,572,964**	**18,133,139**	**19,980,375**	**22,132,864**	**24,608,346**	**27,424,198**	**30,597,513**
I_{y1}	828,837	828,837	828,837	828,837	828,837	828,837	828,837	828,837	828,837
I_{y2}	3,323	3,323	3,323	3,323	3,323	3,323	3,323	3,323	3,323
I_{y3}	2,800,071	2,800,071	2,800,071	2,800,071	2,800,071	2,800,071	2,800,071	2,800,071	2,800,071
I_{y4}	0	1,050,867	2,101,734	3,152,602	4,203,469	5,254,336	6,305,203	7,356,070	8,406,937
I_{yTotal} (mm^4)	**3,632,231**	**4,683,098**	**5,733,965**	**6,784,833**	**7,835,700**	**8,886,567**	**9,937,434**	**10,988,301**	**12,039,168**
A	68	64	59	55	50	45	40	35	30
B	85	89	93	98	103	108	113	118	123
C	72	72	72	72	72	72	72	72	72

Sectorial Product Areas									
α (mm)	0	12.5	25	37.5	50	62.5	75	87.5	100
$I_{x\omega o2}$	0	3,280,627	13,122,506	29,525,639	52,490,025	82,015,664	118,102,556	160,750,702	209,960,100
$I_{x\omega o4}$	0	3,280,627	13,122,506	29,525,639	52,490,025	82,015,664	118,102,556	160,750,702	209,960,100
$I_{x\omega o6}$	61,375,384	61,375,384	61,375,384	61,375,384	61,375,384	61,375,384	61,375,384	61,375,384	61,375,384
$I_{x\omega o7}$	61,375,384	61,375,384	61,375,384	61,375,384	61,375,384	61,375,384	61,375,384	61,375,384	61,375,384
$I_{x\omega oTotal}$	**122,750,768**	**129,312,021**	**148,995,781**	**181,802,046**	**227,730,818**	**286,782,096**	**358,955,881**	**444,252,171**	**542,670,968**
$I_{y\omega o2}$	0	-3,266,068	-13,767,782	-32,485,338	-60,318,326	-98,104,426	-146,633,134	-206,655,995	-278,894,325
$I_{y\omega o4}$	0	3,266,068	13,767,782	32,485,338	60,318,326	98,104,426	146,633,134	206,655,995	278,894,325
$I_{y\omega o6}$	153,179,219	160,825,506	168,864,945	177,237,216	185,893,735	194,794,938	203,908,275	213,206,728	222,667,676
$I_{y\omega o7}$	-153,179,219	-160,825,506	-168,864,945	-177,237,216	-185,893,735	-194,794,938	-203,908,275	-213,206,728	-222,667,676
$I_{y\omega oTotal}$	**0**	**0**	**0**	**0**	**0**	**0**	**0**	**0**	**0**
Origin Co-ordinates from Centroid									
x_o (mm)	0	0	0	0	0	0	0	0	0
y_o (mm)	63.33	59.10	54.65	50.01	45.22	40.30	35.25	30.11	24.87
Shear Centre Co-ordinates from Centroid									
x_a (mm)	0	0	0	0	0	0	0	0	0
y_a (mm)	29.53	31.48	28.66	23.22	16.16	8.02	-0.87	-10.32	-20.21
Shear Centre from bottom of Section									
y-bar$_{sc}$ (mm)	119.01	125.19	126.82	126.00	123.74	120.53	116.68	112.37	107.72

Below is the general geometry figure of the H-section with 1/3 width of the bottom flange and tables extracted from Excel that were used to determine the shear centres.

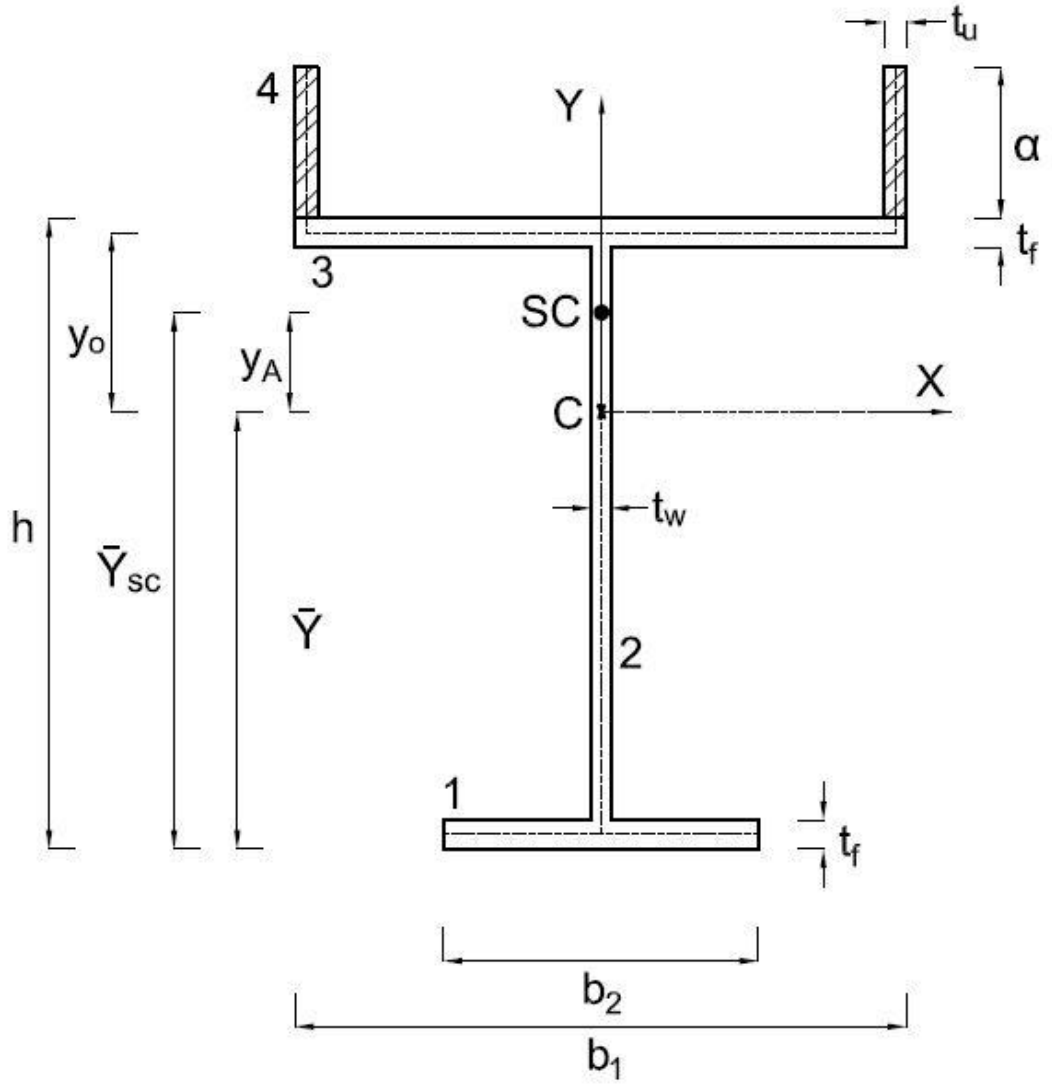

Section	152x152x30 UC								
h (mm)	157.5			I_x (mm4)	17,500,000				
b_1 (mm)	152.9			I_y (mm4)	5,600,000				
b_2 (mm)	51	1/3 of bottom flange ... 51mm							
t_w (mm)	6.6								
t_f (mm)	9.4								
α incriment (mm)	12.5								
α (mm)	0	12.5	25	37.5	50	62.5	75	87.5	100
t_u (mm)	8	8	8	8	8	8	8	8	8
Output from equations									
First Moments of Areas									
x bar (mm)	**0**	**0**	**0**	**0**	**0**	**0**	**0**	**0**	**0**
y bar (mm)	**103.80**	**107.75**	**111.99**	**116.46**	**121.13**	**125.96**	**130.94**	**136.03**	**141.23**
Second Moments of Areas									
I_{x1}	4,711,154	5,094,398	5,521,819	5,991,560	6,502,311	7,053,139	7,643,364	8,272,490	8,940,146
I_{x2}	2,041,748	2,237,402	2,478,902	2,769,431	3,111,743	3,508,205	3,960,853	4,471,435	5,041,458
I_{x3}	3,462,144	2,927,539	2,404,451	1,908,446	1,452,089	1,045,621	697,465	414,606	202,883
I_{x4}	0	629,810	1,366,966	2,215,098	3,179,635	4,267,547	5,487,100	6,847,647	8,359,444
I_{xTotal} (mm^4)	**10,215,046**	**10,889,149**	**11,772,139**	**12,884,535**	**14,245,777**	**15,874,512**	**17,788,783**	**20,006,178**	**22,543,931**
I_{y1}	103,910	103,910	103,910	103,910	103,910	103,910	103,910	103,910	103,910
I_{y2}	3,323	3,323	3,323	3,323	3,323	3,323	3,323	3,323	3,323
I_{y3}	2,800,071	2,800,071	2,800,071	2,800,071	2,800,071	2,800,071	2,800,071	2,800,071	2,800,071
I_{y4}	0	1,050,867	2,101,734	3,152,602	4,203,469	5,254,336	6,305,203	7,356,070	8,406,937
I_{yTotal} (mm^4)	**2,907,304**	**3,958,171**	**5,009,038**	**6,059,906**	**7,110,773**	**8,161,640**	**9,212,507**	**10,263,374**	**11,314,241**
A	54	50	46	41	36	32	27	21	16
B	99	103	107	112	116	121	126	131	137
C	72	72	72	72	72	72	72	72	72

Sectorial Product Areas									
α (mm)	0	12.5	25	37.5	50	62.5	75	87.5	100
$I_{x\omega o2}$	0	3,280,627	13,122,506	29,525,639	52,490,025	82,015,664	118,102,556	160,750,702	209,960,100
$I_{x\omega o4}$	0	3,280,627	13,122,506	29,525,639	52,490,025	82,015,664	118,102,556	160,750,702	209,960,100
$I_{x\omega o6}$	7,694,532	7,694,532	7,694,532	7,694,532	7,694,532	7,694,532	7,694,532	7,694,532	7,694,532
$I_{x\omega o7}$	7,694,532	7,694,532	7,694,532	7,694,532	7,694,532	7,694,532	7,694,532	7,694,532	7,694,532
$I_{x\omega oTotal}$	**15,389,064**	**21,950,317**	**41,634,076**	**74,440,342**	**120,369,114**	**179,420,392**	**251,594,176**	**336,890,467**	**435,309,264**
$I_{y\omega o2}$	0	-2,630,098	-11,262,018	-26,912,675	-50,499,670	-82,867,202	-124,804,279	-177,057,756	-240,341,846
$I_{y\omega o4}$	0	2,630,098	11,262,018	26,912,675	50,499,670	82,867,202	124,804,279	177,057,756	240,341,846
$I_{y\omega o6}$	44,852,345	46,642,324	48,560,875	50,585,522	52,698,737	54,886,655	57,138,158	59,444,231	61,797,488
$I_{y\omega o7}$	-44,852,345	-46,642,324	-48,560,875	-50,585,522	-52,698,737	-54,886,655	-57,138,158	-59,444,231	-61,797,488
$I_{y\omega oTotal}$	**0**	**0**	**0**	**0**	**0**	**0**	**0**	**0**	**0**
Origin Co-ordinates from Centroid									
x_o (mm)	0	0	0	0	0	0	0	0	0
y_o (mm)	49.00	45.05	40.81	36.34	31.67	26.84	21.86	16.77	11.57
Shear Centre Co-ordinates from Centroid									
x_a (mm)	0	0	0	0	0	0	0	0	0
y_a (mm)	43.71	39.50	32.50	24.05	14.74	4.85	-5.45	-16.06	-26.91
Shear Centre from bottom of Section									
y-bar$_{sc}$(mm)	147.51	147.25	144.49	140.52	135.87	130.82	125.49	119.98	114.33

Below is the general geometry figure of the T-section and tables extracted from Excel that were used to determine the shear centres.

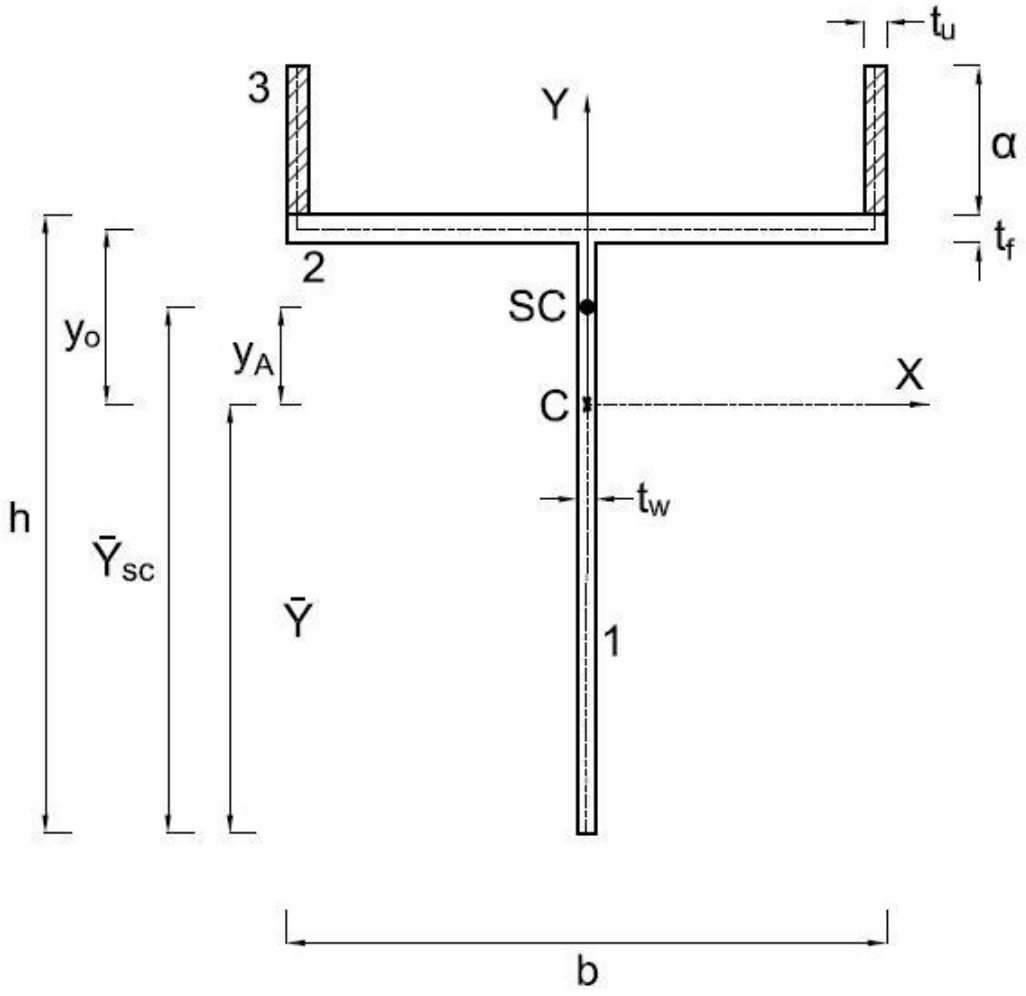

Section	203x178x30								
h (mm)	203.2			I_x (mm4)	13,800,000				
b (mm)	177.8			I_y (mm4)	6,000,000				
t_w (mm)	7.8								
t_f (mm)	12.8								
α incriment (mm)	12.5								
α (mm)	0	12.5	25	37.5	50	62.5	75	87.5	100
t_u (mm)	8	8	8	8	8	8	8	8	8
Output from equations									
First Moments of Areas									
x bar (mm)	**0**	**0**	**0**	**0**	**0**	**0**	**0**	**0**	**0**
y bar (mm)	**156.68**	**159.34**	**162.35**	**165.66**	**169.23**	**173.02**	**177.00**	**181.17**	**185.49**
Second Moments of Areas									
-	0	0	0	0	0	0	0	0	0
I_{x1}	10,100,084	10,597,193	11,183,964	11,859,712	12,624,594	13,479,288	14,424,783	15,462,240	16,592,900
I_{x2}	3,694,224	3,223,815	2,731,409	2,237,886	1,761,570	1,318,547	922,951	587,224	322,340
I_{x3}	0	504,709	1,159,149	1,971,418	2,949,101	4,099,748	5,431,148	6,951,483	8,669,400
I_{xTotal} (mm^4)	**13,794,307**	**14,325,717**	**15,074,523**	**16,069,016**	**17,335,265**	**18,897,583**	**20,778,883**	**23,000,947**	**25,584,641**
-	0	0	0	0	0	0	0	0	0
I_{y1}	7,530	7,530	7,530	7,530	7,530	7,530	7,530	7,530	7,530
I_{y2}	5,995,480	5,995,480	5,995,480	5,995,480	5,995,480	5,995,480	5,995,480	5,995,480	5,995,480
I_{y3}	0	1,442,669	2,885,337	4,328,006	5,770,675	7,213,343	8,656,012	10,098,681	11,541,349
I_{yTotal} (mm^4)	**6,003,010**	**7,445,679**	**8,888,347**	**10,331,016**	**11,773,685**	**13,216,353**	**14,659,022**	**16,101,691**	**17,544,359**
A	47	44	41	38	34	30	26	22	18
B	0	0	0	0	0	0	0	0	0
C	85	85	85	85	85	85	85	85	85

Sectorial Product Areas									
α (mm)	0	12.5	25	37.5	50	62.5	75	87.5	100
$I_{x\omega o2}$	0	4,505,006	18,020,025	40,545,056	72,080,100	112,625,156	162,180,225	220,745,306	288,320,400
$I_{x\omega o4}$	0	4,505,006	18,020,025	40,545,056	72,080,100	112,625,156	162,180,225	220,745,306	288,320,400
-	0	0	0	0	0	0	0	0	0
-	0	0	0	0	0	0	0	0	0
$I_{x\omega oTotal}$	**0**	**9,010,013**	**36,040,050**	**81,090,113**	**144,160,200**	**225,250,313**	**324,360,450**	**441,490,613**	**576,640,800**
$I_{y\omega o2}$	0	-2,769,249	-12,207,051	-29,866,529	-57,144,723	-95,315,381	-145,553,805	-208,955,930	-286,553,127
$I_{y\omega o4}$	0	2,769,249	12,207,051	29,866,529	57,144,723	95,315,381	145,553,805	208,955,930	286,553,127
-	0	0	0	0	0	0	0	0	0
-	0	0	0	0	0	0	0	0	0
$I_{y\omega oTotal}$	**0**	**0**	**0**	**0**	**0**	**0**	**0**	**0**	**0**
Origin Co-ordinates from Centroid									
x_o (mm)	0	0	0	0	0	0	0	0	0
y_o (mm)	40.12	37.46	34.45	31.14	27.57	23.78	19.80	15.63	11.31
Shear Centre Co-ordinates from Centroid									
x_a (mm)	0	0	0	0	0	0	0	0	0
y_a (mm)	40.12	36.25	30.39	23.29	15.33	6.74	-2.33	-11.79	-21.55
Shear Centre from bottom of Section									
y-bar$_{sc}$ (mm)	196.80	195.59	192.75	188.95	184.56	179.76	174.67	169.38	163.93

APPENDIX B: PROKON (PROSEC) OUTPUT OF I-BEAMS WITH UPSTANDS

0mm Upstand

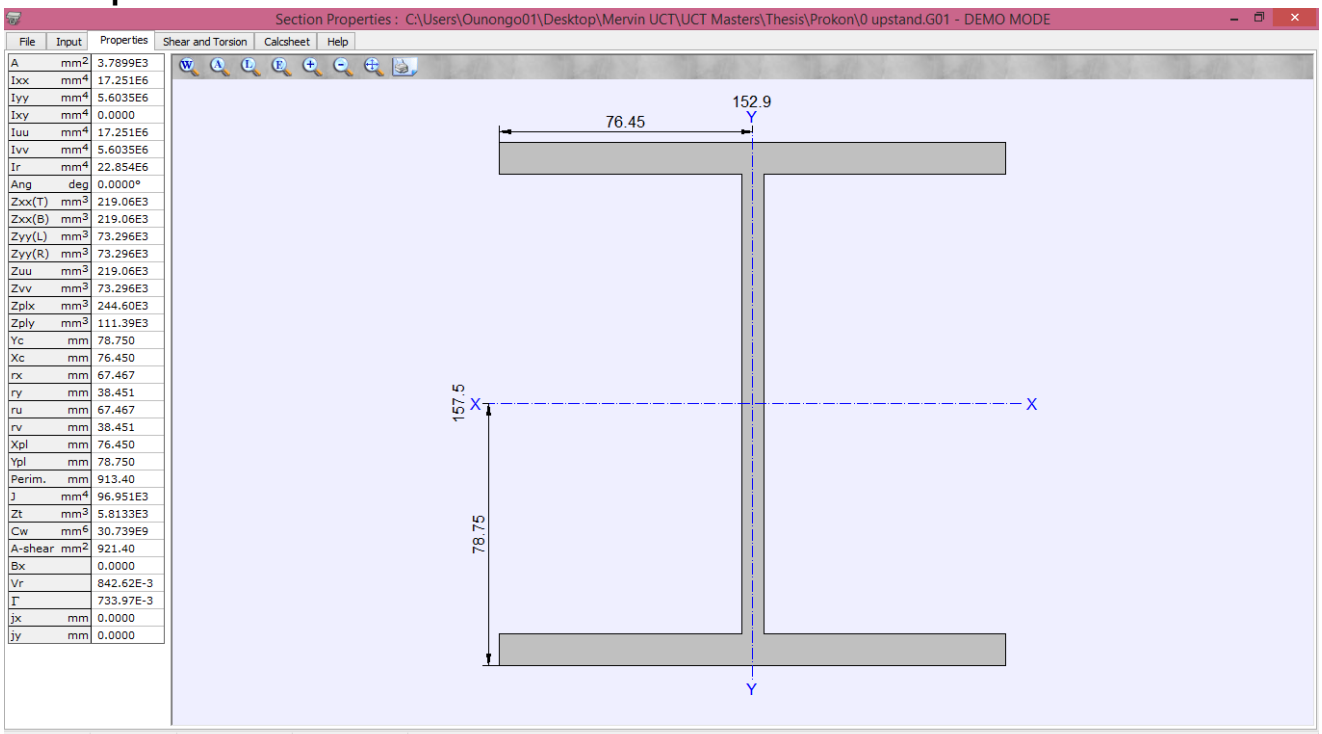

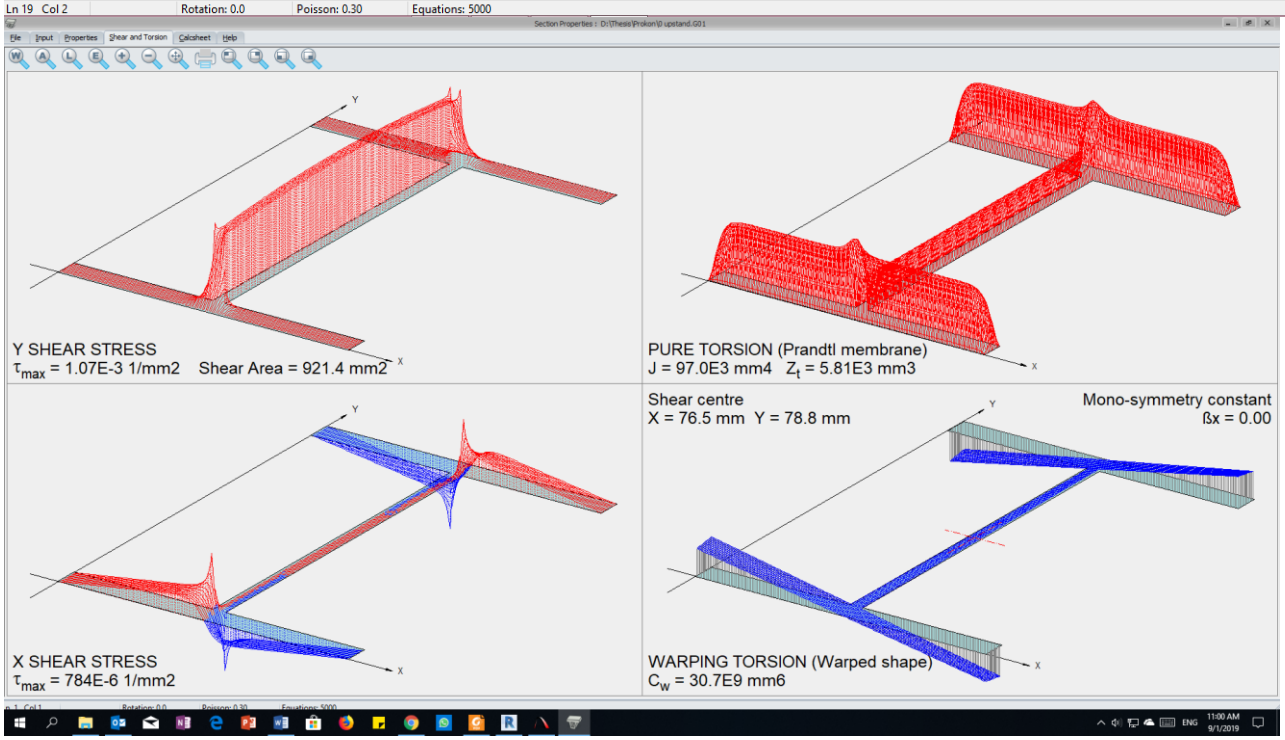

12.5mm Upstand

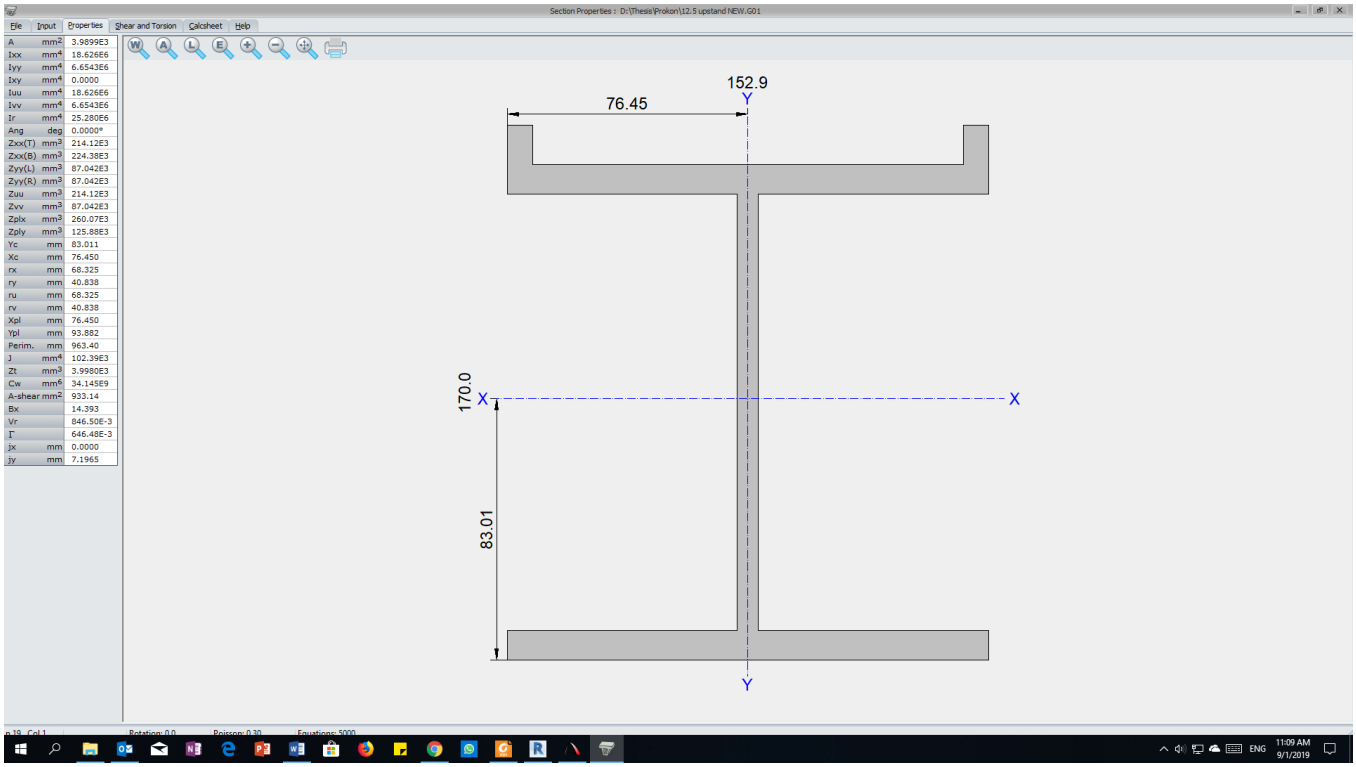

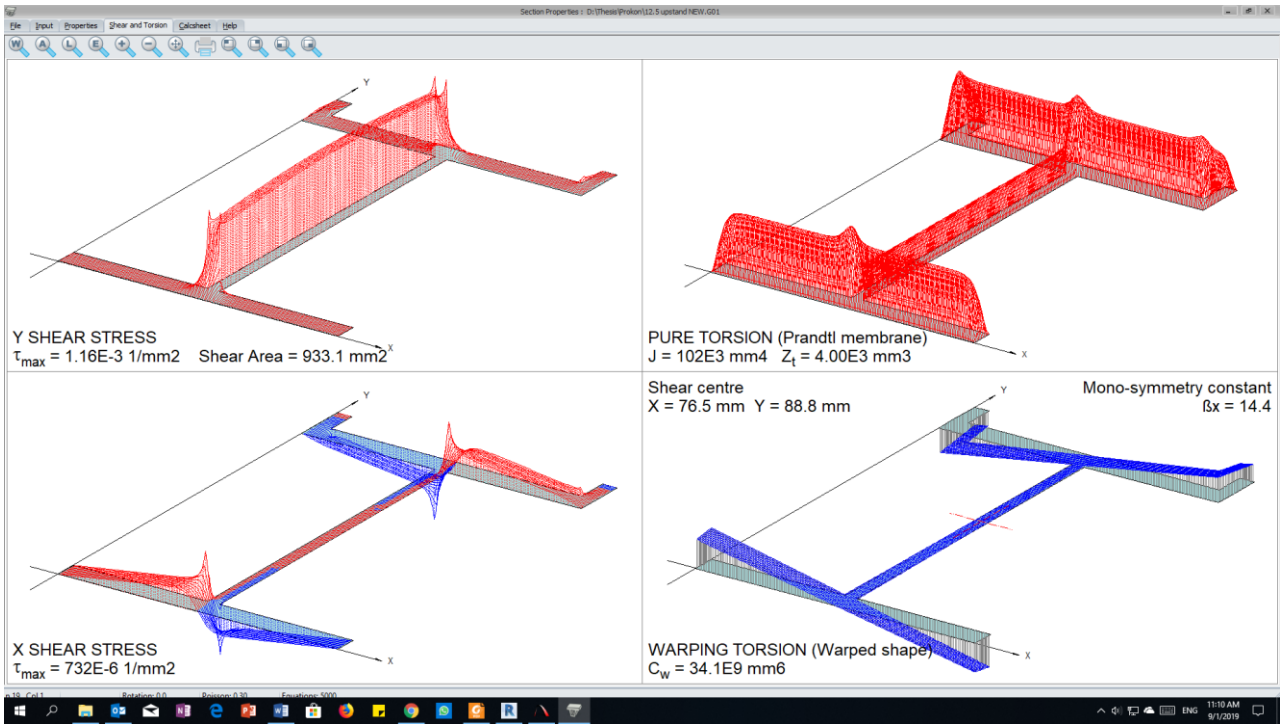

25mm Upstand

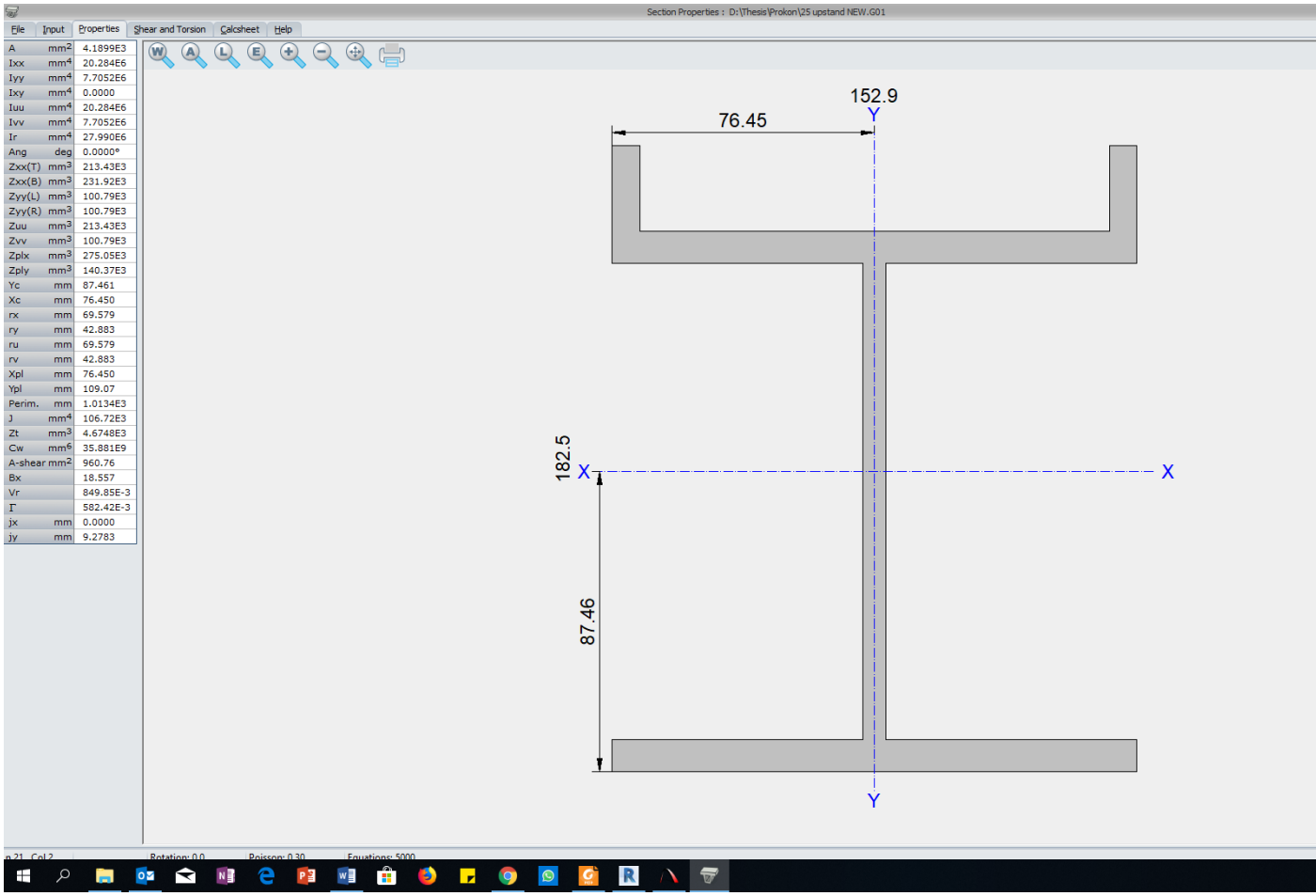

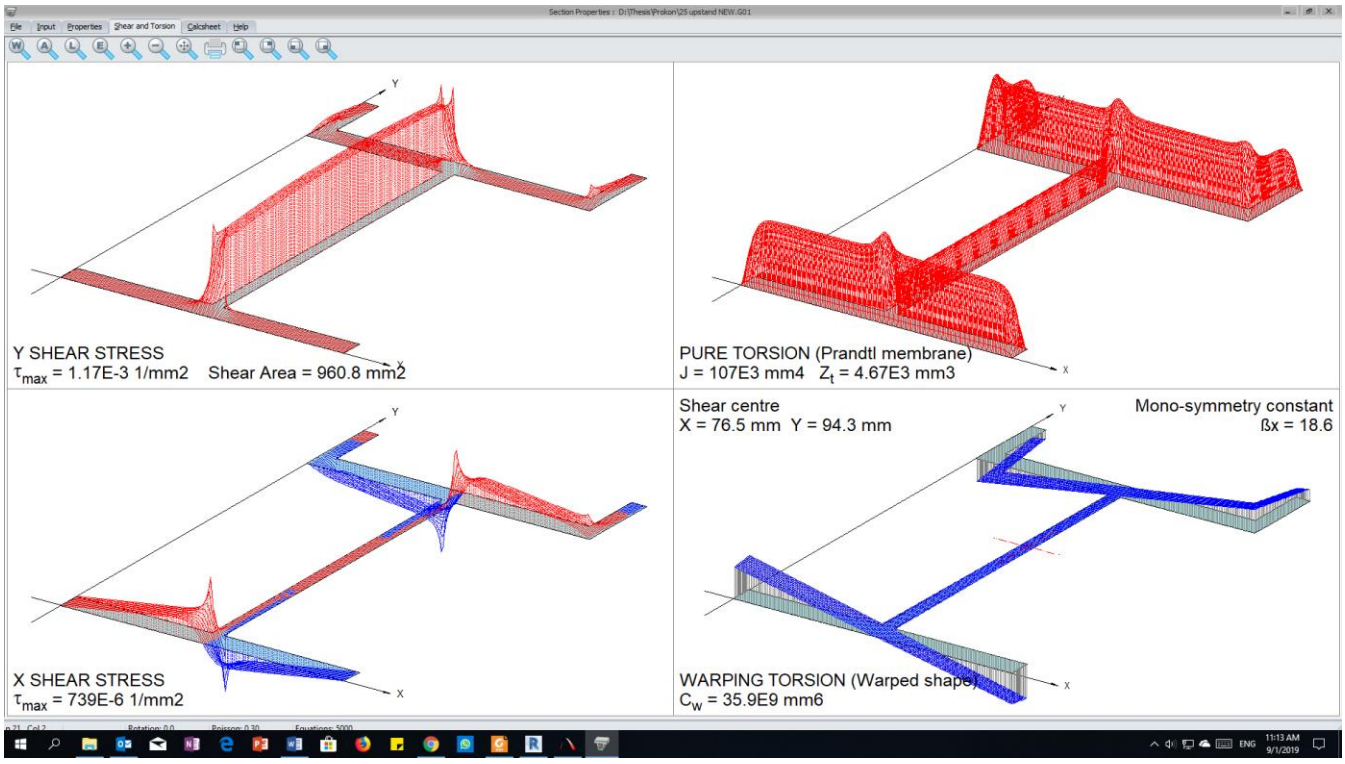

37.5mm Upstand

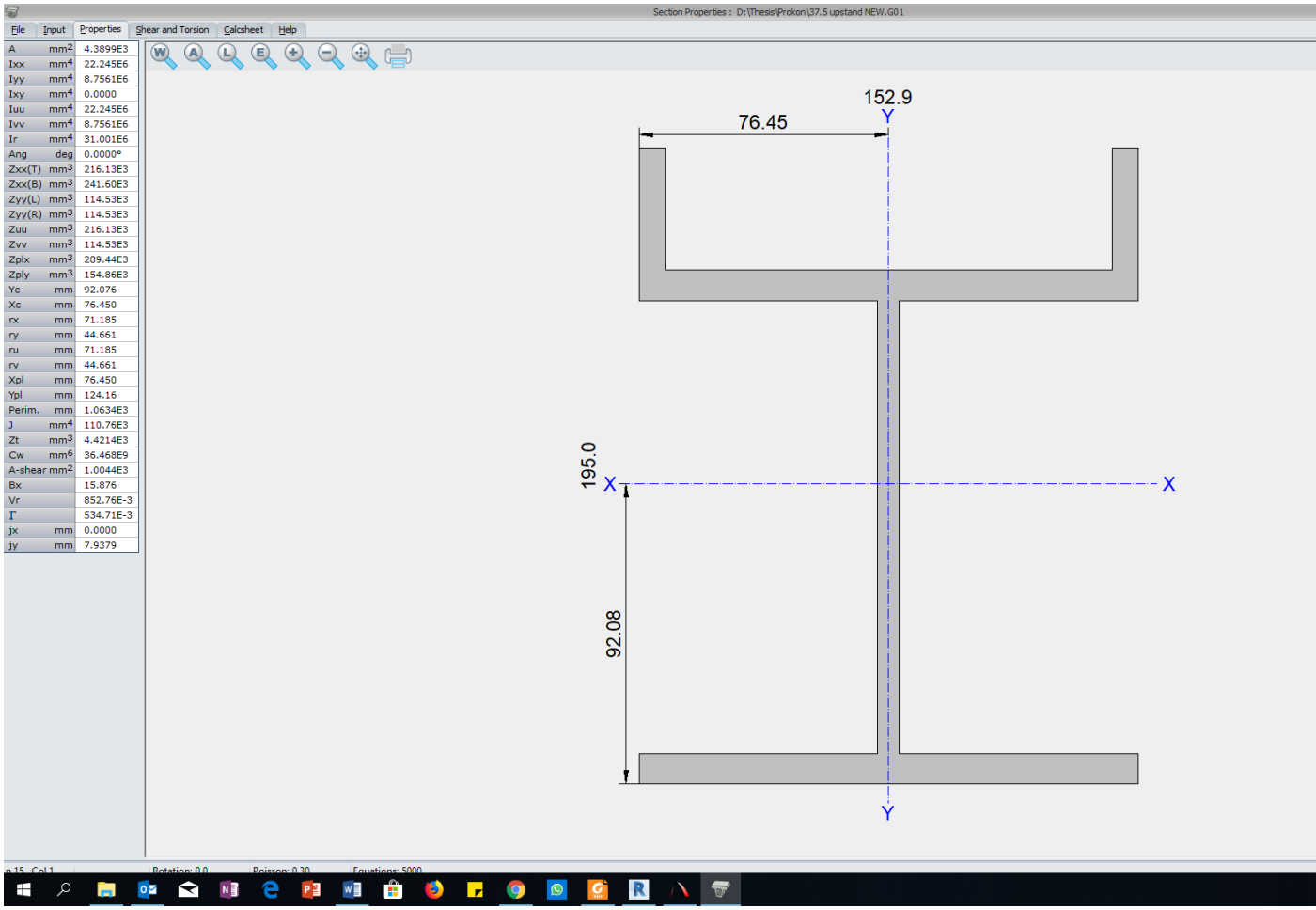

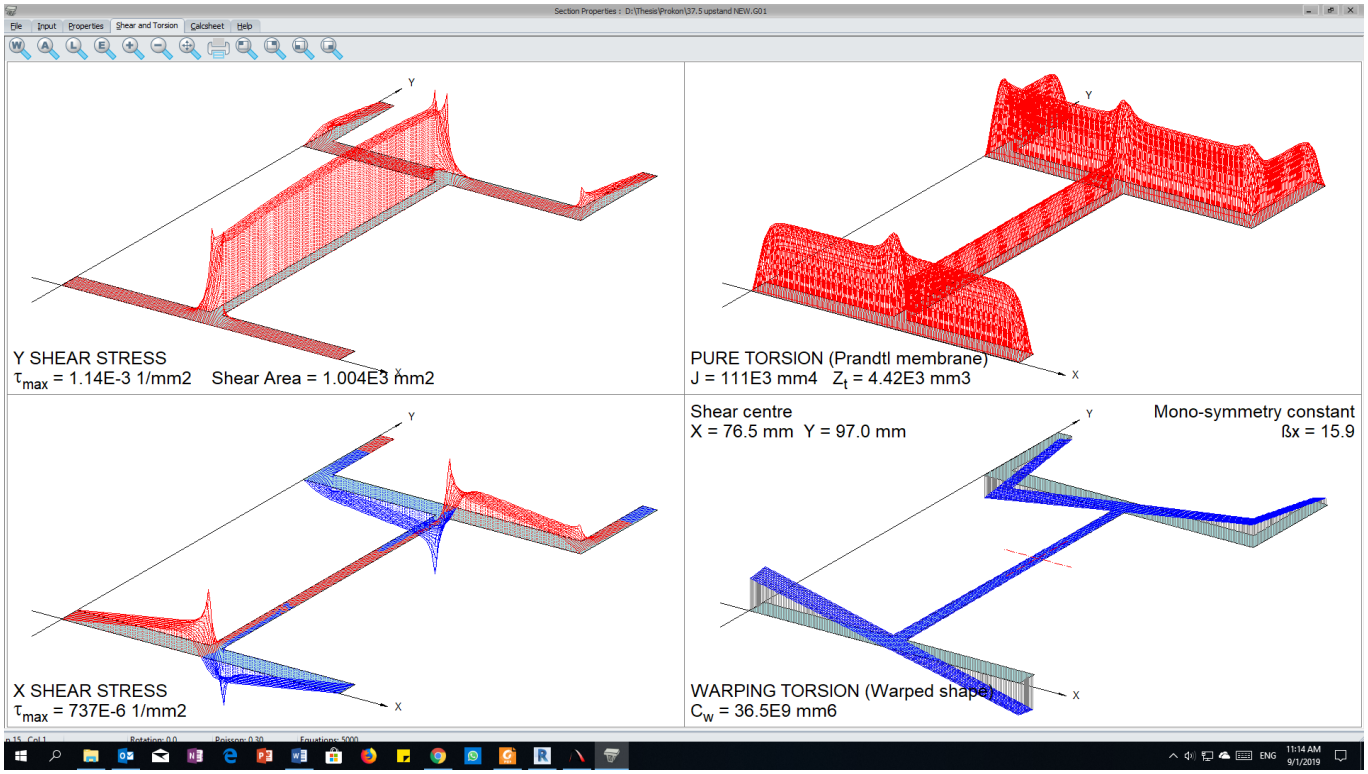

50mm Upstand

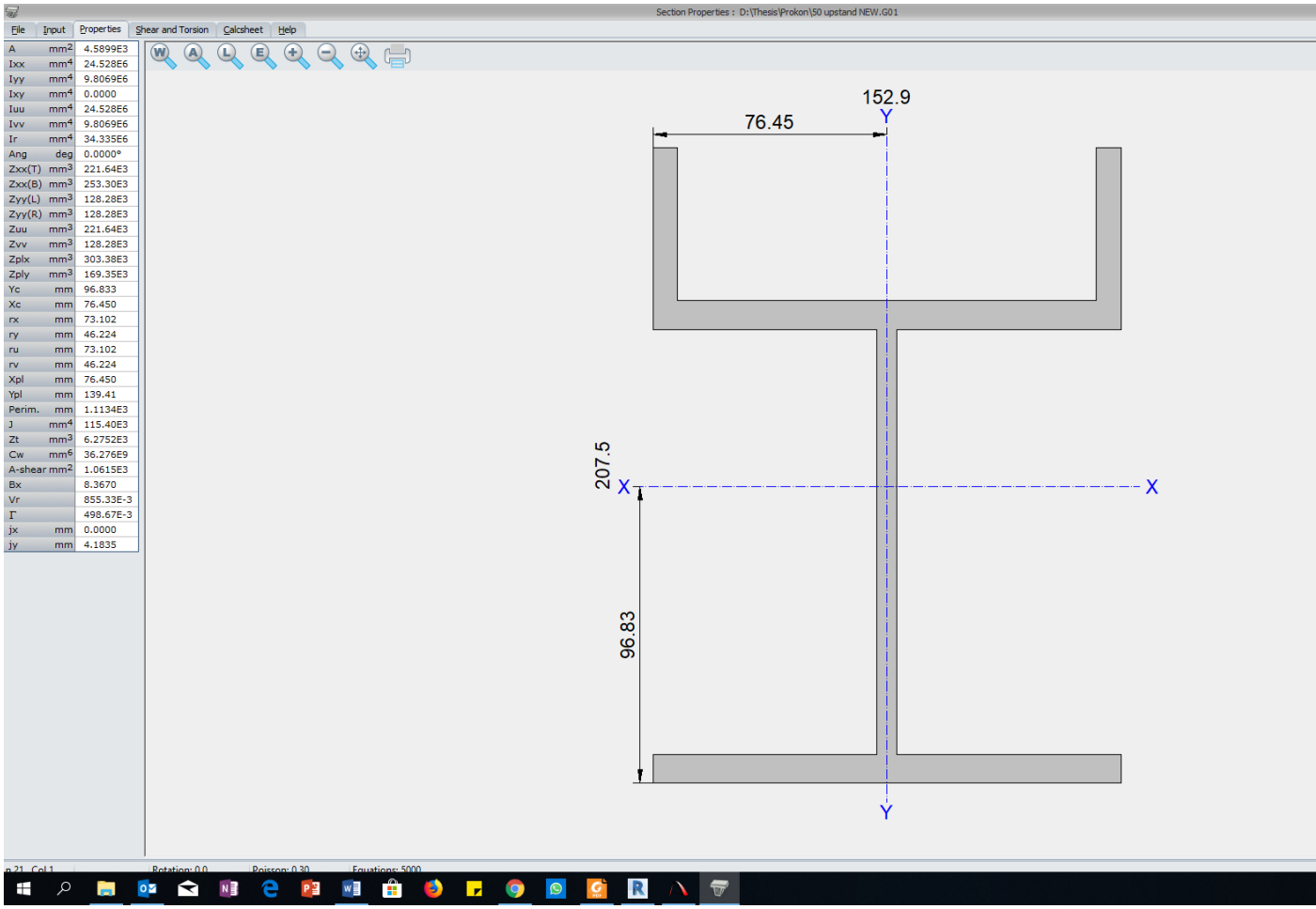

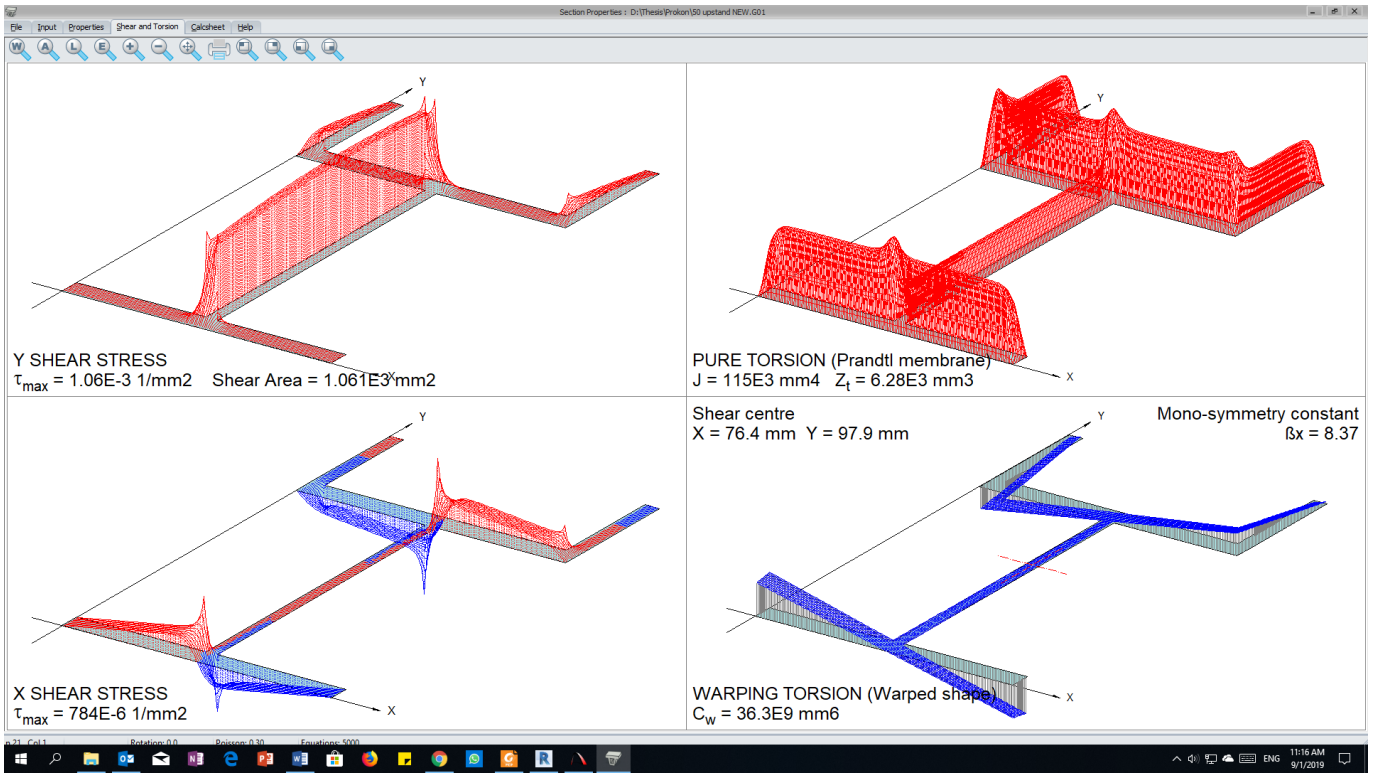

62.5mm Upstand

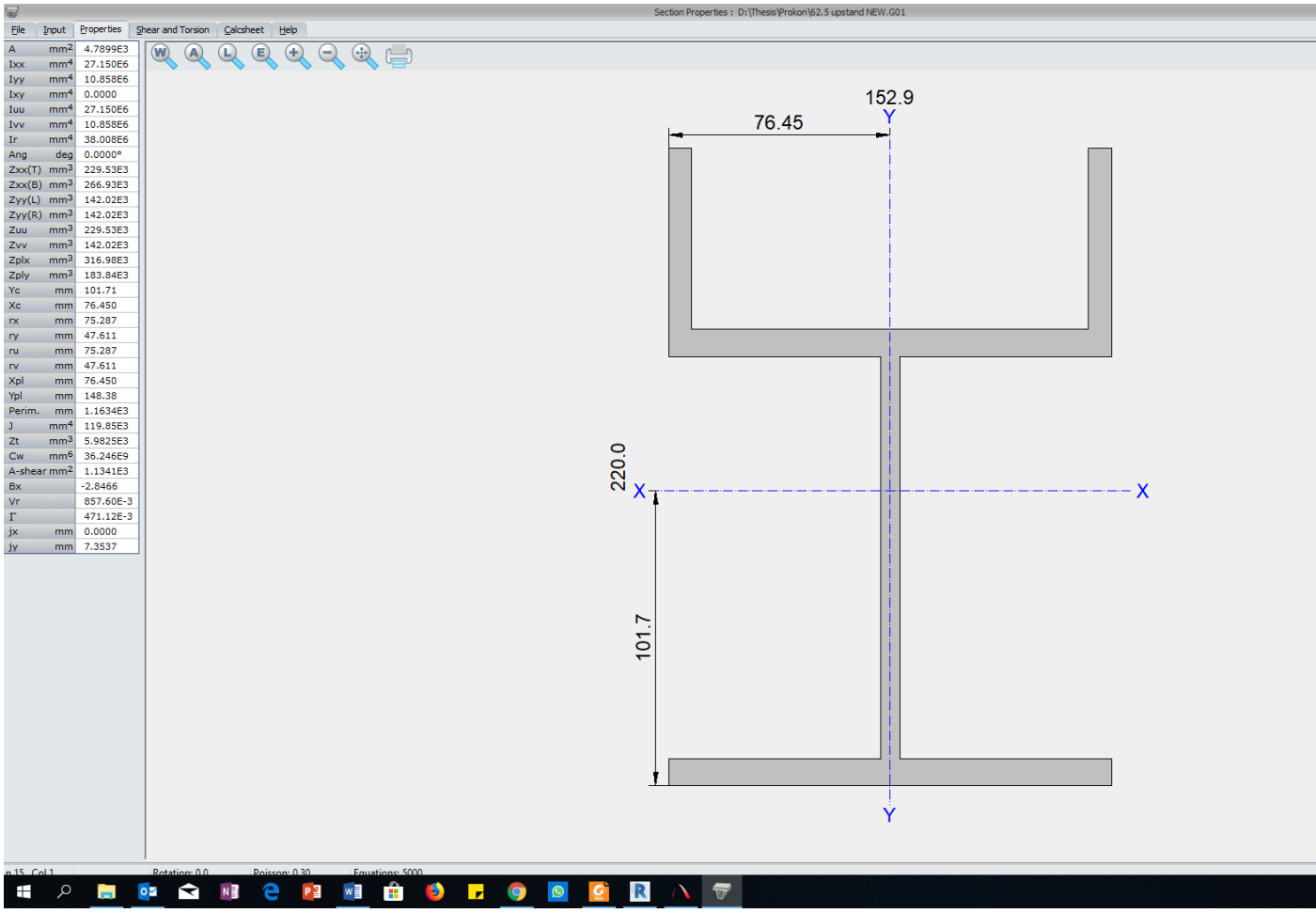

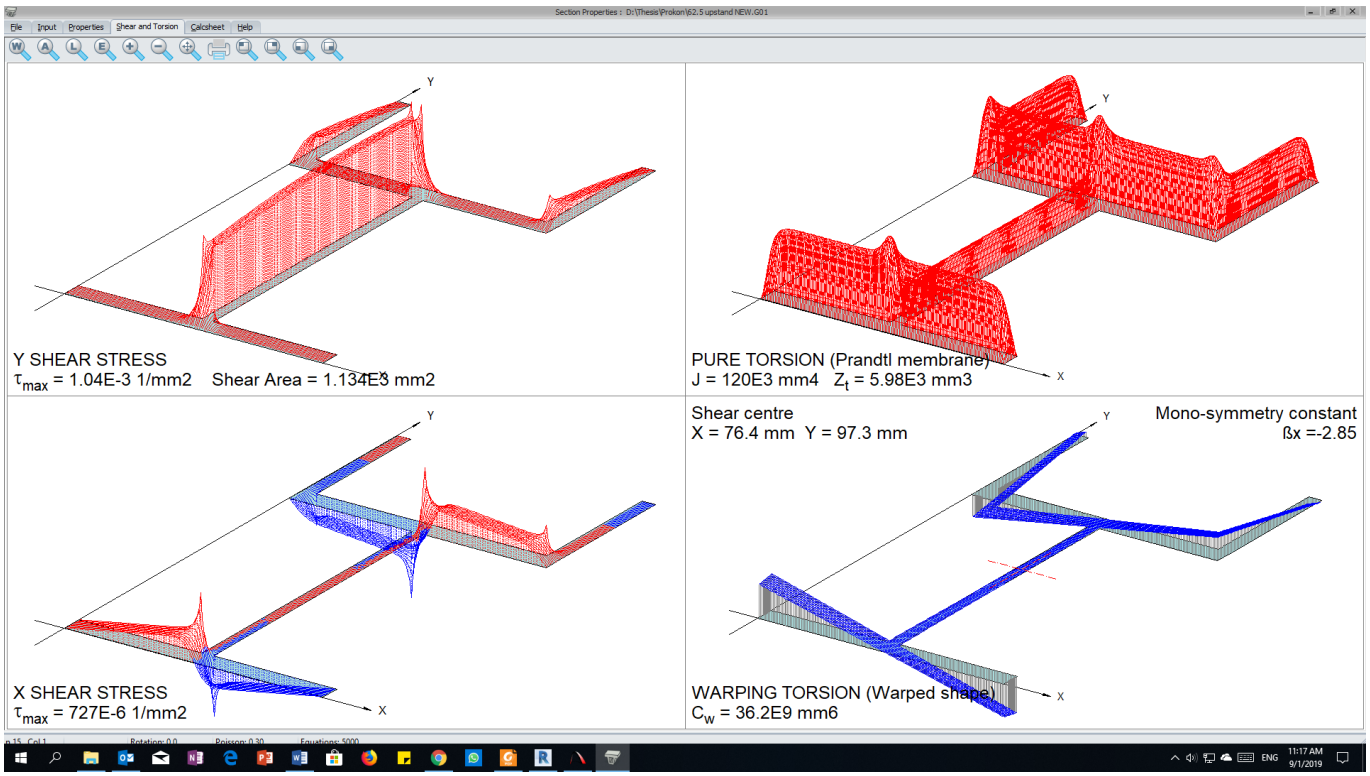

75mm Upstand

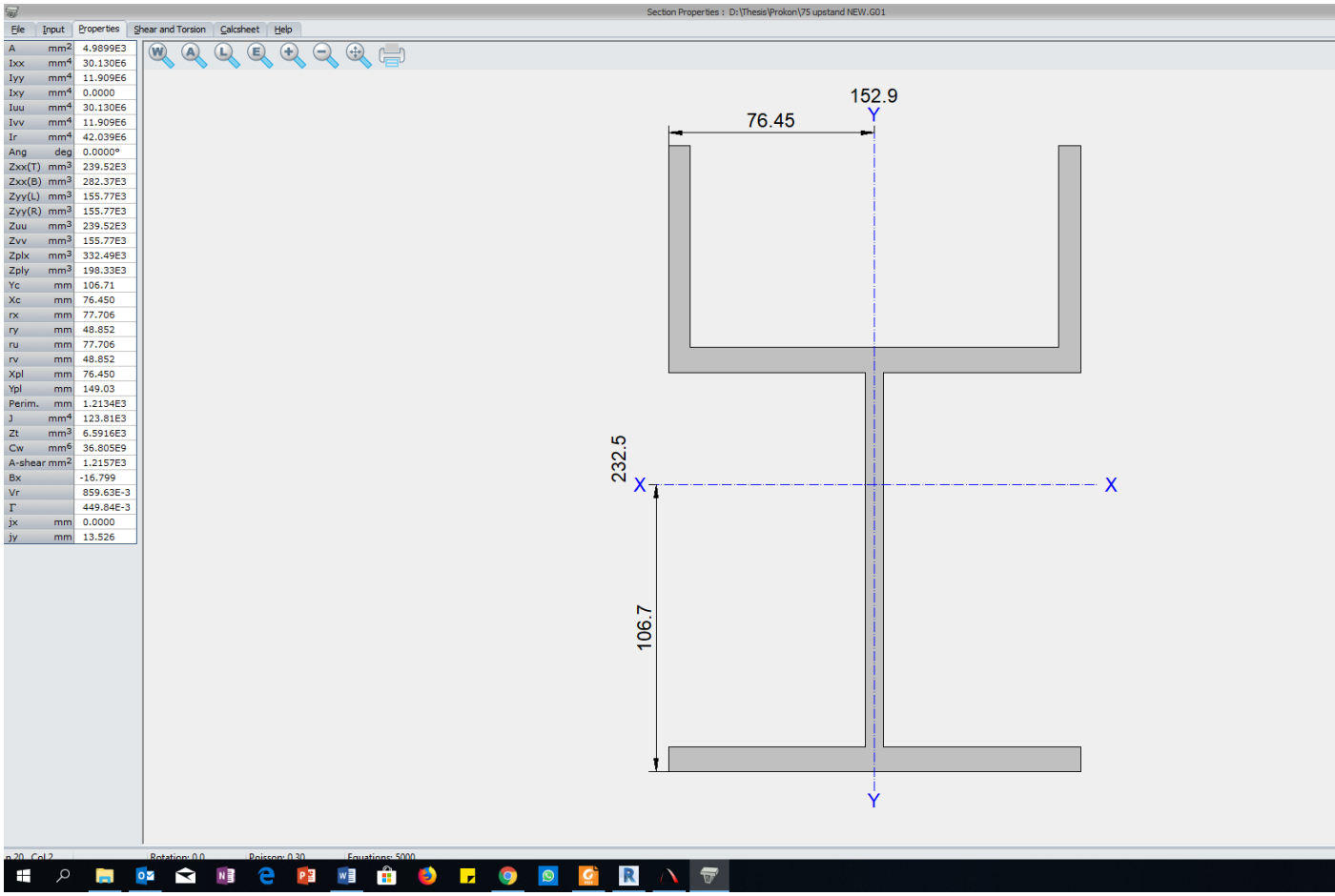

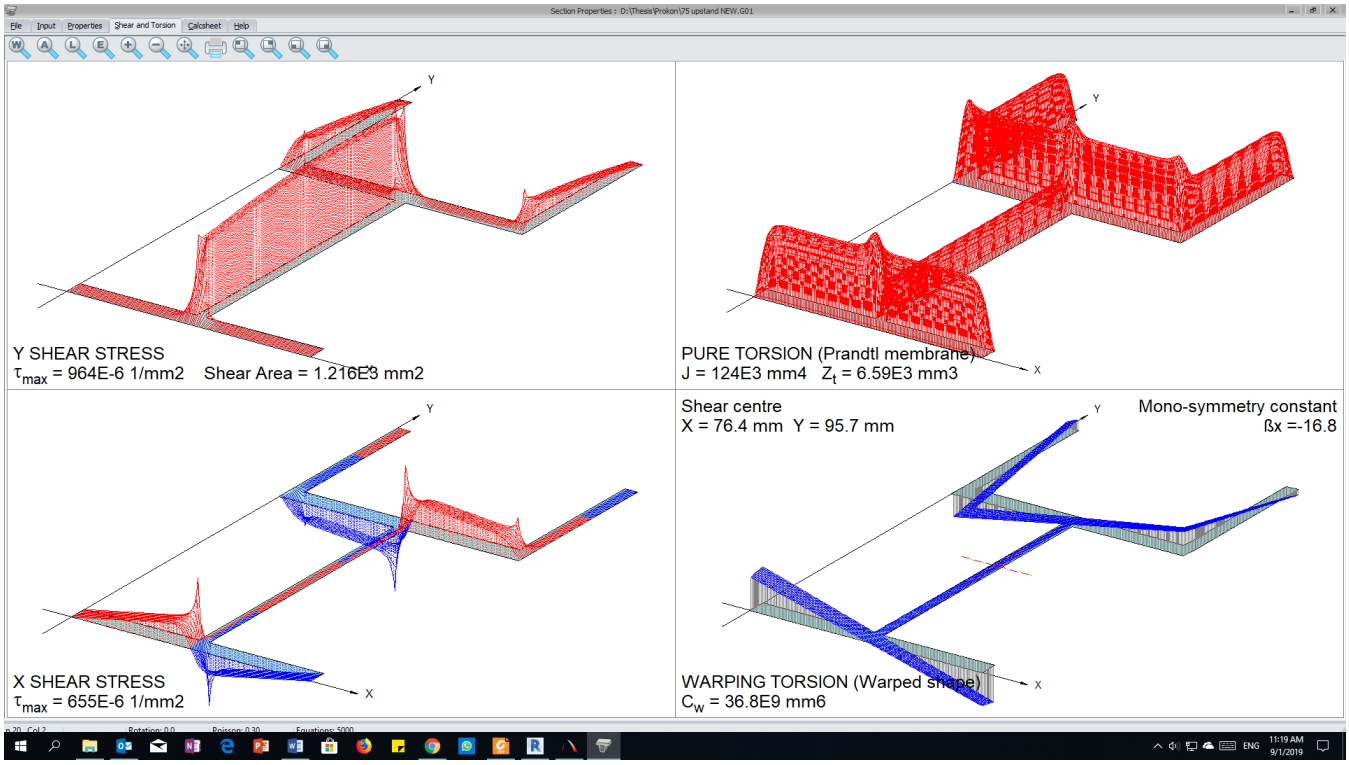

87.5mm Upstand

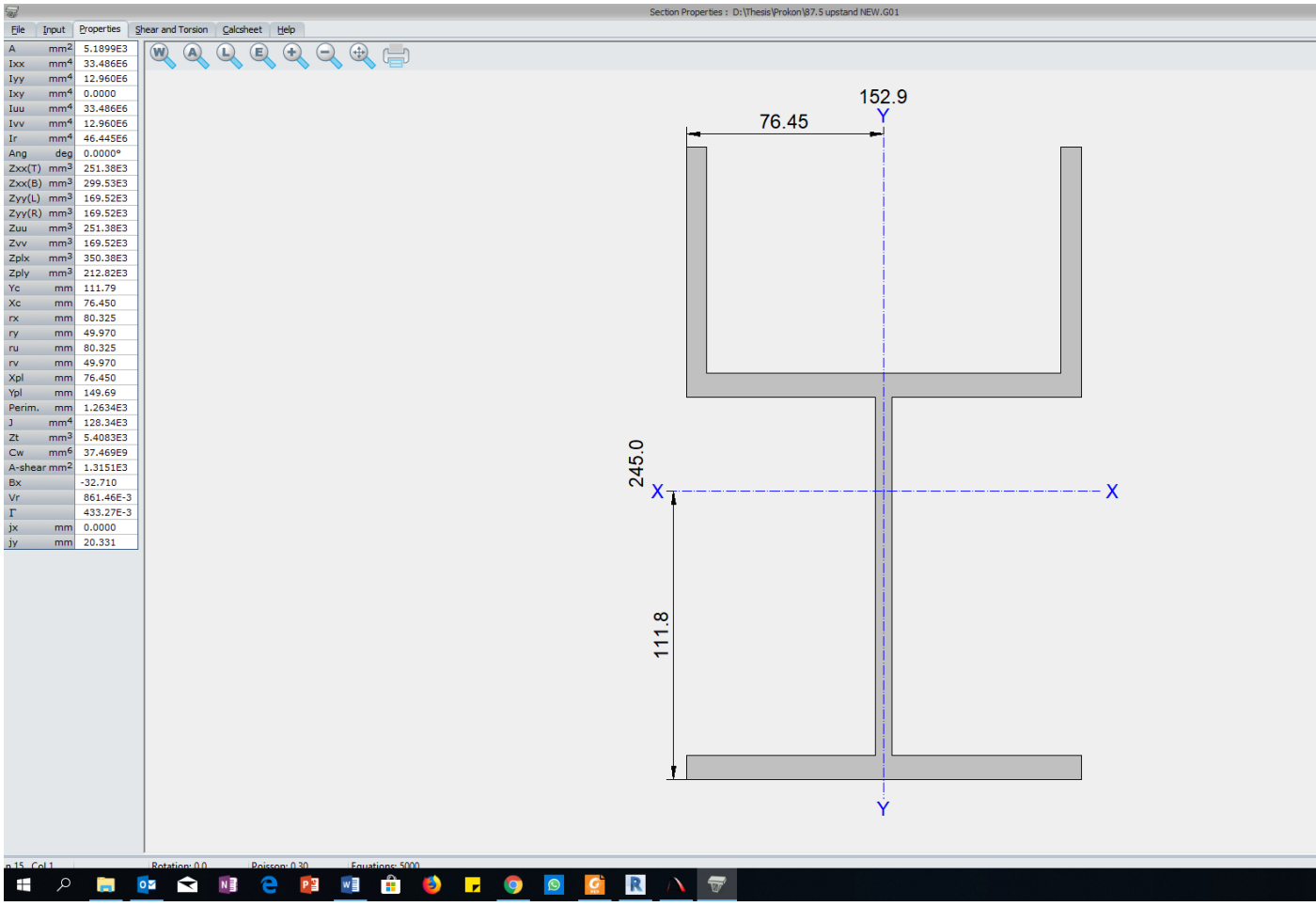

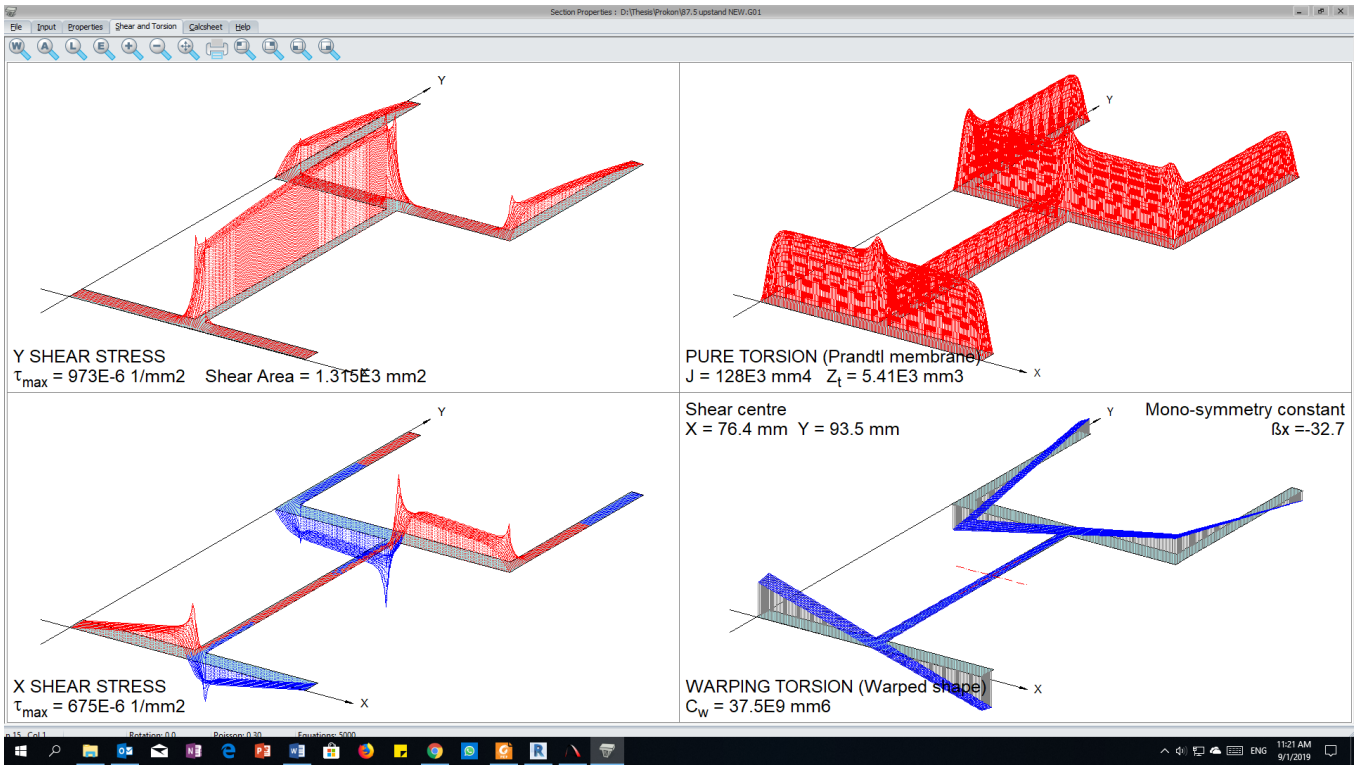

100mm Upstand